Resource Allocation in Service Area based Networks

Dissertation

zur

Erlangung des akademischen Grades

Doktor-Ingenieur (Dr.-Ing.)

der Fakultät für Informatik und Elektrotechnik

der Universität Rostock

vorgelegt von

Shiyang Deng, geb. am 22. August 1977 in China

aus Stuttgart

Stuttgart, 24. Oktober 2008

urn:nbn:de:gbv:28-diss2009-0080-0

Als Dissertation genehmigt von der
Fakultät für Informatik und Elektrotechnik
der Universität Rostock

Gutachter: Prof. Dr.-Ing. habil. Tobias Weber (Universität Rostock)
Prof. Dr.-Ing. Anja Klein (Technische Universität Darmstadt)
Prof. Dr.-Ing. habil. Volker Kühn (Universität Rostock)

Tag der öffentlichen Verteidigung: 26. März 2009

Vorwort

Die vorliegende Arbeit entstand im Rahmen meiner Tätigkeit als wissenschaftlicher Mitarbeiter am Lehrstuhl für hochfrequente Signalübertragung und –verarbeitung der Technischen Universität Kaiserslautern von September 2004 bis September 2005 und am Institut für Nachrichtentechnik der Fakultät für Informatik und Elektrotechnik der Universität Rostock von Oktober 2005 bis Janur 2008. Ich möchte all jenen danken, die mich bei der Entstehung dieser Arbeit unterstützt haben.

Mein besonderer Dank ergeht an Herrn Prof. Dr.–Ing. habil. T. Weber für die Anregung, die Betreuung und die Föderung meiner Arbeit. Durch seine stete Diskussionsbereitschaft sowie durch zahlreiche Ratschläge und Hinweise hat er einen entscheidenden Beitrag zum Gelingen dieser Arbeit geleistet.

Herrn Prof. Dr.–Ing. habil. Dr.–Ing. E. h. P. W. Baier danke ich für die Unterstützung und Anregung während meiner Beschäftigung in seiner Arbeitsgruppe. Diese Arbeit entstand in enger Zusammenarbeit mit der Arbeitsgruppe von Prof. Dr. rer. nat. H. Rohling, Technische Universität Hamburg–Harburg, im Rahmen eines Verbundprojekts im DFG–Schwerpunktprogramm TakeOFDM (Techniken, Algorithmen und Konzepte für zukünftige COFDM Systeme). Für die fruchtbaren Diskussionen aus denen wichtige Ideen für meine Arbeit resultierten sei Herrn Prof. Dr. rer. nat. H. Rohling herzlich gedankt. Frau Prof. Dr.–Ing. A. Klein von der Technischen Universität Darmstadt danke ich für die Übernahme des Korreferats und die im Rahmen unserer Kooperation enstandenen hilfreichen Hinweise und Anregungen. Herrn Prof. Dr.–Ing. habil. V. Kühn danke ich für das Interesse an meiner Arbeit und für die Übernahme des Korreferats. Weiterhin danke ich dem Vorsitzenden der Promotionskommission, Herrn Prof. Dr.–Ing. habil. H. Beikrich.

Den ehemaligen Kollegen an der Universität Rostock sowie an der Technischen Universität Kaiserslautern möchte ich für die angenehme Arbeitsatmosphäre und freundliche Hilfe herzlich danken.

Nicht zuletzt möchte ich mich bei meiner Frau und meiner Familie bedanken, die mir immer ein großer Rückhalt waren. Ihnen ist diese Arbeit gewidmet.

Stuttgart, im März 2009

Shiyang Deng

Contents

1 Introduction **1**
1.1 Preliminary remarks 1
1.2 JOINT – a future mobile radio system concept 5
1.3 Resource allocation in the OFDM based JOINT system 10
1.4 Related work 13
1.5 Structure of the thesis 18

2 Transmission model of JOINT **20**
2.1 General linear transmission model 20
2.2 Joint detection in the uplink of JOINT 22
2.3 Joint transmission in the downlink of JOINT 25
2.4 Time division duplex 27

3 Performance assessment of JOINT **29**
3.1 Single service area scenarios 29
3.1.1 Uplink performance 29
3.1.2 Downlink performance 37
3.2 Multiple service area scenarios 38
3.2.1 Uplink performance 38
3.2.2 Downlink performance 40

4 Transmit power allocation in interference channels **44**
4.1 Preliminary remarks 44
4.2 Interference channel model 46
4.3 Power allocation in interference channels 48
4.3.1 Signal-to-interference ratio balancing 48
4.3.2 Sum rate maximizing power allocation 50

4.3.3 Equal power allocation 53
4.3.4 Greedy power allocation 54
4.3.5 Conventional waterfilling 54
4.3.6 Iterative waterfilling 56
4.3.7 Noniterative waterfilling 60
4.4 Performance analysis 61

5 Subcarrier and power allocation in service area networks 71
5.1 Preliminary remarks 71
5.2 Subcarrier allocation in service area networks 72
5.2.1 Overview 72
5.2.2 Optimum subcarrier allocation 73
5.2.3 Sequential subcarrier allocation 77
5.2.4 Binary integer programming based subcarrier allocation . 79
5.2.5 Three dimensional channel gain array based subcarrier allocation 81
5.2.6 Fixed subcarrier allocation 83
5.3 Power allocation in service area networks 84
5.3.1 Service area interference channel 84
5.3.2 Signal-to-interference ratio balancing in service area networks 86
5.3.3 Greedy power allocation in service area networks 88
5.3.4 Conventional waterfilling in service area networks 89
5.3.5 Iterative waterfilling in service area networks 90

6 Performance evaluation of adaptive resource allocation in JOINT 91
6.1 Preliminary remarks 91
6.2 Simulation model 92
6.2.1 Reference scenario 92
6.2.2 Figure of merit 94
6.3 Performance of subcarrier allocation 95
6.3.1 Performance evaluation in the reference service area scenario 95
6.3.2 Service area networks versus conventional cellular networks 98

6.3.3 Exploitation of frequency selectivity 100
6.3.4 Adaptation of spatial correlation 102
6.3.5 Interferer diversity and interference adaptation 106
6.4 Performance of power allocation 109
6.4.1 Power allocation in the reference service area scenario . . 109
6.4.2 Power allocation in a conventional cellular network . . . 113
6.4.3 Power allocation in a frequency planned network 114

7 Summary **117**
7.1 English 117
7.2 Deutsch 119

A List of frequently used abbreviations and symbols **121**
A.1 Abbreviations 121
A.2 Symbols 122

Literature **126**

List of Figures **138**

List of Tables **142**

Thesen **144**

Chapter 1

Introduction

1.1 Preliminary remarks

In the last decade wireless communication has been evolving and growing rapidly all over the world. On the one hand, both the number of subscribers and the demands for novel multimedia applications are increasing dramatically with the introduction of the 3rd generation (3G) cellular networks and wireless LAN (WLAN) networks. On the other hand, radio resources needed for wireless communications continue to be most valuable and scarce for network operators. To accommodate as many as possible users while maintaining their diverse quality of service (QoS) requirements with minimum cost is of great interest to both network operators and the communication community.

Interference is an essential issue in communication systems which severely limits the system capacity. In wired communication systems such as digital subscriber line (DSL) systems interference may be caused by crosstalk [SCS98]. In wireless communication systems interference is unavoidable because a large number of users have to compete for limited radio resources. Reducing interference to an acceptable level is a challenging task and has been drawing a lot of attention. In general, interference management can be done in the following ways:

- Separate users in orthogonal channels, e.g., time slots, frequencies and spreading codes, so that they do not interfere with each other at all. In cellular systems, users in the same cell are usually separated by applying time/frequency/code division multiple access (TDMA/FDMA/CDMA) and users in neighboring cells can be separated by frequency planning which allocates disjoint subsets of frequencies to neighboring cells [MD79]. Moreover, rather than fixed channel assignment it is more efficient to adaptively assign the channels to the users depending on the channel conditions. Unfortunately, due to the fact that the number of channels is often not sufficient to accommodate a large number of users, especially in high user density scenarios like airports and shopping malls, some users have to share the same channels. Even users active at different channels may cause inter-channel interferences (ICIs) to each other due to synchronization errors, imperfect filtering or imperfect code orthogonality. In the context of this thesis the term interference will exclusively refer to co-channel interference (CCI) caused by channel-sharing users, unless other stated.

- Allocate transmit powers to co-channel users in an intelligent way so that the interference level is acceptable and the system performance is optimized. Unlike thermal noise which can be overcome by simply increasing the transmit powers, interference caused by co-channel users depends on the relative relationship among their transmit powers. For instance, increasing the transmit power of a specific user increases its signal-to-interference-plus-noise ratio (SINR) and enables a lower bit error rate (BER) or a higher data rate. On the other hand, however, this means a higher power consumption and leads to stronger interference to its co-channel users which consequently degrades their SINRs. Therefore, proper power allocation strategies that strike a balance between the benefits and drawbacks depending on the performance criteria have to be incorporated while designing communication systems. A well known example is the IS-95 system where power control is used to combat the near-far problem in the uplink, i.e., the interference from the users close to a base station should not overwhelm those users far away [Gar99].

- Apply interference cancellation techniques to co-channel users. By do-

ing so interference is reduced or eliminated at a cost of transceiver complexity. Various linear and nonlinear interference cancellation techniques applicable to single antenna elements or antenna arrays have been developed [And05]. Traditionally, interference cancellation is carried out at the receiver side through multiuser detection [Ver98]. For instance, in the uplink of mobile radio systems multiple receive antennas at the base station allow spatial separation of the signals of different users, which is known as space division multiple access (SDMA) [TV05]. Interference cancellation with single receive antennas can be achieved by joint maximum likelihood estimation [Ett76] and its derivatives [CLTC98, HHA03, HBHD$^+$06, SH04]. Rather than cancelling interference at the receiver side, in the downlink of mobile radio systems it is desirable to avoid interference at the transmitter side, i.e., at the base stations, in order to save signal processing complexity at the mobile stations which are typically size and power limited. Such interference mitigation strategies can be accomplished by applying precoding techniques [Fis02]. Examples of precoding techniques include linear transmit beamforming [TV05] and nonlinear dirty paper coding (DPC) [Cos83].

In practice, the above mentioned interference management strategies can be combined to improve the system performance. It should be noted that channel allocation and power allocation can be executed without changing the transceiver design or system architecture. Therefore, they are compatible to current systems in use. In contrast to this, applying co-channel interference cancellation techniques normally requires modifications to the transceiver design and is more expensive.

Multiple-input multiple-output (MIMO) and orthogonal frequency division multiplexing (OFDM) have been acknowledged as the most promising techniques for beyond 3rd generation (B3G) mobile radio systems. Using multiple antennas at the transmitter and at the receiver side, MIMO systems provide extra degrees of freedom in the spatial domain as compared to single-input single-output (SISO) systems. These extra degrees of freedom can be exploited to provide diversity to improve the reliability of transmission or alternatively to

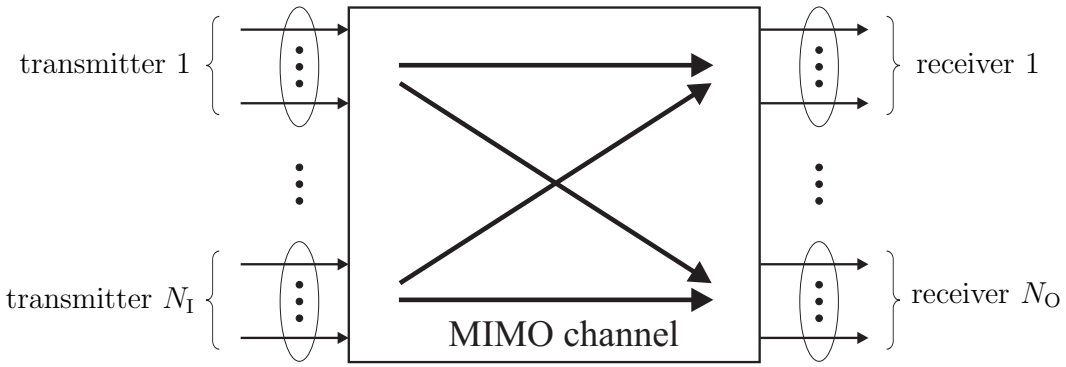

Figure 1.1: General MIMO system

multiplex multiple data streams in order to increase the throughput. The fundamental tradeoff between diversity and multiplexing in point-to-point MIMO systems is analyzed in [ZT03]. Depending on the number of transmitters and receivers a few varieties of the MIMO systems exist. Fig. 1.1 illustrates a general MIMO system, where N_{I} transmitters and N_{O} receivers are communicating through the MIMO channel. Each transmitter and receiver may be equipped with a single antenna or with multiple antennas. In the case that $N_{\mathrm{I}} > 1$ and $N_{\mathrm{O}} > 1$ Fig. 1.1 represents a multipoint-to-multipoint MIMO system. If there are $N_{\mathrm{I}} > 1$ transmitters and $N_{\mathrm{O}} = 1$ receiver, such a MIMO system is referred to as multipoint-to-point MIMO system with a multiple access channel (MAC) [Ahl71, CT91] in between. Oppositely, a MIMO system with $N_{\mathrm{I}} = 1$ transmitter and $N_{\mathrm{O}} > 1$ receivers is known as point-to-multipoint MIMO system with a broadcast channel (BC) [Cov72, CT91] in between. When there are exactly one transmitter and one receiver present, Fig. 1.1 degenerates into a point-to-point MIMO system. Because of its great potential in increasing data throughput and link quality without additional bandwidth or transmit power and achieving higher spectral efficiencies [FG98, Tel99], MIMO is being considered by the high-speed packet access plus (HSPA+) standard and the long term evolution (LTE) project. The IEEE 802.16e standard dubbed mobile WiMAX [Har06] also incorporates MIMO.

OFDM [vNP00] is a multi-carrier modulation (MCM) technique which divides a high bit rate data stream into multiple parallel low bit rate data streams and uses them to modulate multiple carriers [Bin90]. In the frequency domain the

entire bandwidth is composed of densely spaced subcarriers. Unlike conventional frequency division multiplexing (FDM) where inter-carrier guard bands are required to mitigate undesired crosstalk between subcarriers, in OFDM the overlapping subcarriers are orthogonal to each other, which implies that ICI is avoided and a higher spectrum efficiency is achievable. Another primary advantage of OFDM over single-carrier schemes is its ability to cope with severe channel conditions such as multipath and narrowband interference. By expanding the symbol duration in the time domain and inserting a guard interval between OFDM symbols each subcarrier is frequency non-selective, so that inter-symbol interferences (ISIs) are avoided and complex equalization becomes unnecessary at the receivers. Furthermore, the cyclic prefix transmitted during guard interval allows efficient modulator implementation using IFFT and demodulator implementation using FFT. OFDM has some inherent drawbacks including the high peak-to-average power ratio (PAPR) and frequency synchronization sensitiveness. Nevertheless, due to its elegant delay spread tolerant and spectrum efficient properties OFDM has been integrated into numerous standards such as digital video broadcasting (DVB) [ETS97a], digital audio broadcasting (DAB) [ETS97b], HIPERLAN/2 [ETS99], IEEE 802.11a [80299], IEEE 802.11g [80203], IEEE 802.16d which is also known as WiMAX [Har06], high data rate DSL (HDSL) [CTC91] and power line communication (PLC) [Koc07], etc. In mobile radio community OFDM is being considered as a leading candidate technique for B3G systems [RGG01]. For example, high speed OFDM packet access (HSOPA) is proposed for 3GPP LTE. The OFDM based mobile broadband wireless access (MBWA) specification is under development in the framework of IEEE 802.20 and a commercial MBWA system called Flash-OFDM (Fast Low-latency Access with Seamless Handoff OFDM) [KL03] has already been deployed in America and Europe.

1.2 JOINT – a future mobile radio system concept

As a novel B3G system proposal, the joint transmission and detection integrated network (JOINT) [WSLW03] takes advantage of both MIMO and

OFDM techniques. It aims at increasing the capacity as compared to 3G cellular systems and WLAN systems while keeping the complexity of the mobile stations (MSs) low. JOINT is built on the novel service area (SA) architecture. Before introducing the SA concept let us review the conventional cellular architecture.

The advent of the cellular concept proposed by D. H. Ring in an internal memorandum at Bell Laboratories in 1947 was a milestone in the evolution of mobile radio communications. It has been employed by all the three generations of mobile radio systems. By partitioning the whole region to be served into a number of cells and assigning subsets of frequencies to individual cells the interferences are greatly reduced as compared to the case without partitioning. The conventional cellular architecture is reviewed in Fig. 1.2. There each hexagon represents a cell, which defines the radio coverage region served by the base station (BS) at cell center. The MSs located in a cell are radio linked to the BS of the same cell and all BSs are connected to the core network. In this way a link between any two MSs can be established.

It is well known that conventional cellular networks are interference rather than noise limited [Lee97]. Depending on whether the interferences originate from the same cell or from co-channel cells operating on the same subset of frequencies, the interferences in cellular networks are categorized as intra-cell interferences or inter-cell interferences. Intra-cell interferences can be combated by employing precoding [Fis02] or multiuser detection [Ver98] techniques. Inter-cell interferences are reduced by increasing the spatial separations between co-channel cells. Apart from the cell size, the spatial separations between co-channel cells are determined by the cluster size which defines how many cells collectively use the complete set of available frequencies [Rap96]. For instance, in Fig. 1.2 the cluster size is three. As long as the inter-cell interference does not exceed an acceptable level, the cluster size should be as small as possible so that the spectrum is efficiently used.

In order to reduce the inter-cell interference of cellular networks and to improve the spectrum efficiency, the novel SA architecture is introduced, see Fig. 1.3. As the basic entity of the JOINT system a SA is formed by a cluster of neighboring cells. A SA can also be viewed as a hyper-cell whose shape depends on

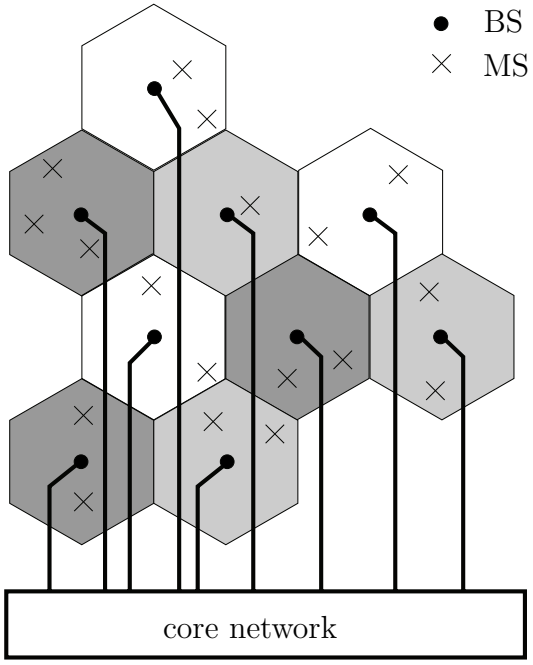

Figure 1.2: Conventional cellular architecture with cluster size three

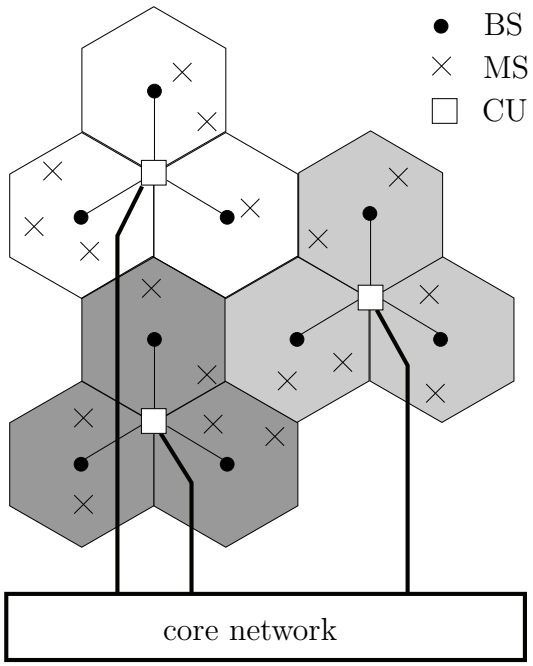

Figure 1.3: SA architecture with SA size three

which cells are clustered together. Unlike conventional cellular networks where adjacent cells usually use disjoint subsets of frequencies as a result of frequency planning, in SA based networks the neighboring cells inside the same SA operate on the same frequency band and frequency planning treats an entire SA as a unit. The inter-cell interferences among the cells belonging to the same SA become intra-SA interferences. The BSs of a SA are coordinated by linking them to a SA specific central unit (CU) where joint signal processing is carried out. The CUs are then connected to the core network. In the uplink (UL), the signals stemming from multiple MSs can be jointly detected [Ver98, Kle96] at the CU by exploiting the receive signals of the connected BSs. In the downlink (DL), the transmit signals for the BSs of each SA are jointly generated [Fis02, MBW$^+$00] at the CU in such a way that the intra-SA interferences are mitigated. In contrast to conventional cellular systems where each channel is exclusively occupied by one MS, the introduction of the SA concept and the application of joint transmission (JT) and joint detection (JD) in JOINT allow multiple MSs to be simultaneously active, which represents a SDMA component. The rationale used in JD and JT can be zero forcing or minimum mean square error [KKB96]. Through JD in the UL and JT in the DL the interferences in SA based networks are reduced as compared to conventional cellular networks. The number K_{B} of cells making up of a SA is referred to as the SA size. Conventional cellular networks are actually special cases of SA based networks with SA size being one. A larger SA size means more cells are clustered together which leads to a higher infrastructure cost and signal processing complexity. Therefore, the performance improvement of SA based networks over conventional cellular networks is at a price of complexity.

From the physical layer perspective, the BSs of a SA at one end and the MSs in the same SA at the other end form a multiuser MIMO system. Precisely, in the UL the uncoordinated MSs as separate transmitters and the coordinated BSs as a common receiver represent a multipoint-to-point MIMO system. In the DL the coordinated BSs as a common transmitter and the uncoordinated MSs as separate receivers represent a point-to-multipoint MIMO system. In principle, both single antenna elements and antenna arrays can be deployed at each BS and MS. For the sake of simplicity in this thesis it is assumed that single antenna elements are installed at all BSs. Furthermore, it is reasonable

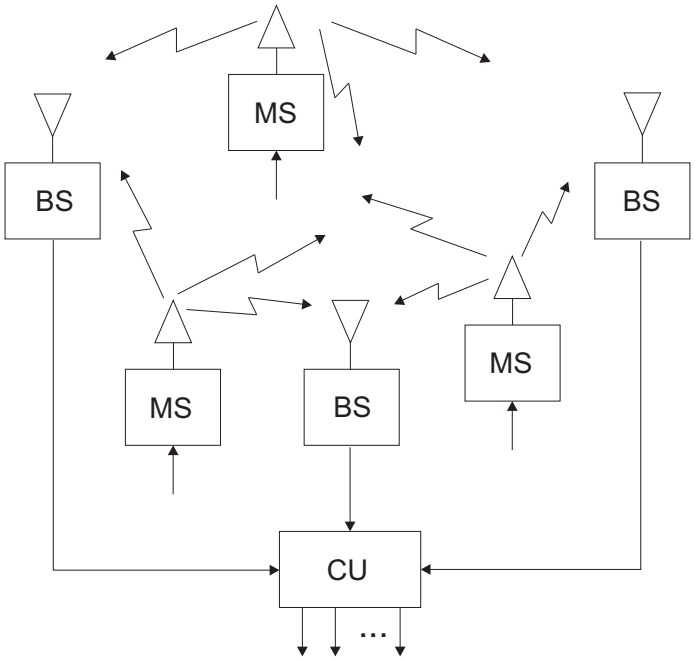

Figure 1.4: Multiuser MIMO scenarios in a service area, uplink

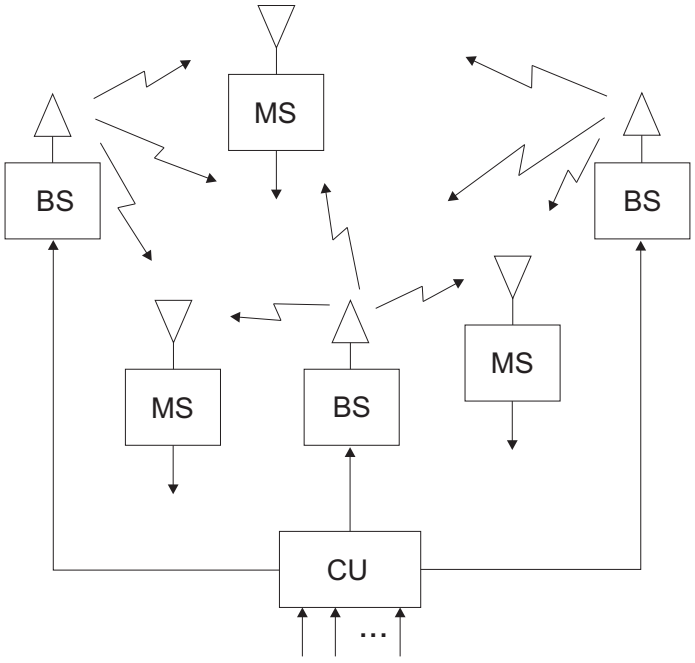

Figure 1.5: Multiuser MIMO scenarios in a service area, downlink

to assume that the MSs are equipped with single antennas due to cost, volume, power consumption and design aspects. The corresponding UL and DL multiuser MIMO scenarios are illustrated in Fig. 1.4 and Fig. 1.5, respectively.

Since the cells within a SA operate on the same subset of frequencies, a moving MS does not trigger handoff as long as it is served by the same CU regardless in which cell of the SA the MS is located. In other words, in SA based networks handoff happens less frequently than in conventional cellular networks.

A group cell concept which is very similar to the SA concept is studied under the framework of the FuTURE (Future Technologies for Universal Radio Environment) project in China [ZTZ+05, TXX+05, XTWZ06]. A group cell is equivalent to a service area. The SA based JOINT system can also be viewed as a distributed antenna system [SRR87, MF07].

JOINT utilizes time division duplex (TDD) as the duplex scheme to benefit from the reciprocity of the UL channel and the DL channel. Thus the channel state information (CSI) obtained by pilot aided joint channel estimation (JCE) [SMW+01, MWS+02] performed at the CU can be used for both JD in the UL and JT in the DL. Besides the SA architecture and TDD, OFDM is another crux of the JOINT system. By adopting OFDM the JOINT system can benefit from simplified transceiver design without complex equalization stage. For the BS side only JT and JD signal processing needs to be implemented at the CUs. Furthermore, since JT and JD are performed at the BS side, only traditional OFDM transceivers are needed at the MSs without requiring extra signal processing tasks, which keeps the complexities of the MSs low. The use of OFDM also enables flexible resource allocation in JOINT, which will be discussed in next section.

1.3 Resource allocation in the OFDM based JOINT system

OFDM's inherent multicarrier nature allows flexible subcarrier-wise adaptation of transmit power, constellation size and channel coding, so that the

power and spectrum efficiency can be significantly enhanced. Moreover, in multiuser OFDM systems multiuser diversity [KH95] provides another degree of freedom for adaptation. Although OFDM was originally proposed as a modulation technique used for transmitting the data stream of a single user, in multiuser scenarios it can also be combined with multiple access using time, frequency or code separation of multiple users. In particular, the combination of OFDM and FDMA known as orthogonal frequency division multiple access (OFDMA) assigns different OFDM subcarriers to different users. [RG97] shows that OFDMA, also called OFDM-FDMA, outperforms OFDM-CDMA and OFDM-TDMA, if proper subcarrier allocation is performed. OFDMA also supports differentiated QoS by assigning different number of subcarriers to different users.

Adaptive resource allocation in multiuser OFDM systems is attracting more and more interest in recent years due to its capability of improving system performance [WCLM99, RC00, KL00, KT02, YGC02, MPS02, SL03, WSEA04, ZL04, KHK05, ZL05, MB05, KAS05, WDM05, SR06]. In OFDM based JOINT system resource allocation is also a key issue which has a great impact on the system performance. In the context of this thesis resources refer to OFDM subcarriers and transmit powers, although resources may also refer to time slots, spreading codes or constellation size in literature. Therefore, resource allocation in JOINT in the following means allocation of subcarriers to different users and distribution of the available transmit power to different users and to different subcarriers. In principle, the following aspects should be taken into consideration while developing adaptive resource allocation algorithms:

- The subcarrier specific channel condition. Frequency selectivity caused by multipath propagation is a basic characteristic of wireless channels and can be detrimental to communications [Rap96]. In pure TDMA or CDMA systems where the entire system bandwidth is utilized by every user, deep fading can degrade spectral efficiency. However, the presence of OFDMA in JOINT offers a great potential for performance optimization by exploiting frequency selectivity induced multiuser diversity [KH95]. In multiuser scenarios different users experience different channel conditions on the same subcarrier. It is very likely that on every

subcarrier there exist some users who see favorable channel conditions. This phenomenon reflects the beneficial multiuser diversity which can be exploited by adaptive subcarrier allocation in OFDMA systems. Besides, transmit power allocation should adapt to OFDM subcarrier dependent channel conditions to increase the power efficiency.

- The spatial correlations of the users' channels. Unlike conventional subcarrier allocation problems where a single best MS is selected for each subcarrier, in JOINT the use of SDMA enables intra-SA frequency reuse by multiplexing spatially separable users and hence subcarrier allocation deals with assignment of groups of users to subcarriers. Grouping users differently yield different performance. For instance, if the subcarrier-sharing users have very similar channels on that subcarrier, i.e., the channels are tightly correlated, it will be difficult to separate the signals by JD in the UL and to avoid interferences by JT in the DL. Even for the case that different subcarriers fade identically the way how the users are combined has a great impact on the performance, because the combinations of users provide another source of multiuser diversity. Therefore, not only the channel conditions of individual users but also the spatial correlations among the users play an important role in resource allocation in SDMA based systems, which imposes a challenge and meanwhile provides extra potentials for optimization.

- Inter-SA interferences. Although intra-SA interferences can be completely eliminated by applying ZF JD in the UL and ZF JT in the DL, inter-SA interferences that come from the SAs operating on the same subset of subcarriers still remain in the JOINT system. Due to mutual influence among the co-channel SAs, the allocation of subcarriers and transmit powers to different users must be carefully determined. On the one hand, for a specific user the subcarriers exhibiting small interference from the co-channel SAs should be chosen. On the other hand, power and subcarrier allocation for the user should cause small interferences to its co-channel SAs. The interactive nature of co-channel users in different SAs implies difficulties in resource allocation in multi-SA scenarios.

The aforementioned aspects also suggest how we potentially can benefit from

adaptive resource allocation. In reality some of the potential benefits may be of minor importance and can be ignored to reduce the complexity of resource allocation. For instance, in a scenario with large interferer diversity resource allocation adapting to interference may yield only marginal performance improvement as compared to allocating resources without considering interferences. It should also be mentioned that in practical applications adaptive resource allocation is subject to certain QoS requirements while adapting to frequency selectivity, spatial correlations and interferences.

1.4 Related work

Driven by the continuously increasing demands on spectrum efficiency in both wired and wireless communication systems a lot of effort has been devoted to adaptive resource allocation techniques, among which different types of resources such as time slots, subcarriers, rates and transmit power are concerned. Some researchers solve cell selection problems additionally. For convenience some selected references dealing with different types of resources in various systems are listed in Table 1.1, which provides an overview of resource allocation.

Originally, scheduling refers to the process of determining which users are served at which time in queuing systems. As a simple scheduling algorithm round-robin scheduling fairly allocates time slots to users without optimizing the throughput [HG86]. However, the time variance of wireless channels caused by relative motion between transmitters and receivers provides the possibility of throughput optimization by applying channel-dependent scheduling algorithms so that multiuser diversity is exploited. Well known channel-dependent scheduling algorithms include maximum throughput scheduling [TE92] and proportionally fair (PF) scheduling [JPP00]. The former optimizes system throughput without taking care of fairness, whereas the latter achieves a favorable compromise between system throughput and fairness. PF scheduling has been included in the downlink specification of IS-856 (cdma2000 EV-DO) [EV-01]. In this thesis, however, the focus is not on temporally scheduling users

Table 1.1: Selected publications on resource allocation

references	remarks
[HG86], [TE92], [JPP00]	temporal scheduling
[Aei73], [AN82], [NA83], [Zan92], [Wu00]	classic power control and its variants
[HH87], [Kal89], [CCB95], [WW97], [JLL02], [Bin90], [SS00]	power/bit allocation in single-user OFDM
[WCLM99], [RC00], [KL00], [MPS02], [JL03], [SAE03], [WSEA04], [KHK05], [MB05]	subcarrier and power/bit allocation in multiuser OFDM (SISO, interference-unaware)
[KT02], [YL02], [FGH05], [SS04], [SSH04], [WDM05], [ZL05], [XL06], [ZCZ+06], [FGH06], [Mac08]	resource allocation in SDMA based systems
[PJ04], [ZL04], [KAS05], [SR06]	interference-aware resource allocation

to different time slots, but on assigning users to subcarriers in the frequency dimension for every channel snapshot.

Power control is an effective means for interference management. In the early 70's power control was suggested by Aein [Aei73] as a method for ensuring that all co-channel users in satellite systems experience the same carrier-to-interference ratio (CIR), i.e., CIR balancing is achieved. Later on Nettleton and Alavi investigated the CIR balancing problem in spread spectrum cellular systems [AN82, NA83] and Zander considered FDMA/TDMA cellular systems [Zan92]. In [Wu00] Wu extended Zander's work to the case of unbalanced CIR levels, i.e., heterogenous CIR targets are assumed. The present thesis will extend previously considered conventional cellular networks to SA based networks. It will be shown that the CIR balancing problem in SA based networks can be efficiently solved.

As mentioned before, in OFDM based systems the use of multiple orthogonal subcarriers allows flexible subcarrier-wise adaptation of transmit power and constellation size. In single-user OFDM systems, the transmit power can be adaptively distributed to subcarriers to exploit frequency diversity so that the

throughput is increased. Due to the ICI-free feature of OFDM, the throughput in a single-user OFDM system is maximized when the transmit power allocation constrained by a total transmit power follows the waterfilling principle in frequency domain [Kal89, WW97]. Under the constraint of average transmit power, waterfilling should be performed in both frequency and time domain for throughput maximization [JLL02]. Power allocation in multicarrier systems is usually combined with bit loading which adjusts the number of transmitted bits on each subcarrier according to the subcarrier specific channel quality [HH87, Bin90, CCB95, SS00]. In general, subcarriers with high channel gains should employ large constellation size to carry more bits per OFDM symbol in order to take advantage of the good channel quality, whereas subcarriers in deep fade should carry one or even zero bit per OFDM symbol. In this thesis, however, bit loading is not our primary focus.

In multiuser OFDM, not only the transmit power and constellation size can be adapted for every subcarrier, but also the multiple access can be controlled through adaptive subcarrier allocation. By doing so, frequency domain diversity as well as multiuser diversity is effectively exploited and thus the system performance is significantly improved. Subcarrier allocation problems in multiuser OFDM systems have been studied in many publications [WCLM99, KL00, RC00, MPS02, JL03, SAE03, WSEA04, KHK05, MB05, SR06]. Some of them focus on subcarrier allocation using fixed power allocation [SR06, MPS02]. In [SR06] the cell-wide subcarrier allocation problem aiming at maximizing the sum signal-to-noise ratio (SNR) is modelled as a bipartite matching problem which is solvable via the Hungarian method. In [MPS02] a multiuser waterfilling [CV93] based subcarrier allocation technique aiming at maximizing the total data rate subject to per user power budgets is presented. Some publications deal with both adaptive subcarrier allocation and adaptive power allocation [WCLM99, KL00, RC00, JL03, SAE03, WSEA04, MB05, KHK05]. In [RC00] the optimal subcarrier and power allocation that maximizes the minimum capacity of all users under the zero delay and total transmit power constraint is analyzed. It is shown that a suboptimum solution with uniform power allocation performs almost as well as the optimal power and subcarrier allocation. In [WCLM99] the authors propose an iterative subcarrier-bit-and-power allocation algorithm based on the Lagrangian method for minimizing

the total transmit power under a fixed set of user data rate and BER requirements. However, the high computational complexity of the iterative algorithm makes it impractical. Some other suboptimal solutions that perform subcarrier and power allocation jointly can be found in [MB05, KHK05]. The joint optimization problem can be divided into separate steps to reduce the complexity [KL00, JL03, SAE03, WSEA04]. For instance, in [KL00] the first step determines the number of subcarriers that each user will get based on the users' average SNR. The subcarriers are then assigned to the users at the second step. Finally, single-user power allocation is performed. It is shown that the proposed low complexity algorithms offer a performance comparable to that of the iterative algorithm in [WCLM99]. In [JL03] the subcarriers are assigned to the users first and the transmit power and the number of bits on each subcarrier are determined afterwards by using single-user power/bit loading algorithms. It is proven in [JL03] that in order to maximize the total capacity under the constraint of total transmit power and BER, each subcarrier should be allocated exclusively to the user with the best channel gain on it and the power should be distributed over the subcarriers using the waterfilling algorithm. The present thesis will also handle subcarrier allocation and power allocation separately in multiuser OFDM based JOINT system.

Resource allocation in SDMA based systems is drawing considerable attention recently with the consensus that MIMO technology is indispensable in future wireless systems. In contrast to SISO systems where each frequency or time slot is dedicated to one user [WCLM99, KL00, RC00, MPS02, JL03, SAE03, WSEA04, KHK05, MB05, SR06], in SDMA based systems, e.g., the JOINT system, sharing the same frequency or time slot by multiple users is allowed. The presence of multiple antennas provides extra degrees of freedom in the spatial domain which can be exploited by channel-aware subcarrier allocation or scheduling [KT02, YL02, FGH05, ZL05, WDM05, XL06, ZCZ+06, SSH04, SS04, FGH06, Mac08]. Either maximizing throughput or minimizing transmit power, the essential goal of channel-aware subcarrier allocation or scheduling in SDMA based systems is to arrange multiple users in groups such that the users belonging to a group can be efficiently multiplexed in space, while the different groups are served in different frequency or time slots. The underlying principle to achieve the goal is to arrange the users with weakly correlated

spatial signatures in the same group. In this thesis, the subcarrier allocation problem dealing with assigning groups of users to multiple subcarriers will be studied.

Most previous work concentrates on single cell scenarios or models co-channel interferences as white noises [WCLM99, KL00, RC00, MPS02, SAE03, FGH05, KHK05, ZL05, MB05, WDM05, XL06, ZCZ+06], i.e., the performance limiting interferences are ignored. However, the existence of colorful interferences in reality requires more sophisticated interference-aware resource allocation techniques to improve the system performance [PJ04, ZL04, KAS05, SR06]. For instance, in [SR06] it is demonstrated that in cellular OFDMA systems self-organized subcarrier allocation based on interference measurements outperforms frequency planning with interference-unaware subcarrier allocation in hotspot scenarios and in nearly flat fading scenarios. Although in certain scenarios ignoring the interferences may simplify resource allocation algorithms without considerable performance loss, in this thesis both interference-aware and interference-unaware resource allocation techniques are studied. The performance will be mainly evaluated in interference limited scenarios consisting of multiple co-channel SAs and the influence of inter-SA interference will be explicitly investigated.

The employment of adaptive resource allocation in OFDM based systems clearly requires extra signalling overhead to describe which time slots, subcarriers and constellation size are assigned to a specific user. A large amount of signalling overhead can waste a significant portion of the improved power and spectrum efficiency resulting from adaptive resource allocation. However, in environments where the channels are not severely frequency selective, a contiguous band of subcarriers with similar fading characteristics can be treated as a single unit in subcarrier allocation instead of subcarrier-by-subcarrier assignment. In this way the signalling overhead can be saved. Similarly, in low mobility environments it is more efficient to perform scheduling for multiple consecutive time slots together rather than for each time slot individually. In this thesis, however, we will neither quantify the amount of signalling overhead incurred by resource allocation nor consider how the signalling is transferred between BSs and MSs. Instead, we focus on developing practical resource

allocation techniques in SA based networks and evaluating their performance.

1.5 Structure of the thesis

The rest of this thesis consists of six chapters which are organized as follows.

In Chapter 2 the basic system model and the signal structures of JOINT are introduced. Starting with a generalized linear transmission model, the ZF JD based UL transmission and ZF JT based DL transmission in JOINT are described. The relevant time division duplex (TDD) frame structure is briefly reviewed as well.

Performance assessment in SA based networks is discussed in Chapter 3. In single SA scenarios the SNR, the user data rate and the energy efficiency are interesting performance measures which show duality between the UL and the DL. In scenarios with multiple SAs the performance is mainly measured by SINR and the corresponding data rate.

Theoretically, any system exhibiting interference can be modelled as an interference channel. In Chapter 4 transmit power allocation in generic interference channels is studied. After briefly reviewing classic CIR balancing power allocation, sum rate maximizing power allocation under a total power constraint is addressed in this chapter. The optimum power allocation in two-user interference channels is derived mathematically and several suboptimum power allocation schemes applicable in generic interference channels are discussed, among which the proposed iterative and noniterative waterfilling algorithms based on the conventional waterfilling principle are highlighted. The investigations in this chapter provide insights helpful for understanding the behavior of power and channel allocation in realistic networks.

The emphasis of Chapter 5 is on adaptive resource allocation in SA based networks. The joint subcarrier and power allocation problem is separated into two stages to make the complexity manageable. At the first stage adaptive subcarrier allocation with equal power allocation is performed. Several practical

subcarrier allocation algorithms applicable to SA based networks are discussed. They exploit the previously mentioned potential benefits in different ways and present different complexities. At the second stage adaptive power allocation follows. The suboptimum power allocation strategies discussed in Chapter 4 for generic interference channels are extended to SA based networks.

In Chapter 6 the performance of various subcarrier and power allocation techniques are evaluated through simulations in a reference multi-SA scenario. The performance improvement of SA based networks over conventional cellular networks is demonstrated here as well. To which extent the discussed resource allocation techniques adapt to the frequency selectivity of the channels, the spatial correlations of the users and the inter-SA interferences is investigated by considering some specific scenarios.

Finally, Chapter 7 summaries this thesis.

Throughout this thesis time discrete equivalent lowpass representation is used. Complex quantities are underlined. Vectors and matrices are written in lower and upper cases, respectively, both printed in bold face. $(\cdot)^*$ and $(\cdot)^{\mathrm{T}}$ designate the complex conjugation and the transposition, respectively.

Chapter 2

Transmission model of JOINT

2.1 General linear transmission model

The transmission model of the JOINT system can be generalized as a data transmission scheme with linear pre- and post-processing stages as depicted in Fig. 2.1. Due to the orthogonality of the subcarriers it is sufficient to consider a single subcarrier here. The signals on the considered subcarrier are described by their complex amplitudes.

In Fig. 2.1 the subcarrier specific data vector $\underline{\mathbf{d}}$ contains the information bearing data symbols to be transmitted. The transmit powers allocated to each symbol are explicitly contained in the diagonal matrix $\mathbf{P}$. The transmit signal $\underline{\mathbf{s}}$ is a linear function of the data vector $\underline{\mathbf{d}}$, i.e.,

$$\underline{\mathbf{s}} = \underline{\mathbf{M}} \cdot \mathbf{P}^{\frac{1}{2}} \underline{\mathbf{d}}, \tag{2.1}$$

where the modulation matrix $\underline{\mathbf{M}}$ describes the transmitter. The physical channel between the transmitter and the receiver is characterized by the complex channel matrix $\underline{\mathbf{H}}$. The signal at the output of the channel is corrupted by additive noise $\underline{\mathbf{n}}$ which may model thermal noise only or both thermal noise and interference. In the former case the noise elements are uncorrelated white

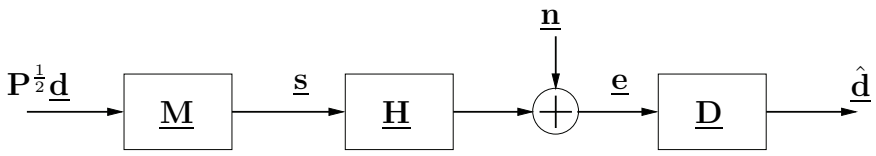

Figure 2.1: Generalized linear data transmission

Gaussian noises, while in the latter case one can assume the noise elements are approximately Gaussian distributed based on the central limit theory.

The receive signal

$$\underline{\mathbf{e}} = \underline{\mathbf{H}} \cdot \underline{\mathbf{s}} + \underline{\mathbf{n}} = \underline{\mathbf{H}} \cdot \underline{\mathbf{M}} \cdot \mathbf{P}^{\frac{1}{2}} \underline{\mathbf{d}} + \underline{\mathbf{n}} \tag{2.2}$$

is processed at the receiver according to the linear operation described by the demodulation matrix $\underline{\mathbf{D}}$, which results in the data estimates

$$\hat{\underline{\mathbf{d}}} = \underline{\mathbf{D}} \cdot \underline{\mathbf{e}} = \underline{\mathbf{D}} \cdot \underline{\mathbf{H}} \cdot \underline{\mathbf{M}} \cdot \mathbf{P}^{\frac{1}{2}} \underline{\mathbf{d}} + \underline{\mathbf{D}} \cdot \underline{\mathbf{n}}. \tag{2.3}$$

If we view the concatenation of the transmitter, the physical channel and the receiver as an overall channel, (2.3) also characterizes the relationship between the input $\mathbf{P}^{\frac{1}{2}} \underline{\mathbf{d}}$ and the output $\hat{\underline{\mathbf{d}}}$ of the overall channel.

To determine the modulation matrix $\underline{\mathbf{M}}$ and the demodulation matrix $\underline{\mathbf{D}}$ is a key issue in transmission system design. In principle there exist three options [MBQ04]:

- Transmitter orientation. In transmitter orientated transmission schemes the modulation matrix $\underline{\mathbf{M}}$ is a priori given and the channel matrix $\underline{\mathbf{H}}$ is known to the receiver, whereas the demodulation matrix $\underline{\mathbf{D}}$ is a posteriori determined based on $\underline{\mathbf{M}}$ and $\underline{\mathbf{H}}$, i.e.,

$$\underline{\mathbf{D}} = f\left(\underline{\mathbf{H}}, \underline{\mathbf{M}}\right). \tag{2.4}$$

- Receiver orientation. Unlike transmitter orientation, in receiver orientated transmission schemes in addition to $\underline{\mathbf{H}}$ the demodulation matrix $\underline{\mathbf{D}}$ instead of the modulation matrix $\underline{\mathbf{M}}$ is a priori given. $\underline{\mathbf{M}}$ is a posteriori determined according to

$$\underline{\mathbf{M}} = f\left(\underline{\mathbf{H}}, \underline{\mathbf{D}}\right). \tag{2.5}$$

- Channel orientation. In this case both $\underline{\mathbf{M}}$ and $\underline{\mathbf{D}}$ are determined based on $\underline{\mathbf{H}}$, i.e.,

$$(\underline{\mathbf{M}}, \underline{\mathbf{D}}) = f\left(\underline{\mathbf{H}}\right). \tag{2.6}$$

As will be shown in the following sections, transmitter orientation and receiver orientation are employed in the JOINT system. Channel orientated transmission schemes are beyond the scope of this thesis.

2.2 Joint detection in the uplink of JOINT

Consider the UL scenario of a SA in JOINT as shown in Fig. 1.4, where K MSs transmit their data symbols to K_{B} coordinated BSs simultaneously. The corresponding transmission model is depicted in Fig. 2.2.

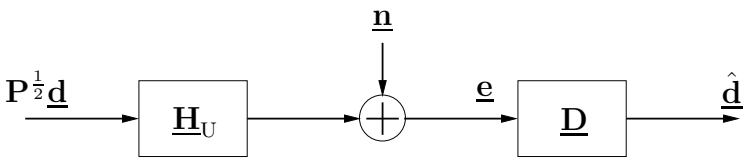

Figure 2.2: UL transmission model

The data vector

$$\underline{\mathbf{d}} = \left(\underline{d}_1 \ldots \underline{d}_K\right)^{\mathrm{T}} \tag{2.7}$$

contains statistically independent complex data symbols of the K MSs. Without loss of generality the data symbols $\underline{d}_k$, $k = 1 \ldots K$, are assumed to have average unit energy, i.e.,

$$\mathrm{E}\left\{\left|\underline{d}_k\right|^2\right\} = 1, \quad \forall k. \tag{2.8}$$

The transmit powers P_k, $k = 1 \ldots K$, allocated to each symbol reside along the main diagonal of the power matrix, namely,

$$\mathbf{P} = \begin{pmatrix} P_1 & & \mathbf{0} \\ & \ddots & \\ \mathbf{0} & & P_K \end{pmatrix}. \tag{2.9}$$

Due to the fact that the MSs are uncoordinated and due to the assumption that a single antenna is equipped at each MS, the modulation matrix in the generic linear transmission model of Fig. 2.1 becomes an identity matrix, i.e.,

$$\underline{\mathbf{M}} = \mathbf{I}^{K \times K}. \tag{2.10}$$

In other words, only traditional OFDM transmitters are required at MSs without extra signal processing tasks.

The transmit signal which carries the data symbols is passed through a MIMO channel characterized by the channel matrix

$$\underline{\mathbf{H}}_{\mathrm{U}} = \left(\underline{\mathbf{h}}_{\mathrm{U},1} \dots \underline{\mathbf{h}}_{\mathrm{U},K}\right) = \begin{pmatrix} \underline{H}_{\mathrm{U},1,1} & \cdots & \underline{H}_{\mathrm{U},1,K} \\ \vdots & & \vdots \\ \underline{H}_{\mathrm{U},K_{\mathrm{B}},1} & \cdots & \underline{H}_{\mathrm{U},K_{\mathrm{B}},K} \end{pmatrix} \tag{2.11}$$

of size $K_{\mathrm{B}} \times K$ containing the instantaneous channel transfer functions (CTFs) of the channels from each MS to each BS in the SA. The vector

$$\underline{\mathbf{h}}_{\mathrm{U},k} = \left(\underline{H}_{\mathrm{U},1,k} \dots \underline{H}_{\mathrm{U},K_{\mathrm{B}},k}\right)^{\mathrm{T}} \tag{2.12}$$

is often referred to as the spatial signature [TV05] of the k-th MS impinged on the antennas of the coordinated BSs. At the output of the channel the signals are corrupted by complex noise modelled by the vector

$$\underline{\mathbf{n}} = \left(\underline{n}_1 \dots \underline{n}_{K_{\mathrm{B}}}\right)^{\mathrm{T}}. \tag{2.13}$$

Considering thermal noise only, the elements $\underline{n}_{k_{\mathrm{B}}}$ of $\underline{\mathbf{n}}$, $k_{\mathrm{B}} = 1 \dots K_{\mathrm{B}}$, corresponding to different BSs are uncorrelated additive white Gaussian noises (AWGNs) having zero mean and variance σ^2. In this case the noise covariance matrix reads

$$\mathbf{R}_{\mathrm{n}} = \mathrm{E}\left\{\underline{\mathbf{n}} \cdot \underline{\mathbf{n}}^{*\mathrm{T}}\right\} = \sigma^2 \mathbf{I}^{K_{\mathrm{B}} \times K_{\mathrm{B}}}. \tag{2.14}$$

The vector $\underline{\mathbf{e}}$ comprising the complex amplitudes of the receive signals at all the K_{B} BSs reads

$$\underline{\mathbf{e}} = \left(\underline{e}_1 \dots \underline{e}_{K_{\mathrm{B}}}\right)^{\mathrm{T}} = \underline{\mathbf{H}}_{\mathrm{U}} \mathbf{P}^{\frac{1}{2}} \underline{\mathbf{d}} + \underline{\mathbf{n}}. \tag{2.15}$$

In the UL of the JOINT system the concept of transmitter orientation [MBQ04] is applied, i.e.,

$$\underline{\mathbf{D}} = f\left(\underline{\mathbf{H}}_{\mathrm{U}}, \underline{\mathbf{M}}\right), \tag{2.16}$$

where $\underline{\mathbf{H}}_{\mathrm{U}}$ is obtained by executing joint channel estimation (JCE) [SMW+01, MWS+02] at the CU and $\underline{\mathbf{M}}$ is given by (2.10). Note that in this thesis we do not distinguish between the true and the estimated channel state information, although in reality they are not the same. The demodulation matrix according to the linear zero forcing (ZF) criterion follows to be [Ver98, SSH04]

$$\begin{aligned} \underline{\mathbf{D}} &= \begin{pmatrix} \underline{D}_{1,1} & \cdots & \underline{D}_{1,K_{\mathrm{B}}} \\ \vdots & & \vdots \\ \underline{D}_{K,1} & \cdots & \underline{D}_{K,K_{\mathrm{B}}} \end{pmatrix} \\ &= \left(\underline{\mathbf{H}}_{\mathrm{U}}^{*\mathrm{T}} \underline{\mathbf{H}}_{\mathrm{U}}\right)^{-1} \underline{\mathbf{H}}_{\mathrm{U}}^{*\mathrm{T}}. \end{aligned} \tag{2.17}$$

Besides the ZF detector, the matched filter (MF) and the minimum mean square error (MMSE) detector are frequently utilized joint detectors. In this thesis, however, we restrict ourself to ZF JD.

Inserting (2.10) and (2.17) into (2.3) yields the continuous valued estimated data vector

$$\begin{aligned} \hat{\underline{\mathbf{d}}} &= \left(\underline{\mathbf{H}}_{\mathrm{U}}^{*\mathrm{T}} \underline{\mathbf{H}}_{\mathrm{U}}\right)^{-1} \underline{\mathbf{H}}_{\mathrm{U}}^{*\mathrm{T}} \underline{\mathbf{H}}_{\mathrm{U}} \mathbf{P}^{\frac{1}{2}} \underline{\mathbf{d}} + \left(\underline{\mathbf{H}}_{\mathrm{U}}^{*\mathrm{T}} \underline{\mathbf{H}}_{\mathrm{U}}\right)^{-1} \underline{\mathbf{H}}_{\mathrm{U}}^{*\mathrm{T}} \underline{\mathbf{n}} \\ &= \mathbf{P}^{\frac{1}{2}} \underline{\mathbf{d}} + \left(\underline{\mathbf{H}}_{\mathrm{U}}^{*\mathrm{T}} \underline{\mathbf{H}}_{\mathrm{U}}\right)^{-1} \underline{\mathbf{H}}_{\mathrm{U}}^{*\mathrm{T}} \underline{\mathbf{n}}, \end{aligned} \tag{2.18}$$

i.e., the intra-SA interferences are completely eliminated at the CU. Therefore the ZF receiver is also known as interference nulling receiver. Because of the linear ZF constraint the estimated data vector $\hat{\underline{\mathbf{d}}}$ of (2.18) only exists if

$$K \leq K_{\mathrm{B}} \tag{2.19}$$

holds, i.e., the number of subcarrier-sharing MSs in a SA is limited by the SA size. The separation of the data symbols of multiple users by exploiting the fact that different users impinge different spatial signatures on the coordinated receive antennas is known as SDMA.

For conventional cellular networks which are special cases of SA based networks with $K_{\mathrm{B}} = 1$, only $K = 1$ MS can be served per subcarrier per cell. In this case the demodulation matrix $\underline{\mathbf{D}}$ of (2.17) degenerates into a scalar which is the inverse of the channel transfer function.

2.3 Joint transmission in the downlink of JOINT

In the DL scenario of the JOINT system, see Fig. 1.5, the signals are jointly generated at the CU based on the data vector $\underline{\mathbf{d}}$ to be transmitted and are radiated from the K_B coordinated BSs to the K MSs simultaneously. The corresponding transmission model is depicted in Fig. 2.3.

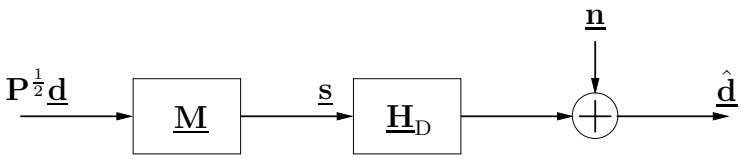

Figure 2.3: DL transmission model

Since the MSs are uncoordinated, the demodulation matrix $\underline{\mathbf{D}}$ in the DL is a diagonal matrix. Furthermore, to keep the complexity of the MSs as low as possible, in the DL of the JOINT system the receivers of the MSs are designed as traditional low complexity OFDM receivers without any equalizers, which means that

$$\underline{\mathbf{D}} = \mathbf{I}^{K\times K} \tag{2.20}$$

holds and thus the receive signal is taken as the continuous valued estimated data symbol. The DL channel matrix $\underline{\mathbf{H}}_\mathrm{D}$ has the structure

$$\underline{\mathbf{H}}_\mathrm{D} = \left(\underline{\mathbf{h}}_{\mathrm{D},1}\dots\underline{\mathbf{h}}_{\mathrm{D},K}\right)^\mathrm{T} = \begin{pmatrix} \underline{H}_{\mathrm{D},1,1} & \cdots & \underline{H}_{\mathrm{D},1,K_\mathrm{B}} \\ \vdots & & \vdots \\ \underline{H}_{\mathrm{D},K,1} & \cdots & \underline{H}_{\mathrm{D},K,K_\mathrm{B}} \end{pmatrix} \tag{2.21}$$

with

$$\underline{\mathbf{h}}_{\mathrm{D},k} = \left(\underline{H}_{\mathrm{D},k,1}\dots\underline{H}_{\mathrm{D},k,K_\mathrm{B}}\right)^\mathrm{T} \tag{2.22}$$

being the spatial signature of the k-th MS and $\underline{H}_{\mathrm{D},k,k_\mathrm{B}}$ being the CTF of the channel from the k_B-th BS to the k-th MS. The noise vector

$$\underline{\mathbf{n}} = \left(\underline{n}_1\dots\underline{n}_K\right)^\mathrm{T} \tag{2.23}$$

models complex noises at receiver input of the K MSs. The noise elements $\underline{n}_k$, $k = 1\dots K$, are Gaussian distributed and are assumed to have zero mean and the same variance of σ^2 as in the UL case if only thermal noise is considered.

In the DL of the JOINT system the concept of receiver orientation [MBQ04] is applied, i.e.,

$$\underline{\mathbf{M}} = f\left(\underline{\mathbf{H}}_{\mathrm{D}}, \underline{\mathbf{D}}\right), \tag{2.24}$$

where $\underline{\mathbf{H}}_{\mathrm{D}}$ is known to the transmitter thanks to the channel reciprocity, see Section 2.4, and $\underline{\mathbf{D}}$ is given by (2.20). Hence the modulation matrix according to the linear ZF criterion follows [Fis02, MBW$^+$00, SSH04]

$$\begin{aligned} \underline{\mathbf{M}} &= \begin{pmatrix} \underline{M}_{1,1} & \cdots & \underline{M}_{1,K} \\ \vdots & & \vdots \\ \underline{M}_{K_{\mathrm{B}},1} & \cdots & \underline{M}_{K_{\mathrm{B}},K} \end{pmatrix} \\ &= \underline{\mathbf{H}}_{\mathrm{D}}^{*\mathrm{T}} \left(\underline{\mathbf{H}}_{\mathrm{D}} \underline{\mathbf{H}}_{\mathrm{D}}^{*\mathrm{T}}\right)^{-1} \left(\mathrm{diag}\left(\left(\underline{\mathbf{H}}_{\mathrm{D}} \underline{\mathbf{H}}_{\mathrm{D}}^{*\mathrm{T}}\right)^{-1}\right)\right)^{-\frac{1}{2}}, \end{aligned} \tag{2.25}$$

where $\mathrm{diag}(\cdot)$ denotes a diagonal matrix whose diagonal elements are the diagonal elements of the matrix in brackets. In what follows, $[\cdot]_{k,k'}$ represents the element at the k-th row and the k'-th column of a matrix in brackets. The term $\left(\mathrm{diag}\left(\left(\underline{\mathbf{H}}_{\mathrm{D}} \underline{\mathbf{H}}_{\mathrm{D}}^{*\mathrm{T}}\right)^{-1}\right)\right)^{-\frac{1}{2}}$ in (2.25) is introduced for ensuring

$$\left[\underline{\mathbf{M}}^{*\mathrm{T}} \underline{\mathbf{M}}\right]_{k,k} = 1, \quad k = 1 \ldots K, \tag{2.26}$$

so that the average transmit power associated with a data symbol $\underline{d}_k$ at the output of the transmitter is equal to the transmit power P_k invested to the data symbol at the input of the transmitter, i.e.,

$$\mathrm{E}\left\{\left[\underline{\mathbf{s}}^{*\mathrm{T}} \underline{\mathbf{s}}\right]_{k,k}\right\} = \left[\underline{\mathbf{M}}^{*\mathrm{T}} \underline{\mathbf{M}}\right]_{k,k} P_k \mathrm{E}\left\{|\underline{d}_k|^2\right\} = P_k, \quad k = 1 \ldots K, \tag{2.27}$$

holds.

Note that the transmit signal

$$\begin{aligned} \underline{\mathbf{s}} &= \left(\underline{s}_1 \ldots \underline{s}_{K_{\mathrm{B}}}\right)^{\mathrm{T}} \\ &= \underline{\mathbf{H}}_{\mathrm{D}}^{*\mathrm{T}} \left(\underline{\mathbf{H}}_{\mathrm{D}} \underline{\mathbf{H}}_{\mathrm{D}}^{*\mathrm{T}}\right)^{-1} \left(\mathrm{diag}\left(\left(\underline{\mathbf{H}}_{\mathrm{D}} \underline{\mathbf{H}}_{\mathrm{D}}^{*\mathrm{T}}\right)^{-1}\right)\right)^{-\frac{1}{2}} \mathbf{P}^{\frac{1}{2}} \underline{\mathbf{d}} \end{aligned} \tag{2.28}$$

only exists if (2.19) holds due to the linear ZF constraint. In addition to ZF, MF and MMSE are also popular options in JT. For the investigations in this thesis, however, ZF JT is considered.

Inserting (2.20) and (2.25) into (2.3) yields the continuous valued estimated data vector

$$\begin{aligned}\hat{\underline{\mathbf{d}}} &= \underline{\mathbf{H}}_{\mathrm{D}}\underline{\mathbf{H}}_{\mathrm{D}}^{*\mathrm{T}}\left(\underline{\mathbf{H}}_{\mathrm{D}}\underline{\mathbf{H}}_{\mathrm{D}}^{*\mathrm{T}}\right)^{-1}\left(\mathrm{diag}\left(\left(\underline{\mathbf{H}}_{\mathrm{D}}\underline{\mathbf{H}}_{\mathrm{D}}^{*\mathrm{T}}\right)^{-1}\right)\right)^{-\frac{1}{2}}\mathbf{P}^{\frac{1}{2}}\underline{\mathbf{d}}+\underline{\mathbf{n}} \\ &= \left(\mathrm{diag}\left(\left(\underline{\mathbf{H}}_{\mathrm{D}}\underline{\mathbf{H}}_{\mathrm{D}}^{*\mathrm{T}}\right)^{-1}\right)\right)^{-\frac{1}{2}}\mathbf{P}^{\frac{1}{2}}\underline{\mathbf{d}}+\underline{\mathbf{n}}. \qquad (2.29)\end{aligned}$$

Since $\left(\mathrm{diag}\left(\left(\underline{\mathbf{H}}_{\mathrm{D}}\underline{\mathbf{H}}_{\mathrm{D}}^{*\mathrm{T}}\right)^{-1}\right)\right)^{-\frac{1}{2}}$ is diagonal, the intra-SA interferences in the DL are avoided and the desired data symbols can be retrieved at the MSs up to a scalar factor in the absence of noise.

For conventional cellular networks with $K_{\mathrm{B}} = K = 1$ the modulation matrix $\underline{\mathbf{M}}$ of (2.25) degenerates into $e^{-j\arg\{\underline{H}_{\mathrm{D}}\}}$ and (2.29) is simplified as

$$\hat{\underline{d}} = |\underline{H}_{\mathrm{D}}|\sqrt{P}\underline{d}+\underline{n}. \qquad (2.30)$$

2.4 Time division duplex

Utilizing time division duplex (TDD) as the duplex scheme, the JOINT frame is composed of an UL part and a DL part, as depicted in Fig. 2.4. The UL part and the DL part are further divided into OFDM symbol slots which include a cyclic prefix. In the UL, the symbol slots are used for data transmission and pilot transmission. The symbol slots in the DL are dedicated to data transmission. During each OFDM symbol slot multiple data or pilot symbols are transmitted in parallel on different orthogonal subcarriers. With an adjustable length of the UL and the DL segments, TDD allows to allocate more symbol slots on the link that requires more throughput. Therefore, TDD supports data transmission with asymmetric traffic such as FTP and web browsing and is more bandwidth efficient than the frequency division duplex (FDD) scheme in data applications.

With the aid of the pilot symbol slots inserted between the UL data symbol slots and the DL data symbol slots, JCE is performed at the CU to provide

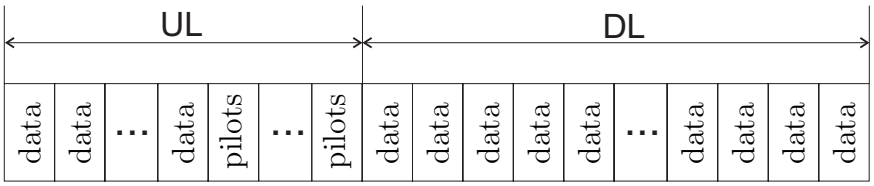

Figure 2.4: TDD frame structure of JOINT

the channel estimates of the UL. As described in Section 2.2 the UL channel estimates are used for JD at the CU.

The wireless channels are assumed to be block fading, i.e., within the duration of the frame the channels are quasi time invariant. This is the case whenever the frame duration is significantly smaller than the coherence time of the channels. Moreover, thanks to the reciprocity of the UL and DL channels

$$\underline{H}_{\mathrm{U},k_\mathrm{B},k} = \underline{H}_{\mathrm{D},k,k_\mathrm{B}}, \quad \forall k, k_\mathrm{B}, \tag{2.31}$$

in TDD based systems, the UL spatial signature $\underline{\mathbf{h}}_{\mathrm{U},k}$ of (2.12) is identical to the DL spatial signature $\underline{\mathbf{h}}_{\mathrm{D},k}$ of (2.22) and thus the DL channel matrix is simply the transpose of the UL channel matrix, i.e.,

$$\underline{\mathbf{H}}_\mathrm{D} = \underline{\mathbf{H}}_\mathrm{U}^\mathrm{T} \tag{2.32}$$

holds. Therefore, JT in the DL can make use of the channel estimates obtained in the UL. In contrast to FDD based systems where training sequences are often used in both links, TDD based JOINT system performs training based channel estimation only in the UL and is more efficient.

Throughout the rest of this thesis perfect channel knowledge at the CUs is assumed. The impact of imperfect CSI on JD and JT in JOINT is studied in [Man05, Liu05].

Chapter 3

Performance assessment of JOINT

3.1 Single service area scenarios

3.1.1 Uplink performance

Consider a single SA which contains K_{B} BSs and $K \leq K_{\mathrm{B}}$ MSs active on a specific subcarrier. Rewrite (2.18) for the UL transmission as

$$\underline{\hat{\mathbf{d}}} = \mathbf{P}^{\frac{1}{2}}\underline{\mathbf{d}} + \underbrace{\left(\underline{\mathbf{H}}_{\mathrm{U}}^{*\mathrm{T}}\underline{\mathbf{H}}_{\mathrm{U}}\right)^{-1}\underline{\mathbf{H}}_{\mathrm{U}}^{*\mathrm{T}}}_{\underline{\mathbf{D}}}\underline{\mathbf{n}} = \mathbf{P}^{\frac{1}{2}}\underline{\mathbf{d}} + \underline{\tilde{\mathbf{n}}}. \tag{3.1}$$

With (2.14) and (2.17) the covariance matrix of the enhanced noise $\underline{\tilde{\mathbf{n}}}$ at receiver output follows

$$\underline{\mathbf{R}}_{\tilde{\mathrm{n}}} = \mathrm{E}\left\{\underline{\tilde{\mathbf{n}}} \cdot \underline{\tilde{\mathbf{n}}}^{*\mathrm{T}}\right\} = \mathrm{E}\left\{\underline{\mathbf{D}} \cdot \underline{\mathbf{n}} \cdot \underline{\mathbf{n}}^{*\mathrm{T}} \cdot \underline{\mathbf{D}}^{*\mathrm{T}}\right\} = \sigma^2 \underline{\mathbf{D}} \cdot \underline{\mathbf{D}}^{*\mathrm{T}} = \sigma^2 \left(\underline{\mathbf{H}}_{\mathrm{U}}^{*\mathrm{T}}\underline{\mathbf{H}}_{\mathrm{U}}\right)^{-1}. \tag{3.2}$$

Therefore, the UL SNR of the k-th user is given by

$$\gamma_k = \frac{P_k}{\sigma^2 \left[\left(\underline{\mathbf{H}}_{\mathrm{U}}^{*\mathrm{T}}\underline{\mathbf{H}}_{\mathrm{U}}\right)^{-1}\right]_{k,k}}. \tag{3.3}$$

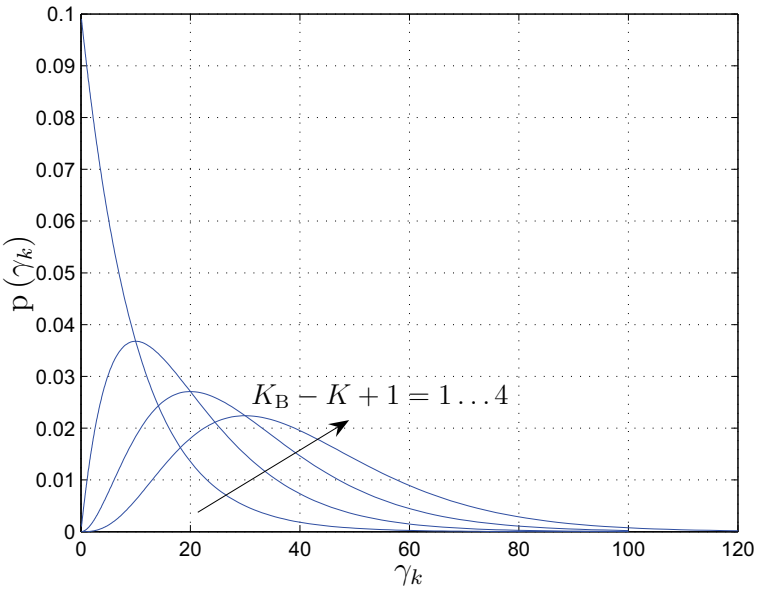

Figure 3.1: pdf of the SNR γ_k under the i.i.d. assumption of (3.4), $10 \log \frac{P_k}{\sigma^2} = 10$ dB

Assume the entries of the UL channel matrix $\underline{\mathbf{H}}_\mathrm{U}$ are independent and identically distributed (i.i.d.) complex Gaussian variables with zero mean and unit variance, i.e.,

$$\underline{H}_{\mathrm{U},k_\mathrm{B},k} \sim \mathcal{CN}(0,1), \quad \forall k_\mathrm{B}, k. \tag{3.4}$$

With (3.4) the probability density function (pdf) of the SNR γ_k can be derived with the aid of random matrix theory [Meh91]

$$\mathrm{p}(\gamma_k) = \begin{cases} \frac{\left(\frac{\sigma^2}{P_k}\right)^{K_\mathrm{B}-K+1}}{\gamma_k \Gamma(K_\mathrm{B}-K+1)} \gamma_k^{K_\mathrm{B}-K+1} e^{-\frac{\sigma^2}{P_k}\gamma_k}, & \gamma_k \geq 0 \\ 0, & \text{else} \end{cases} \tag{3.5}$$

with

$$\Gamma(\mu) = \int_0^\infty e^{-t} t^{\mu-1} \mathrm{d}t \tag{3.6}$$

being the gamma function [AS65]. Note that the pdf of (3.5) is not determined by the absolute value of K_B or of K, but by $K_\mathrm{B} - K + 1$ which quantifies the spatial degrees of freedom in SDMA based systems. In Fig. 3.1 the pdf is visualized for different spatial degrees of freedom and $10 \log_{10} \frac{P_k}{\sigma^2}$ equal to 10 dB. Obviously, with increasing number of spatial degrees of freedom the mean

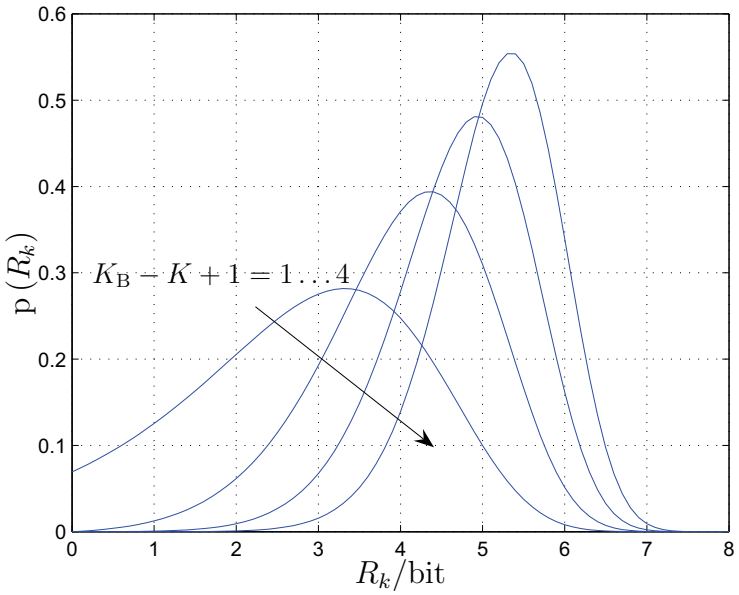

Figure 3.2: pdf of the bit rate R_k under the i.i.d. assumption of (3.4), $10 \log \frac{P_k}{\sigma^2} = 10$ dB

value and the variance of the SNR increase. In particular, when there is only one spatial degree of freedom, the SNR follows an exponential distribution. Without the i.i.d. assumption of (3.4), however, a closed form solution of the pdf is in general not known and the statistics of the SNR have to be obtained by simulations.

With the SNR γ_k of (3.3), the UL bit rate of the k-th user reads

$$R_k = \log_2 (1 + \gamma_k) \tag{3.7}$$

$$= \log_2 \left(1 + \frac{P_k}{\sigma^2 \left[\left(\underline{\mathbf{H}}_\mathrm{U}^{*\mathrm{T}} \underline{\mathbf{H}}_\mathrm{U} \right)^{-1} \right]_{k,k}} \right). \tag{3.8}$$

With (3.5) and (3.7) it is straightforward to derive the pdf of the bit rate

$$\mathrm{p}(R_k) = \begin{cases} \frac{2^{R_k} \ln 2 \left(\frac{\sigma^2}{P_k} \right)^{K_\mathrm{B}-K+1}}{\left(2^{R_k} - 1 \right) \Gamma(K_\mathrm{B}-K+1)} \left(2^{R_k} - 1 \right)^{K_\mathrm{B}-K+1} e^{-\frac{\sigma^2}{P_k}\left(2^{R_k}-1 \right)}, & R_k \geq 0 \\ 0, & \text{else} \end{cases}, \tag{3.9}$$

which is also a function of the number of spatial degrees of freedom for given ratio between P_k and σ^2. In Fig. 3.2 the pdf of (3.9) is plotted for different spatial degrees of freedom with $10\log_{10}\frac{P_k}{\sigma^2}$ being 10 dB. It can be seen that as the number of spatial degrees of freedom increases the mean value increases and the variance degreases.

Joint signal processing is a key feature in the JOINT system. Due to the correlated spatial signatures of subcarrier-sharing users, part of the transmit energy has to be sacrificed for separating signals by means of linear ZF JD in the UL. In order to quantitatively measure the price to be paid for interference cancellation the concept of energy efficiency is introduced. Energy efficiency characterizes how efficient the transmit energy is converted to useful receive signal energy. For linear ZF JD in the UL of the JOINT system the energy efficiency of the k-th MS reads [Liu05]

$$\varepsilon_k = \frac{1}{\left[\left(\underline{\mathbf{H}}_{\mathrm{U}}^{*\mathrm{T}}\underline{\mathbf{H}}_{\mathrm{U}}\right)^{-1}\right]_{k,k}\left[\underline{\mathbf{H}}_{\mathrm{U}}^{*\mathrm{T}}\underline{\mathbf{H}}_{\mathrm{U}}\right]_{k,k}}, \tag{3.10}$$

which takes values ranging from zero to one, with one being the optimum. Essentially, energy efficiency reflects the separability among the signals of co-channel users through linear ZF JD. A low energy efficiency indicates a poor signal separability, whereas a high energy efficiency means that the signals can be easily separated with minor energy consumption. Note that the concept of energy efficiency applies not only to linear ZF scheme but also to other types of linear transmission schemes such as MMSE and MF.

Under the assumption of (3.4), the energy efficiency of (3.10) is proven to be beta distributed with the pdf [Meh91, Mül01]

$$\mathrm{p}(\varepsilon_k) = \begin{cases} \frac{\varepsilon_k^{K_\mathrm{B}-K}(1-\varepsilon_k)^{K-2}}{B(K_\mathrm{B}-K+1,K-1)}, & 0 \le \varepsilon_k \le 1 \\ 0, & \text{else} \end{cases}, \tag{3.11}$$

where

$$B(\mu,\nu) = \int_0^1 t^{\mu-1}(1-t)^{\nu-1}\mathrm{d}t = \frac{\Gamma(\mu)\Gamma(\nu)}{\Gamma(\mu+\nu)} \tag{3.12}$$

indicates the beta function [AS65]. (3.11) is plotted in Fig. 3.3 for several examples under the constraint of $K \le K_\mathrm{B}$. It can be observed that two pdfs

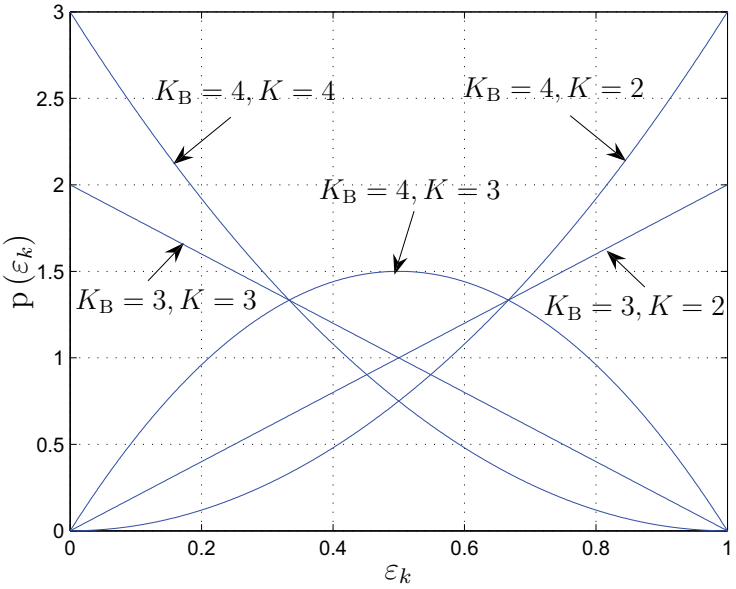

Figure 3.3: pdf of the energy efficiency ε_k under the i.i.d. assumption of (3.4)

corresponding to (K_B, K) and (K'_B, K') are symmetric with respect to $\varepsilon_k = 0.5$ if $K_\mathrm{B} = K'_\mathrm{B} = K + K' - 2$ holds. In particular, if $K_\mathrm{B} = 2K - 2$ holds, the corresponding pdf is self-symmetric with respect to $\varepsilon_k = 0.5$. Without the i.i.d. assumption of (3.4), a closed form solution of the pdf is in general not known and the statistics of the energy efficiency have to be obtained by means of simulations.

In the following we define

$$\tilde{\gamma}_k = \frac{\gamma_k}{\frac{P_k}{\sigma^2}} = \frac{1}{\left[\left(\underline{\mathbf{H}}_\mathrm{U}^{*\mathrm{T}} \underline{\mathbf{H}}_\mathrm{U}\right)^{-1}\right]_{k,k}} \tag{3.13}$$

as the normalized SNR. Comparing (3.10) with (3.13) one can see that the energy efficiency ε_k and the normalized SNR $\tilde{\gamma}_k$ have the relationship

$$\tilde{\gamma}_k = \varepsilon_k \left\| \underline{\mathbf{h}}_{\mathrm{U},k} \right\|_2^2, \tag{3.14}$$

where

$$\left\| \underline{\mathbf{h}}_{\mathrm{U},k} \right\|_2^2 = \underline{\mathbf{h}}_{\mathrm{U},k}^{*\mathrm{T}} \underline{\mathbf{h}}_{\mathrm{U},k} = \left[\underline{\mathbf{H}}_\mathrm{U}^{*\mathrm{T}} \underline{\mathbf{H}}_\mathrm{U}\right]_{k,k} = \sum_{k_\mathrm{B}} \left| \underline{H}_{\mathrm{U},k_\mathrm{B},k} \right|^2 \tag{3.15}$$

designates the squared l_2 norm of the spatial signature $\underline{\mathbf{h}}_{\mathrm{U},k}$, i.e., the channel energy of user k.

In the case that only a single user is active on the considered subcarrier, the UL channel matrix $\underline{\mathbf{H}}_{\mathrm{U}}$ degenerates into a column vector $\underline{\mathbf{h}}_{\mathrm{U}}$ which is the spatial signature of the user. The ZF JD is then equivalent to matched filtering. The energy efficiency is exactly one since no interference cancellation is performed and the normalized SNR is equal to the channel energy of the user.

Note that the computation of both the normalized SNR of (3.13) and the energy efficiency of (3.10) involve matrix inversions. Let $\underline{\mathbf{H}}'_{\mathrm{U}} = \left(\underline{\mathbf{h}}_{\mathrm{U},1} \ldots \underline{\mathbf{h}}_{\mathrm{U},K-1}\right)$ be the UL channel matrix containing the spatial signatures of the first $K-1$ users. Thus the UL channel matrix corresponding to all the K users can be written as $\underline{\mathbf{H}}_{\mathrm{U}} = \left(\underline{\mathbf{H}}'_{\mathrm{U}} \;\; \underline{\mathbf{h}}_{\mathrm{U},K}\right)$. With the help of the matrix inversion lemma [GVL86] one obtains

$$\begin{aligned}
\left(\underline{\mathbf{H}}_{\mathrm{U}}^{*\mathrm{T}} \cdot \underline{\mathbf{H}}_{\mathrm{U}}\right)^{-1} &= \left(\begin{pmatrix}\underline{\mathbf{H}}_{\mathrm{U}}^{\prime *\mathrm{T}} \\ \underline{\mathbf{h}}_{\mathrm{U},K}^{*\mathrm{T}}\end{pmatrix} \cdot \left(\underline{\mathbf{H}}'_{\mathrm{U}} \;\; \underline{\mathbf{h}}_{\mathrm{U},K}\right)\right)^{-1} \\
&= \begin{pmatrix}\underline{\mathbf{H}}_{\mathrm{U}}^{\prime *\mathrm{T}}\underline{\mathbf{H}}'_{\mathrm{U}} & \underline{\mathbf{H}}_{\mathrm{U}}^{\prime *\mathrm{T}}\underline{\mathbf{h}}_{\mathrm{U},K} \\ \underline{\mathbf{h}}_{\mathrm{U},K}^{*\mathrm{T}}\underline{\mathbf{H}}'_{\mathrm{U}} & \underline{\mathbf{h}}_{\mathrm{U},K}^{*\mathrm{T}}\underline{\mathbf{h}}_{\mathrm{U},K}\end{pmatrix}^{-1} \\
&= \begin{pmatrix}\left(\underline{\mathbf{H}}_{\mathrm{U}}^{\prime *\mathrm{T}}\underline{\mathbf{H}}'_{\mathrm{U}}\right)^{-1} + a\underline{\mathbf{b}}\,\underline{\mathbf{b}}^{*\mathrm{T}} & -a\underline{\mathbf{b}} \\ -a\underline{\mathbf{b}}^{*\mathrm{T}} & a\end{pmatrix},
\end{aligned} \tag{3.16}$$

where

$$a = \frac{1}{\underline{\mathbf{h}}_{\mathrm{U},K}^{*\mathrm{T}}\underline{\mathbf{h}}_{\mathrm{U},K} - \underline{\mathbf{h}}_{\mathrm{U},K}^{*\mathrm{T}}\underline{\mathbf{H}}'_{\mathrm{U}}\left(\underline{\mathbf{H}}_{\mathrm{U}}^{\prime *\mathrm{T}}\underline{\mathbf{H}}'_{\mathrm{U}}\right)^{-1}\underline{\mathbf{H}}_{\mathrm{U}}^{\prime *\mathrm{T}}\underline{\mathbf{h}}_{\mathrm{U},K}} \tag{3.17}$$

and

$$\underline{\mathbf{b}} = \left(\underline{\mathbf{H}}_{\mathrm{U}}^{\prime *\mathrm{T}}\underline{\mathbf{H}}'_{\mathrm{U}}\right)^{-1}\underline{\mathbf{H}}_{\mathrm{U}}^{\prime *\mathrm{T}}\underline{\mathbf{h}}_{\mathrm{U},K}. \tag{3.18}$$

Therefore, the normalized SNR of the K-th user is given by

$$\tilde{\gamma}_K = \frac{1}{a} = \underline{\mathbf{h}}_{\mathrm{U},K}^{*\mathrm{T}}\underline{\mathbf{h}}_{\mathrm{U},K} - \underline{\mathbf{h}}_{\mathrm{U},K}^{*\mathrm{T}}\underline{\mathbf{H}}'_{\mathrm{U}}\left(\underline{\mathbf{H}}_{\mathrm{U}}^{\prime *\mathrm{T}}\underline{\mathbf{H}}'_{\mathrm{U}}\right)^{-1}\underline{\mathbf{H}}_{\mathrm{U}}^{\prime *\mathrm{T}}\underline{\mathbf{h}}_{\mathrm{U},K} \tag{3.19}$$

and for the energy efficiency

$$\varepsilon_K = \frac{\tilde{\gamma}_K}{\underline{\mathbf{h}}_{\mathrm{U},K}^{*\mathrm{T}}\underline{\mathbf{h}}_{\mathrm{U},K}} = 1 - \frac{\underline{\mathbf{h}}_{\mathrm{U},K}^{*\mathrm{T}}\underline{\mathbf{H}}'_{\mathrm{U}}\left(\underline{\mathbf{H}}_{\mathrm{U}}^{\prime *\mathrm{T}}\underline{\mathbf{H}}'_{\mathrm{U}}\right)^{-1}\underline{\mathbf{H}}_{\mathrm{U}}^{\prime *\mathrm{T}}\underline{\mathbf{h}}_{\mathrm{U},K}}{\underline{\mathbf{h}}_{\mathrm{U},K}^{*\mathrm{T}}\underline{\mathbf{h}}_{\mathrm{U},K}} \tag{3.20}$$

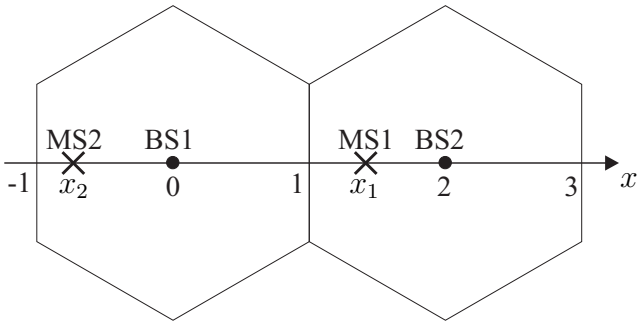

Figure 3.4: Exemplary 2-cell scenario

holds.

From (3.19) it can be clearly seen that the normalized SNR of one user depends not only on its channel energy, but also on the correlation between its spatial signature and the other users' spatial signatures due to the matrix inversion. A high channel energy and weakly correlated spatial signatures lead to a large normalized SNR. On the contrary, the energy efficiency is determined by the correlation of the spatial signatures only, whereas the absolute channel energies are irrelevant. Therefore, user specific energy efficiency is a proper measure of the correlation between the spatial signature of the considered user and the spatial signatures of the other users.

If the spatial signature of the K-th user is orthogonal to the spatial signatures of all the other users, then $\underline{\mathbf{h}}_{\mathrm{U},K}^{*\mathrm{T}}\underline{\mathbf{H}}'_{\mathrm{U}} = \mathbf{0}$ results. In this case the maximal energy efficiency of one is achieved for the K-th user, meaning no transmit energy consumption for cancelling interferences caused by the other users, and the normalized SNR $\tilde{\gamma}_K$ is just the channel energy of the K-th user.

The geographic positions of the subcarrier-sharing MSs have a great impact on the correlations among their spatial signatures and consequently on their energy efficiencies, which can be demonstrated by considering an exemplary scenario as depicted in Fig. 3.4. Two adjacent cells each having a BS at the center form a SA. Two MSs are located at x_1 and x_2 on the x axis, respectively. x_1 and x_2 can be any point on the x axis within the two cells except the positions of the two BSs, i.e., $x_1, x_2 \in [-1, 3] \setminus \{0, 2\}$. For simplicity's sake

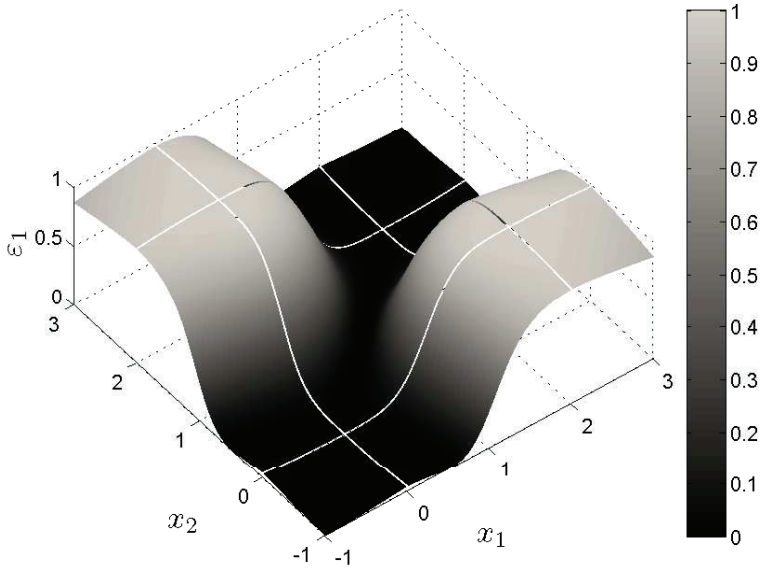

Figure 3.5: Energy efficiency of MS1 in the 2-cell scenario

the channels between the MSs and the BSs are characterized by a single slope path loss model with path loss exponent of 3.0 without fading. As the absolute channel energy is irrelevant, the spatial signature of MS k can be represented by

$$\underline{\mathbf{h}}_{\mathrm{U},k} = \left(\underline{H}_{\mathrm{U},1,k} \;\; \underline{H}_{\mathrm{U},2,k}\right)^{\mathrm{T}} = \left(|x_k|^{-\frac{3}{2}} \quad |x_k - 2|^{-\frac{3}{2}}\right)^{\mathrm{T}}, \quad k = 1, 2. \tag{3.21}$$

The energy efficiencies of both MSs simplify to

$$\varepsilon_1 = \varepsilon_2 = 1 - \frac{\underline{\mathbf{h}}_{\mathrm{U},1}^{*\mathrm{T}} \underline{\mathbf{h}}_{\mathrm{U},2} \underline{\mathbf{h}}_{\mathrm{U},2}^{*\mathrm{T}} \underline{\mathbf{h}}_{\mathrm{U},1}}{\underline{\mathbf{h}}_{\mathrm{U},1}^{*\mathrm{T}} \underline{\mathbf{h}}_{\mathrm{U},1} \underline{\mathbf{h}}_{\mathrm{U},2}^{*\mathrm{T}} \underline{\mathbf{h}}_{\mathrm{U},2}}, \tag{3.22}$$

which is a function of x_1 and x_2.

In Fig. 3.5 the energy efficiency of MS1 as well as MS2 versus x_1 and x_2 is depicted. It can be observed that ε_1 is symmetric with respect to $x_1 = x_2$ and $x_1 = 2 - x_2$. Moreover, a high energy efficiency is obtained if the two MSs are located in different cells, in which case their signals can be easily separated by linear ZF JD. In particular, as both MSs approach the corresponding BSs the

energy efficiency of one is achieved. On the other hand, both MSs being in the same cell leads to a small energy efficiency, which implies that it is rather difficult to separate the signals of the two MSs through linear ZF JD. Indeed, it can be easily proven that when both MSs are located at the same position, i.e., $x_1 = x_2$, the minimum energy efficiency of zero is obtained.

3.1.2 Downlink performance

The DL transmission model of (2.29) corresponding to a single SA is rewritten as

$$\hat{\underline{\mathbf{d}}} = \left(\mathrm{diag}\left(\left(\underline{\mathbf{H}}_{\mathrm{D}}\underline{\mathbf{H}}_{\mathrm{D}}^{*\mathrm{T}}\right)^{-1}\right)\right)^{-\frac{1}{2}} \mathbf{P}^{\frac{1}{2}}\underline{\mathbf{d}} + \underline{\mathbf{n}}, \tag{3.23}$$

with which the DL SNR of the k-th MS

$$\gamma_k = \frac{P_k}{\sigma^2\left[\left(\underline{\mathbf{H}}_{\mathrm{D}}\underline{\mathbf{H}}_{\mathrm{D}}^{*\mathrm{T}}\right)^{-1}\right]_{k,k}} \tag{3.24}$$

follows.

With the channel reciprocity of (2.32) it can be easily seen that the diagonal entries of $\left(\underline{\mathbf{H}}_{\mathrm{D}}\underline{\mathbf{H}}_{\mathrm{D}}^{*\mathrm{T}}\right)^{-1}$ are identical to those of $\left(\underline{\mathbf{H}}_{\mathrm{U}}^{*\mathrm{T}}\underline{\mathbf{H}}_{\mathrm{U}}\right)^{-1}$, therefore the UL SNR of (3.3) is identical to the DL SNR of (3.24).

With (3.24), the DL bit rate of the k-th user is given by

$$R_k = \log_2\left(1 + \frac{P_k}{\sigma^2\left[\left(\underline{\mathbf{H}}_{\mathrm{D}}\underline{\mathbf{H}}_{\mathrm{D}}^{*\mathrm{T}}\right)^{-1}\right]_{k,k}}\right). \tag{3.25}$$

Obviously, the DL bit rate of (3.25) is equal to the UL bit rate of (3.8) due to the duality between the UL SNR and the DL SNR.

Similar to JD in the UL, part of the transmit energy is sacrificed for avoiding interferences by JT in the DL. For linear ZF JT in the DL of the JOINT system the user specific energy efficiency reads [Liu05]

$$\varepsilon_k = \frac{1}{\left[\left(\underline{\mathbf{H}}_{\mathrm{D}}\underline{\mathbf{H}}_{\mathrm{D}}^{*\mathrm{T}}\right)^{-1}\right]_{k,k}\left[\underline{\mathbf{H}}_{\mathrm{D}}\underline{\mathbf{H}}_{\mathrm{D}}^{*\mathrm{T}}\right]_{k,k}}, \tag{3.26}$$

which is equal to the energy efficiency of (3.10) for linear ZF JD in the UL due to the channel reciprocity of (2.32).

The duality of the performance measures between the UL and the DL in single SA scenarios implies that it is sufficient to assess the performance in one of the two links.

3.2 Multiple service area scenarios

3.2.1 Uplink performance

A realistic SA network is composed of multiple SAs which cover the region to be served. Due to the simultaneous use of the same frequency band by co-channel SAs each SA exhibits inter-SA interferences. In principle, interferences can be modelled stochastically or deterministically. In a multi-SA scenario it is too difficult to model inter-SA interferences as stochastic processes since they are neither independent nor identically distributed and sufficient knowledge on the statistics of inter-SA interferences is hard to obtain. Therefore, we use a deterministic interference model in performance assessment, i.e., the interference is explicitly calculated given the transmit powers and the CSI in the whole scenario.

The UL transmission model of a multi-SA scenario is depicted in Fig. 3.6. Without loss of generality a single subcarrier is considered here. The number of co-channel SAs in the scenario is denoted by K_{S}. In each SA with SA size K_{B} there are K MSs active on the considered subcarrier. In comparison to single SA scenarios a superscript has to be introduced to indicate the SA index. The SA specific data vector, power matrix, noise vector, receive signal vector, demodulation matrix and estimated data vector are denoted by $\underline{\mathbf{d}}^{(k_{\mathrm{S}})}$, $\mathbf{P}^{(k_{\mathrm{S}})}$, $\underline{\mathbf{n}}^{(k_{\mathrm{S}})}$, $\underline{\mathbf{e}}^{(k_{\mathrm{S}})}$, $\underline{\mathbf{D}}^{(k_{\mathrm{S}})}$ and $\hat{\underline{\mathbf{d}}}^{(k_{\mathrm{S}})}$, $k_{\mathrm{S}} = 1 \ldots K_{\mathrm{S}}$, respectively. The UL channel matrices

$$\underline{\mathbf{H}}_{\mathrm{U}}^{(k_{\mathrm{S}},k'_{\mathrm{S}})} = \begin{pmatrix} \underline{H}_{\mathrm{U},1,1}^{(k_{\mathrm{S}},k'_{\mathrm{S}})} & \cdots & \underline{H}_{\mathrm{U},1,K}^{(k_{\mathrm{S}},k'_{\mathrm{S}})} \\ \vdots & & \vdots \\ \underline{H}_{\mathrm{U},K_{\mathrm{B}},1}^{(k_{\mathrm{S}},k'_{\mathrm{S}})} & \cdots & \underline{H}_{\mathrm{U},K_{\mathrm{B}},K}^{(k_{\mathrm{S}},k'_{\mathrm{S}})} \end{pmatrix} \tag{3.27}$$

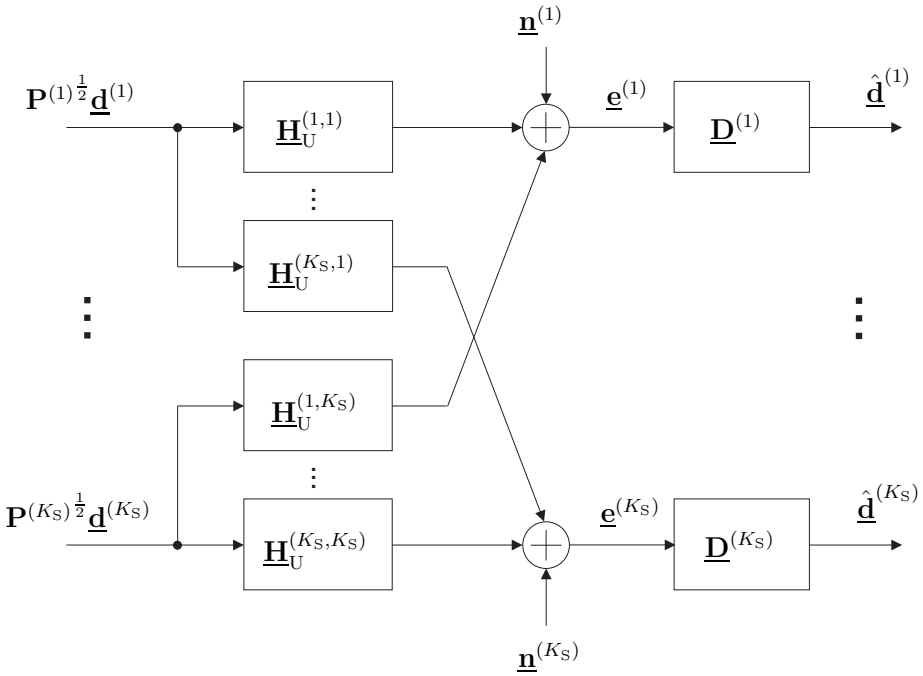

Figure 3.6: UL transmission model in a multi-SA scenario

of dimension $K_{\mathrm{B}} \times K$ contain the CTFs of the channels between the K MSs in the k'_{S}-th SA and the K_{B} BSs in the k_{S}-th SA, $k_{\mathrm{S}}, k'_{\mathrm{S}} = 1 \ldots K_{\mathrm{S}}$. The signals stemming from the MSs of a specific SA impinge not only at the BSs of their own SA, but also at the BSs of the other co-channel SAs. Therefore, the receive signal vector in SA k_{S} reads

$$\underline{\mathbf{e}}^{(k_{\mathrm{S}})} = \underline{\mathbf{H}}_{\mathrm{U}}^{(k_{\mathrm{S}},k_{\mathrm{S}})} \mathbf{P}^{(k_{\mathrm{S}})\frac{1}{2}} \underline{\mathbf{d}}^{(k_{\mathrm{S}})} + \sum_{k'_{\mathrm{S}} \neq k_{\mathrm{S}}} \underline{\mathbf{H}}_{\mathrm{U}}^{(k_{\mathrm{S}},k'_{\mathrm{S}})} \mathbf{P}^{(k'_{\mathrm{S}})\frac{1}{2}} \underline{\mathbf{d}}^{(k'_{\mathrm{S}})} + \underline{\mathbf{n}}^{(k_{\mathrm{S}})}. \tag{3.28}$$

Unlike in single SA scenarios, the desired signals are disturbed by inter-SA interferences apart from thermal noises. The inter-SA interferences can be much stronger than the thermal noise and degrade the system performance drastically. With the intra-SA channel knowledge $\underline{\mathbf{H}}_{\mathrm{U}}^{(k_{\mathrm{S}},k_{\mathrm{S}})}$ the receive signal vector of (3.28) is processed according to the linear ZF criterion

$$\underline{\mathbf{D}}^{(k_{\mathrm{S}})} = \left(\underline{\mathbf{H}}_{\mathrm{U}}^{(k_{\mathrm{S}},k_{\mathrm{S}})*\mathrm{T}} \underline{\mathbf{H}}_{\mathrm{U}}^{(k_{\mathrm{S}},k_{\mathrm{S}})} \right)^{-1} \underline{\mathbf{H}}_{\mathrm{U}}^{(k_{\mathrm{S}},k_{\mathrm{S}})*\mathrm{T}} \tag{3.29}$$

at the CU of SA k_{S}, which results in the estimated data vector

$$\begin{aligned}\hat{\underline{\mathbf{d}}}^{(k_{\mathrm{S}})} &= \underline{\mathbf{D}}^{(k_{\mathrm{S}})}\underline{\mathbf{e}}^{(k_{\mathrm{S}})} \\ &= \underline{\mathbf{D}}^{(k_{\mathrm{S}})}\underline{\mathbf{H}}_{\mathrm{U}}^{(k_{\mathrm{S}},k_{\mathrm{S}})}\mathbf{P}^{(k_{\mathrm{S}})\frac{1}{2}}\underline{\mathbf{d}}^{(k_{\mathrm{S}})} + \underline{\mathbf{D}}^{(k_{\mathrm{S}})}\sum_{k'_{\mathrm{S}}\neq k_{\mathrm{S}}}\underline{\mathbf{H}}_{\mathrm{U}}^{(k_{\mathrm{S}},k'_{\mathrm{S}})}\mathbf{P}^{(k'_{\mathrm{S}})\frac{1}{2}}\underline{\mathbf{d}}^{(k'_{\mathrm{S}})} + \underline{\mathbf{D}}^{(k_{\mathrm{S}})}\underline{\mathbf{n}}^{(k_{\mathrm{S}})} \\ &= \mathbf{P}^{(k_{\mathrm{S}})\frac{1}{2}}\underline{\mathbf{d}}^{(k_{\mathrm{S}})} + \sum_{k'_{\mathrm{S}}\neq k_{\mathrm{S}}}\underline{\mathbf{D}}^{(k_{\mathrm{S}})}\underline{\mathbf{H}}_{\mathrm{U}}^{(k_{\mathrm{S}},k'_{\mathrm{S}})}\mathbf{P}^{(k'_{\mathrm{S}})\frac{1}{2}}\underline{\mathbf{d}}^{(k'_{\mathrm{S}})} + \underline{\mathbf{D}}^{(k_{\mathrm{S}})}\underline{\mathbf{n}}^{(k_{\mathrm{S}})}. \qquad (3.30)\end{aligned}$$

Note that only intra-SA interferences are completely eliminated by applying ZF JD, while inter-SA interferences still remain.

According to (3.30) the SINR with respect to the k-th active MS in SA k_{S} reads

$$\gamma_k^{(k_{\mathrm{S}})} = \frac{P_k^{(k_{\mathrm{S}})}}{\sum\limits_{k'_{\mathrm{S}}\neq k_{\mathrm{S}}}\sum\limits_{k'}\left|\left[\underline{\mathbf{D}}^{(k_{\mathrm{S}})}\underline{\mathbf{H}}_{\mathrm{U}}^{(k_{\mathrm{S}},k'_{\mathrm{S}})}\right]_{k,k'}\right|^2 P_{k'}^{(k'_{\mathrm{S}})} + \sigma^2\left[\left(\underline{\mathbf{H}}_{\mathrm{U}}^{(k_{\mathrm{S}},k_{\mathrm{S}})*\mathrm{T}}\underline{\mathbf{H}}_{\mathrm{U}}^{(k_{\mathrm{S}},k_{\mathrm{S}})}\right)^{-1}\right]_{k,k}}. \qquad (3.31)$$

In comparison to (3.3) for single SA scenarios, the denominator of (3.31) has an additional term representing the interference energy. Treating interferences as Gaussian noise, the user specific UL bit rate is approximated by

$$R_k^{(k_{\mathrm{S}})} = \log_2\left(1 + \frac{P_k^{(k_{\mathrm{S}})}}{\sum\limits_{k'_{\mathrm{S}}\neq k_{\mathrm{S}}}\sum\limits_{k'}\left|\left[\underline{\mathbf{D}}^{(k_{\mathrm{S}})}\underline{\mathbf{H}}_{\mathrm{U}}^{(k_{\mathrm{S}},k'_{\mathrm{S}})}\right]_{k,k'}\right|^2 P_{k'}^{(k'_{\mathrm{S}})} + \sigma^2\left[\left(\underline{\mathbf{H}}_{\mathrm{U}}^{(k_{\mathrm{S}},k_{\mathrm{S}})*\mathrm{T}}\underline{\mathbf{H}}_{\mathrm{U}}^{(k_{\mathrm{S}},k_{\mathrm{S}})}\right)^{-1}\right]_{k,k}}\right). \qquad (3.32)$$

3.2.2 Downlink performance

The DL transmission model of a multi-SA scenario with K_{S} co-channel SAs is illustrated in Fig. 3.7. The SA specific data vector, power matrix, modulation matrix, transmit signal vector, noise vector and estimated data vector are

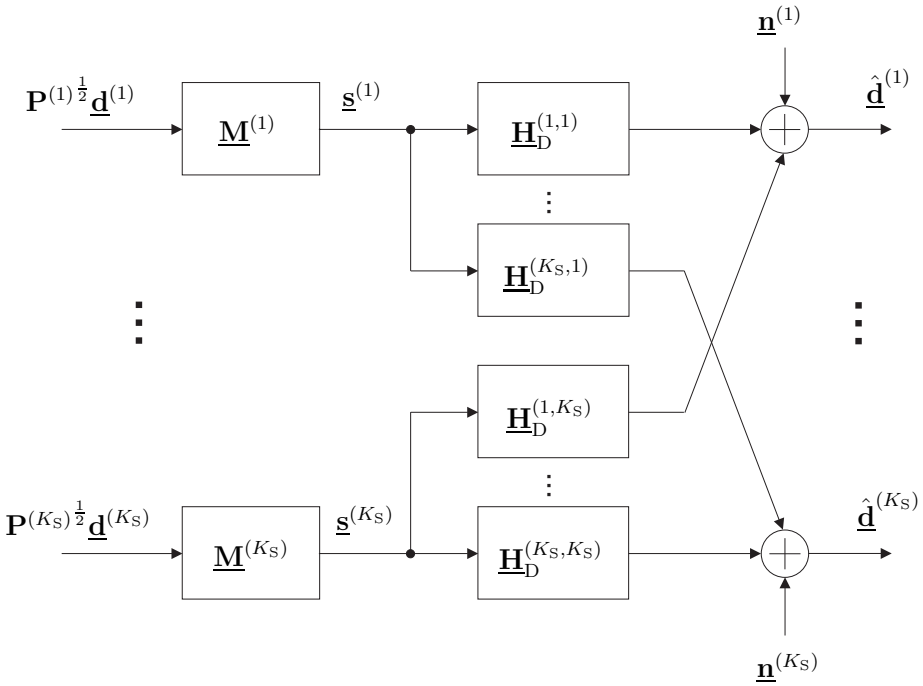

Figure 3.7: DL transmission model in a multi-SA scenario

denoted by $\underline{\mathbf{d}}^{(k_{\mathrm{S}})}$, $\mathbf{P}^{(k_{\mathrm{S}})}$, $\underline{\mathbf{M}}^{(k_{\mathrm{S}})}$, $\underline{\mathbf{s}}^{(k_{\mathrm{S}})}$, $\underline{\mathbf{n}}^{(k_{\mathrm{S}})}$ and $\hat{\underline{\mathbf{d}}}^{(k_{\mathrm{S}})}$, $k_{\mathrm{S}} = 1 \ldots K_{\mathrm{S}}$, respectively. The DL channel matrices

$$\underline{\mathbf{H}}_{\mathrm{D}}^{(k_{\mathrm{S}},k'_{\mathrm{S}})} = \begin{pmatrix} \underline{H}_{\mathrm{D},1,1}^{(k_{\mathrm{S}},k'_{\mathrm{S}})} & \cdots & \underline{H}_{\mathrm{D},1,K_{\mathrm{B}}}^{(k_{\mathrm{S}},k'_{\mathrm{S}})} \\ \vdots & & \vdots \\ \underline{H}_{\mathrm{D},K,1}^{(k_{\mathrm{S}},k'_{\mathrm{S}})} & \cdots & \underline{H}_{\mathrm{D},K,K_{\mathrm{B}}}^{(k_{\mathrm{S}},k'_{\mathrm{S}})} \end{pmatrix} \tag{3.33}$$

of dimension $K \times K_{\mathrm{B}}$ contain the CTFs of the channels from the K_{B} BSs in the k'_{S}-th SA to the K MSs in the k_{S}-th SA, $k_{\mathrm{S}}, k'_{\mathrm{S}} = 1 \ldots K_{\mathrm{S}}$. Due to channel reciprocity in TDD systems

$$\underline{\mathbf{H}}_{\mathrm{D}}^{(k_{\mathrm{S}},k'_{\mathrm{S}})} = \underline{\mathbf{H}}_{\mathrm{U}}^{(k'_{\mathrm{S}},k_{\mathrm{S}})^{\mathrm{T}}} \tag{3.34}$$

holds.

With the intra-SA channel knowledge $\underline{\mathbf{H}}_{\mathrm{D}}^{(k_{\mathrm{S}},k_{\mathrm{S}})}$ available, the SA specific mod-

ulation matrix according to the linear ZF criterion is given by

$$\begin{aligned}\underline{\mathbf{M}}^{(k_\mathrm{S})} &= \underline{\mathbf{H}}_\mathrm{D}^{(k_\mathrm{S},k_\mathrm{S})^{*\mathrm{T}}} \left(\underline{\mathbf{H}}_\mathrm{D}^{(k_\mathrm{S},k_\mathrm{S})} \underline{\mathbf{H}}_\mathrm{D}^{(k_\mathrm{S},k_\mathrm{S})^{*\mathrm{T}}}\right)^{-1} \\ &\quad \cdot \left(\mathrm{diag}\left(\left(\underline{\mathbf{H}}_\mathrm{D}^{(k_\mathrm{S},k_\mathrm{S})} \underline{\mathbf{H}}_\mathrm{D}^{(k_\mathrm{S},k_\mathrm{S})^{*\mathrm{T}}}\right)^{-1}\right)\right)^{-\frac{1}{2}}. \end{aligned} \tag{3.35}$$

In the DL a MS receives signals radiated not only from its BSs, but also from the BSs in the co-channel SAs, therefore the receive signal vector as well as the estimated data vector in SA k_S reads

$$\begin{aligned}\hat{\underline{\mathbf{d}}}^{(k_\mathrm{S})} &= \underline{\mathbf{H}}_\mathrm{D}^{(k_\mathrm{S},k_\mathrm{S})} \underline{\mathbf{M}}^{(k_\mathrm{S})} \mathbf{P}^{(k_\mathrm{S})^{\frac{1}{2}}} \underline{\mathbf{d}}^{(k_\mathrm{S})} \\ &\quad + \sum_{k'_\mathrm{S} \neq k_\mathrm{S}} \underline{\mathbf{H}}_\mathrm{D}^{(k_\mathrm{S},k'_\mathrm{S})} \underline{\mathbf{M}}^{(k'_\mathrm{S})} \mathbf{P}^{(k'_\mathrm{S})^{\frac{1}{2}}} \underline{\mathbf{d}}^{(k'_\mathrm{S})} + \underline{\mathbf{n}}^{(k_\mathrm{S})}. \end{aligned} \tag{3.36}$$

Substituting (3.35) into (3.36) yields

$$\begin{aligned}\hat{\underline{\mathbf{d}}}^{(k_\mathrm{S})} &= \left(\mathrm{diag}\left(\left(\underline{\mathbf{H}}_\mathrm{D}^{(k_\mathrm{S},k_\mathrm{S})} \underline{\mathbf{H}}_\mathrm{D}^{(k_\mathrm{S},k_\mathrm{S})^{*\mathrm{T}}}\right)^{-1}\right)\right)^{-\frac{1}{2}} \mathbf{P}^{(k_\mathrm{S})^{\frac{1}{2}}} \underline{\mathbf{d}}^{(k_\mathrm{S})} \\ &\quad + \sum_{k'_\mathrm{S} \neq k_\mathrm{S}} \underline{\mathbf{H}}_\mathrm{D}^{(k_\mathrm{S},k'_\mathrm{S})} \underline{\mathbf{M}}^{(k'_\mathrm{S})} \mathbf{P}^{(k'_\mathrm{S})^{\frac{1}{2}}} \underline{\mathbf{d}}^{(k'_\mathrm{S})} + \underline{\mathbf{n}}^{(k_\mathrm{S})}. \end{aligned} \tag{3.37}$$

Note that only intra-SA interferences are completely avoided by applying linear ZF JT, whereas inter-SA interferences still remain, which have a great impact on the performance. The DL SINR of the k-th active MS in SA k_S can be calculated to be

$$\gamma_k^{(k_\mathrm{S})} = \frac{\dfrac{P_k^{(k_\mathrm{S})}}{\left[\left(\underline{\mathbf{H}}_\mathrm{D}^{(k_\mathrm{S},k_\mathrm{S})} \underline{\mathbf{H}}_\mathrm{D}^{(k_\mathrm{S},k_\mathrm{S})^{*\mathrm{T}}}\right)^{-1}\right]_{k,k}}}{\displaystyle\sum_{k'_\mathrm{S} \neq k_\mathrm{S}} \sum_{k'} \left|\left[\underline{\mathbf{H}}_\mathrm{D}^{(k_\mathrm{S},k'_\mathrm{S})} \underline{\mathbf{M}}^{(k'_\mathrm{S})}\right]_{k,k'}\right|^2 P_{k'}^{(k'_\mathrm{S})} + \sigma^2}. \tag{3.38}$$

The corresponding user bit rate is given by

$$R_k^{(k_\mathrm{S})} = \log_2\left(1 + \frac{\dfrac{P_k^{(k_\mathrm{S})}}{\left[\left(\underline{\mathbf{H}}_\mathrm{D}^{(k_\mathrm{S},k_\mathrm{S})} \underline{\mathbf{H}}_\mathrm{D}^{(k_\mathrm{S},k_\mathrm{S})^{*\mathrm{T}}}\right)^{-1}\right]_{k,k}}}{\displaystyle\sum_{k'_\mathrm{S} \neq k_\mathrm{S}} \sum_{k'} \left|\left[\underline{\mathbf{H}}_\mathrm{D}^{(k_\mathrm{S},k'_\mathrm{S})} \underline{\mathbf{M}}^{(k'_\mathrm{S})}\right]_{k,k'}\right|^2 P_{k'}^{(k'_\mathrm{S})} + \sigma^2}\right). \tag{3.39}$$

Unlike in single SA scenarios where duality between UL and DL performance measures can be observed, in multi-SA scenarios the UL SINR of (3.31) and the DL SINR of (3.38) is in general unequal due to the different natures of inter-SA interferences in the UL and in the DL. In the UL the interfering signals originating from the MSs in the co-channel SAs arrive at the BSs of the reference SA and are weighted by the demodulation matrix of the reference SA. In the DL the interfering signals radiated from the BSs of the co-channel SAs are generated by multiplying the modulation matrices by the data vectors of the co-channel SAs and impinge on the reference MS.

Chapter 4

Transmit power allocation in interference channels

4.1 Preliminary remarks

Interference channels are basic models that characterize communication networks suffering interferences. The study on interference channels was initiated by Shannon in 1961 [Sha61]. Since then a lot of efforts have been devoted to discovering the capacity region of interference channels [Car78, Sat81, HK81, Kra01, Sas04, LZ06, ETW06]. Unfortunately, even for the simplest two user case the capacity region is not fully explored yet. In this thesis we do not attempt to study the capacity region of interference channels from an information theory standpoint. Instead we focus on the power allocation issue in interference channels.

Adaptive power allocation is proven to be an efficient means in improving system performance. It is well known that waterfilling power allocation is optimum in the sense of capacity maximization in independent parallel channels [CT91]. Power allocation aiming at improving the BER performance in parallel channels is studied in [PL04]. However, power allocation in interference channels is a more challenging task due to crosscoupling among different

sub-channels. Depending on the various features of services and applications different power allocation strategies towards different optimization goals can be adopted in interference channels. For instance, real time voice services which are dominant in 2G cellular networks normally require a fair quality of service. On the other hand, for non-real time data applications including file transfer, emails, web browsing and etc. the aggregate data rate is an important measure of the system performance. Fairness and throughput are essentially a pair of tradeoff. One can hardly ensure fairness and optimize throughput at the same time. A classical way to achieve fairness in cellular networks is to allocate the transmit power among co-channel users so that their signal-to-interference ratios (SIRs) are balanced [AN82, NA83, Zan92]. However, the fairness is at an expense of throughput loss. With the increasing demand on data applications over the last decade, it is becoming more interesting to achieve the other extreme of the tradeoff, i.e., to maximize the sum rate of all users [JL03, PJSL05].

The transmit powers are subject to certain constraints due to regulations and physical limitations. In practical implementations individual power constraints may be reasonable due to the limited dynamic range of the power amplifiers. A total power constraint is interesting from a theoretical point of view as the total power is a suitable measure for the interference caused by the system. Furthermore, the type of power constraint depends on the relationship among the transmitters. For instance, in the UL of cellular systems the uncoordinated transmitters of independent MSs imply individual power constraints. While coordinated transmitters located at a common BS or linked to a common central unit in the DL may be subject to a total power constraint. Besides, combinations of total and individual power constraints may be considered under certain circumstances [Jor06]. Most previous studies [YGC02, CYM+06] deal with individual power constraints, while the problem of sum rate maximizing power allocation in interference channels with a total power constraint is less understood. Only in simplified two-user interference channels the optimum solution is known [PJSL05]. In this thesis a total power constraint will be assumed.

In principle, channel allocation problems can be viewed as binary power allo-

cation in that channel allocation only determines whether a channel resource with a predefined transmit power is assigned to a user or not. While continuous power allocation offers more degrees of freedom as it not only implicitly indicates the assignment of channels but also determines transmit powers invested for each channel. Positive transmit power on a channel with respect to a specific user means the channel is allocated to the user and zero transmit power indicates no assignment. Therefore, understanding power allocation is of great importance and also provides hints on channel allocation problems.

After describing the interference channel model in Section 4.2, various power allocation strategies in interference channels under total power constraint are discussed in Section 4.3, among which the proposed iterative waterfilling and noniterative waterfilling algorithms are highlighted as the major contributions of this thesis. The performance of these power allocation strategies is investigated in Section 4.4.

4.2 Interference channel model

An interference channel [CT91] is a network consisting of multiple transmitter-receiver pairs. There exists a one-to-one correspondence between transmitters and receivers and each transmitter only intends to communicate with its corresponding receiver. However, different transmitter-receiver pairs are coupled through interference links. This model is not only theoretically interesting but also practically important since any system exhibiting interferences can be modelled as an interference channel. For instance, in cellular systems the MSs receive signals not only from their intended BSs but also from the BSs in the co-channel cells. Other examples include DSL systems, satellite systems and etc.

In what follows we consider a generic J-user memoryless interference channel composed of J transmitter-receiver pairs. Each "user" can logically represent a real user or a specific channel resource such as time slot, subcarrier, spreading code or spatial beam. Such an interference channel has J useful links and

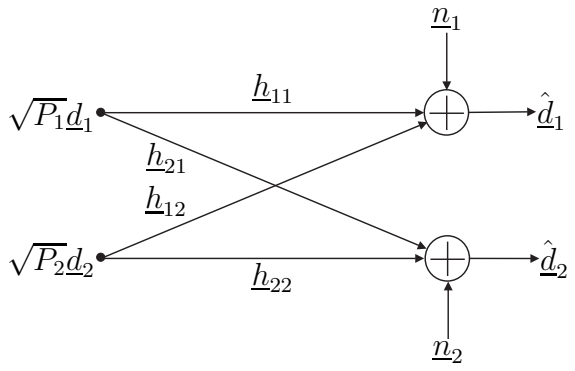

Figure 4.1: Two-user interference channel model

$J(J-1)$ interference links. In addition to physical channels, the links between the transmitters and the receivers in the interference channel may also integrate linear pre-processing and post-processing stages. Let $\underline{h}_{ji}$, $j,i = 1 \dots J$, represent the complex channel coefficient of the link between transmitter i and receiver j. The transmitted and received information bearing data symbols are denoted by $\underline{d}_j$ and $\hat{\underline{d}}_j$, respectively. $\underline{d}_j$, $j = 1 \dots J$, are assumed to be i.i.d. Gaussian variables with zero mean and unit variance. P_j indicates the transmit power allocated to user j. $\underline{n}_j \sim \mathcal{CN}(0, \sigma^2)$ designates complex AWGN with zero mean and variance of σ^2. Hence a J-user interference channel model can be formulated as

$$\hat{\underline{d}}_j = \sqrt{P_j}\underline{h}_{jj}\underline{d}_j + \sum_{i \neq j} \sqrt{P_i}\underline{h}_{ji}\underline{d}_i + \underline{n}_j, \quad j = 1 \dots J. \tag{4.1}$$

As a simple example, a two-user interference channel is illustrated in Fig. 4.1. When both interference links vanish, the interference channel degenerates into parallel channels as shown in Fig. 4.2. A Z-channel is obtained if one of the two interference links disappears, see Fig. 4.3.

In interference channels each receiver only wants to decode the information transmitted by its corresponding transmitter. With (4.1) the SINR of user j is easily computed to be

$$\gamma_j = \frac{P_j g_{jj}}{\sum_{i \neq j} P_i g_{ji} + \sigma^2}, \tag{4.2}$$

where $g_{ji} = \left|\underline{h}_{ji}\right|^2$ denote the channel gains. Treating the interference as noise,

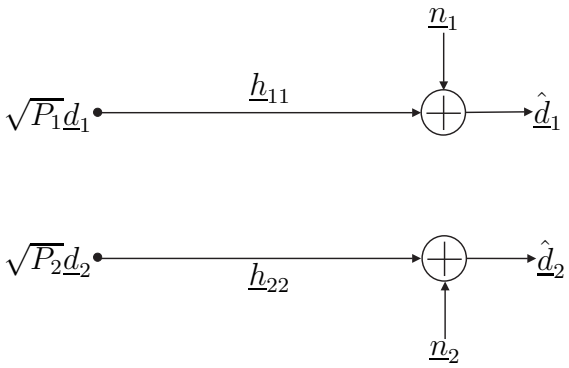

Figure 4.2: Two-user parallel channel model

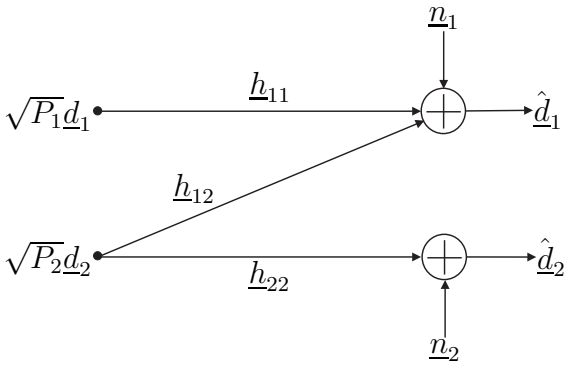

Figure 4.3: Z channel model

the achievable bit rate of user j at which reliable communication is possible is approximated by

$$R_j = \log_2 \left(1 + \frac{P_j g_{jj}}{\sum_{i \neq j} P_i g_{ji} + \sigma^2} \right). \tag{4.3}$$

4.3 Power allocation in interference channels

4.3.1 Signal-to-interference ratio balancing

A classical power allocation strategy in cellular networks is to adjust the transmit powers of co-channel users so that they perceive the same level of SIR. This

is known as SIR balancing or CIR balancing [BS06, Zan92]. For example, in IS-95 systems SIR balancing is employed to effectively combat the near-far effects [Gar99]. The principle of SIR balancing in generic interference channels is reviewed in this subsection.

Neglect thermal noise and assume all users in the interference channel perceive the same SIR level γ, i.e.,

$$\gamma_j = \frac{P_j g_{jj}}{\sum\limits_{i \neq j} P_i g_{ji}} = \gamma, \quad \forall j. \tag{4.4}$$

Rewrite (4.4) as

$$\frac{1}{\gamma} P_j = \sum_{i \neq j} \frac{g_{ji}}{g_{jj}} P_i. \tag{4.5}$$

With the power vector

$$\mathbf{p} = (P_1 \dots P_J)^{\mathrm{T}} \tag{4.6}$$

and the normalized interference channel gain matrix $\mathbf{F} = \{F_{ji}\}$ defined as

$$F_{ji} = \begin{cases} \frac{g_{ji}}{g_{jj}}, & j \neq i \\ 0, & j = i \end{cases}, \tag{4.7}$$

(4.5) can be represented in a matrix-vector form

$$\frac{1}{\gamma} \mathbf{p} = \mathbf{F} \cdot \mathbf{p}, \tag{4.8}$$

which identifies an eigenvalue problem for $\mathbf{p}$. Note that $\mathbf{F}$ is a nonnegative matrix. The Perron-Frobenius theorem [Sen06, SWB06] for nonnegative matrices states that up to a scalar factor there exists a unique eigenvector which consists of nonnegative elements only and satisfies (4.8). The corresponding eigenvalue is $\rho(\mathbf{F})$, where $\rho(\cdot)$ denotes the spectral radius of a matrix. Consequently, the balanced SIR level γ is given by

$$\gamma = \frac{1}{\rho(\mathbf{F})}. \tag{4.9}$$

The eigenvector $\mathbf{p}_{\rho(\mathbf{F})}$ associated with $\rho(\mathbf{F})$ represents the power vector that satisfies (4.8). In case of a total power constraint P_{tot}, the eigenvector should

be scaled by $\frac{P_{\text{tot}}}{\|\mathbf{p}_{\rho(\mathbf{F})}\|_1}$ with $\|\cdot\|_1$ denoting the l_1 norm. In two-user interference channels the spectral radius is $\sqrt{\frac{g_{12}g_{21}}{g_{11}g_{22}}}$ and the associated eigenvector is proportional to $\left(\sqrt{g_{12}g_{22}} \quad \sqrt{g_{11}g_{21}}\right)^{\text{T}}$. Hence the balanced SIR γ equals $\sqrt{\frac{g_{11}g_{22}}{g_{12}g_{21}}}$ and the sum rate approaches

$$R_{\text{sum}} = 2\log_2\left(1+\sqrt{\frac{g_{11}g_{22}}{g_{12}g_{21}}}\right) \tag{4.10}$$

as $\frac{P_{\text{tot}}}{\sigma^2}$ approaches infinity.

Note that although the SIRs of all users achieve the same level through SIR balancing power allocation, the resulting SINRs and consequently the user specific bit rates are not guaranteed to be fair.

The derivation above implies the existence of a central controller with the knowledge of the all channel gains in the interference channel. In reality SIR balancing can be accomplished through a distributed iterative algorithm [FM93] without such a central controller.

SIR balancing is advantageous to real time applications such as voice and video streaming in that all users can communicate relatively fairly and stably. However, the price paid for fairness is a considerable loss in sum rate which is a more crucial figure of merit in data applications, especially in strong interference scenarios. In the following we focus on the other extreme of the fairness-throughput tradeoff.

4.3.2 Sum rate maximizing power allocation

Having channel knowledge at the transmitter side, the objective of power allocation considered here is to maximize the sum rate of the interference channel under a total power constraint, which can be formulated by

$$\max\{R_{\text{sum}}\} = \max\left\{\sum_{j=1}^{J} R_j\right\} \tag{4.11}$$

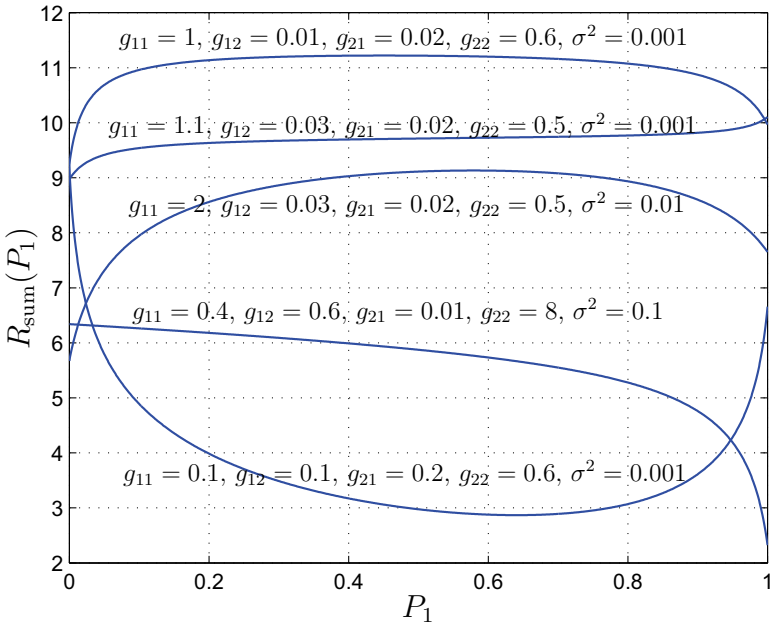

Figure 4.4: Objective function $R_{\mathrm{sum}}(P_1)$ for $P_{\mathrm{tot}} = 1$

subject to

$$\sum_{j=1}^{J} P_j = P_{\mathrm{tot}} \tag{4.12}$$

and to

$$P_j \geq 0, \quad \forall j. \tag{4.13}$$

For two-user interference channels as depicted in Fig. 4.1 the objective function can be written as

$$\begin{aligned} R_{\mathrm{sum}}(P_1) &= \log_2\left(1 + \frac{P_1 g_{11}}{(P_{\mathrm{tot}} - P_1)g_{12} + \sigma^2}\right) \\ &\quad + \log_2\left(1 + \frac{(P_{\mathrm{tot}} - P_1)g_{22}}{P_1 g_{21} + \sigma^2}\right). \end{aligned} \tag{4.14}$$

In Fig. 4.4 several examples of the objective function $R_{\mathrm{sum}}(P_1)$ are plotted, which may have one local maximum, one local minimum, or no local extremum at all. Therefore, the objective function is not guaranteed to be concave.

The non-concavity of the objective function implies that in order to obtain the optimum transmit power P_1^* maximizing (4.14) one should examine the stationary points of (4.14) and the endpoints of the interval $[0, P_{\text{tot}}]$. The stationary points of the objective function (4.14) at which the first derivative is zero read

$$\tilde{P}_1 = \frac{\pm\sqrt{A} - B}{C}, \tag{4.15}$$

where

$$\begin{aligned} A &= g_{11}g_{22}\left(g_{12}P_{\text{tot}} + \sigma^2\right)\left(g_{21}P_{\text{tot}} + \sigma^2\right) \\ &\quad \cdot \left(g_{12}g_{21}P_{\text{tot}} + (g_{12} + g_{21} - g_{22})\,\sigma^2\right) \\ &\quad \cdot \left(g_{12}g_{21}P_{\text{tot}} + (g_{12} + g_{21} - g_{11})\,\sigma^2\right), \end{aligned} \tag{4.16}$$

$$\begin{aligned} B &= g_{12}(g_{11}g_{21} + g_{21}g_{22} + g_{12}g_{22} - g_{11}g_{22})P_{\text{tot}}\sigma^2 \\ &\quad + (g_{11}g_{21} + g_{12}g_{22} - g_{11}g_{22})\sigma^4 + g_{12}^2 g_{21}g_{22}P_{\text{tot}}^2, \end{aligned} \tag{4.17}$$

and

$$\begin{aligned} C &= g_{12}g_{21}(g_{11}g_{21} - g_{12}g_{22})P_{\text{tot}} + g_{11}g_{22}(g_{12} - g_{21})\sigma^2 \\ &\quad + (g_{11}g_{21}^2 - g_{12}^2 g_{22})\sigma^2. \end{aligned} \tag{4.18}$$

Note that $\tilde{P}_1$ of (4.15) does not exist if $A < 0$, i.e., if

$$\min\{g_{11}, g_{22}\} < g_{12}g_{21}\frac{P_{\text{tot}}}{\sigma^2} + g_{12} + g_{21} < \max\{g_{11}, g_{22}\} \tag{4.19}$$

is true. Moreover, both stationary points may not fall within the interval $[0, P_{\text{tot}}]$. It can also happen that the second derivative of $R_{\text{sum}}(P_1)$ at $\tilde{P}_1$ is zero or positive since $R_{\text{sum}}(P_1)$ is not guaranteed to be concave with respect to P_1. In these cases a local maximum does not exist. It is not necessary to verify the second derivative of $R_{\text{sum}}(P_1)$ at $\tilde{P}_1$ to examine whether a stationary point is a local maximum, a local minimum or a saddle point. Instead one can just compare the sum rates at the physically meaningful stationary point $\hat{P}_1 = \left\{\tilde{P}_1 : \tilde{P}_1 \in [0, P_{\text{tot}}]\right\}$ provided $\tilde{P}_1$ exists and at the endpoints $\{0, P_{\text{tot}}\}$ to obtain the optimum transmit power

$$P_1^* = \underset{P_1 \in \{\hat{P}_1, 0, P_{\text{tot}}\}}{\arg\max} \{R_{\text{sum}}(P_1)\} \tag{4.20}$$

and the corresponding sum rate.

The analytical solution of (4.20) is only attainable for the simplest two-user scenarios. For generic interference channels with more than two users an analytical solution is not known. Even numerical methods such as the steepest ascent method and simulated annealing [Che01], which work well for convex optimization problems, are not guaranteed to converge to the global optimum because the optimization problem addressed here is non-convex. In practical implementations transmit power is usually adjusted in discrete steps rather than continuously, in which case the near-optimum power allocation can be found by an exhaustive search. However, due to the fact that the power resolution Δ is normally much smaller than the total power budget P_{tot} and that the number J of users is usually large, such an exhaustive search having a complexity of $\mathcal{O}\left(\left(\frac{P_{\text{tot}}}{\Delta}+1\right)^J\right)$ is infeasible in reality. The prohibitively high complexity in finding the optimum power allocation in multiuser interference channels drives us to resort to suboptimum solutions.

4.3.3 Equal power allocation

As the simplest scheme equal power allocation homogeneously distributes the total transmit power to all users, i.e.,

$$P_j = \frac{P_{\text{tot}}}{J}, \quad \forall j. \tag{4.21}$$

This is a fixed power allocation strategy that does not rely on the channel conditions and can be readily applied even without transmitter side channel knowledge.

The sum rate of two-user interference channels with equal power allocation will asymptotically approach

$$R_{\text{sum}} = \log_2\left(1+\frac{g_{11}}{g_{12}}\right) + \log_2\left(1+\frac{g_{22}}{g_{21}}\right) \tag{4.22}$$

as $\frac{P_{\text{tot}}}{\sigma^2}$ approaches infinity.

4.3.4 Greedy power allocation

Greedy power allocation in interference channels means that all the transmit power is allocated to the user whose useful link has the largest gain, i.e.,

$$P_j = \begin{cases} P_{\text{tot}}, & j = \arg\max_i \{g_{ii}\} \\ 0, & \text{else} \end{cases} . \tag{4.23}$$

By doing so the channel resource is exclusively used by one user. In other words, this power allocation strategy leads to an extreme unfairness in the sense of channel resource utilization. The sum rate resulting from greedy power allocation can be easily obtained as

$$R_{\text{sum}} = \log_2 \left(1 + \frac{P_{\text{tot}} g_{jj}}{\sigma^2} \right) . \tag{4.24}$$

As $\frac{P_{\text{tot}}}{\sigma^2}$ approaches infinity (4.24) can be simplified as

$$R_{\text{sum}} = \log_2 \frac{P_{\text{tot}}}{\sigma^2} + \log_2 g_{jj}. \tag{4.25}$$

4.3.5 Conventional waterfilling

Multicarrier transmission, sequential transmission in time variant channels and singular value decomposition (SVD) based multiantenna transmission are frequently considered transmission schemes in wireless communications. A common property of these transmission schemes is that there is no crosscoupling among the sub-channels, which may represent orthogonal subcarriers, time slots or spatial beams. For such independent parallel channels the sum rate can be simplified as

$$R_{\text{sum}} = \sum_{j=1}^{J} \log_2 \left(1 + \frac{P_j g_{jj}}{\sigma^2} \right) . \tag{4.26}$$

Under a total power constraint among the parallel channels with respect to frequency, time or spatial domain, it is well known that the power allocation maximizing (4.26) follows the waterfilling principle [CT91], which distributes a

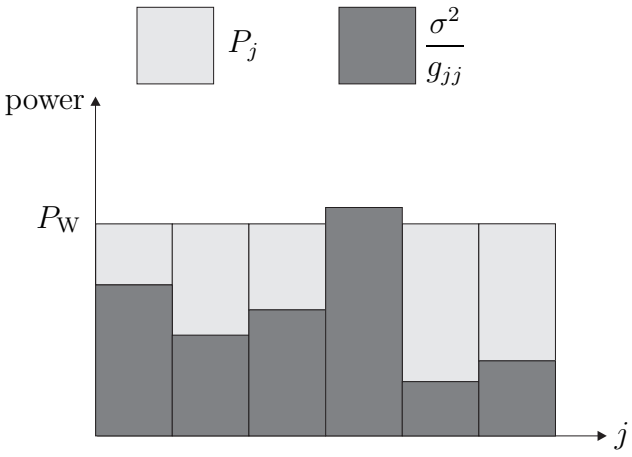

Figure 4.5: Conventional waterfilling

certain amount of transmit power across the uncoupled sub-channels depending on the noise level of each sub-channel as illustrated in Fig. 4.5. The basic idea behind waterfilling is to allocate more power to the sub-channels with good channel condition, i.e., with relatively low noise level, and less power to those with bad channel condition, i.e., with relatively high noise level. Precisely one has

$$P_j = \left(P_{\mathrm{W}} - \frac{\sigma^2}{g_{jj}} \right)^+, \tag{4.27}$$

where $(a)^+ = \max\{0, a\}$ and the water level P_{W} is chosen such that the power constraint of (4.12) is fulfilled. For two parallel channels as depicted in Fig. 4.2 one can explicitly obtain

$$P_1 = \begin{cases} \frac{P_{\mathrm{tot}}}{2} + \frac{\sigma^2}{2}\left(\frac{1}{g_{22}} - \frac{1}{g_{11}}\right), & \frac{P_{\mathrm{tot}}}{\sigma^2} \geq \left|\frac{1}{g_{22}} - \frac{1}{g_{11}}\right| \\ P_{\mathrm{tot}}, & \frac{P_{\mathrm{tot}}}{\sigma^2} < \frac{1}{g_{22}} - \frac{1}{g_{11}} \\ 0, & \frac{P_{\mathrm{tot}}}{\sigma^2} < \frac{1}{g_{11}} - \frac{1}{g_{22}} \end{cases} . \tag{4.28}$$

Obviously, the waterfilling solution (4.28) is equivalent to equal power allocation if $g_{11} = g_{22}$ holds. If $\frac{P_{\mathrm{tot}}}{\sigma^2}$ is smaller than $\left|\frac{1}{g_{22}} - \frac{1}{g_{11}}\right|$ then waterfilling power allocation results in greedy power allocation.

On the other hand, if $\frac{P_{\mathrm{tot}}}{\sigma^2}$ is sufficiently large, the sum rate resulting from conventional waterfilling power allocation in two-user interference channels

follows to be

$$R_{\text{sum}} = \log_2\left(1+\frac{\left(\frac{P_{\text{tot}}}{2}+\frac{\sigma^2}{2}\left(\frac{1}{g_{22}}-\frac{1}{g_{11}}\right)\right)g_{11}}{\left(\frac{P_{\text{tot}}}{2}+\frac{\sigma^2}{2}\left(\frac{1}{g_{11}}-\frac{1}{g_{22}}\right)\right)g_{12}+\sigma^2}\right) + \log_2\left(1+\frac{\left(\frac{P_{\text{tot}}}{2}+\frac{\sigma^2}{2}\left(\frac{1}{g_{11}}-\frac{1}{g_{22}}\right)\right)g_{22}}{\left(\frac{P_{\text{tot}}}{2}+\frac{\sigma^2}{2}\left(\frac{1}{g_{22}}-\frac{1}{g_{11}}\right)\right)g_{21}+\sigma^2}\right). \quad (4.29)$$

As $\frac{P_{\text{tot}}}{\sigma^2}$ approaches infinity, it can be easily derived that (4.29) converges to

$$R_{\text{sum}} = \log_2\left(1+\frac{g_{11}}{g_{12}}\right)+\log_2\left(1+\frac{g_{22}}{g_{21}}\right), \quad (4.30)$$

which is also the limit for equal power allocation as $\frac{P_{\text{tot}}}{\sigma^2}$ approaches infinity.

Unfortunately, in the presence of crosscoupling interferences conventional waterfilling is suboptimum since the interaction among the sub-channels is ignored.

4.3.6 Iterative waterfilling

Although conventional waterfilling fails to maximize the sum rate in interference channels, the waterfilling principle can still be utilized in an iterative fashion by treating the interference as noise. In a J-user interference channel with total power budget of P_{tot}, the proposed iterative waterfilling algorithm can be described as follows: After arbitrary initial power allocation, e.g., equal power allocation, the interference power perceived by every user is calculated. Treating interference calculated from the power allocation in iteration $l-1$ as noise, the power allocation following the waterfilling principle in iteration l reads

$$P_j(l) = \left(P_{\text{W}}(l) - \left(\sum_{i\neq j} P_i(l-1)\frac{g_{ji}}{g_{jj}}+\frac{\sigma^2}{g_{jj}}\right)\right)^+, \quad j=1\ldots J, \quad (4.31)$$

where the water level $P_{\text{W}}(l)$ in iteration l is determined such that

$$\sum_{j=1}^{J} P_j(l) = P_{\text{tot}} \quad (4.32)$$

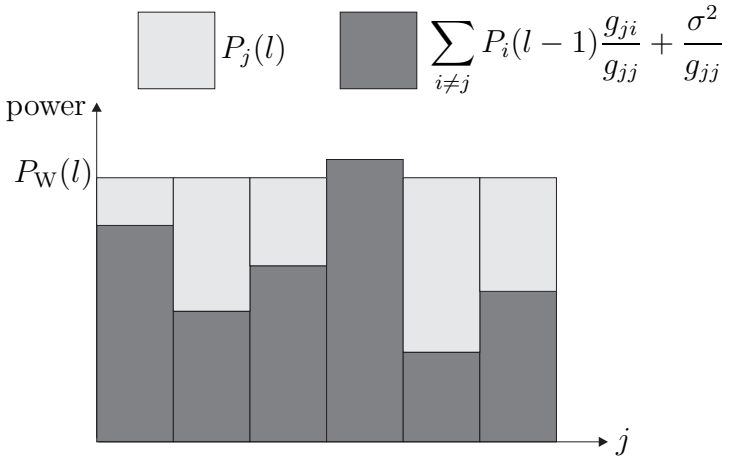

Figure 4.6: Iterative waterfilling

holds. Iterations stop if the power allocation does not change significantly any more. Fig. 4.6 illustrates how power is allocated in one iteration.

It should be emphasized that the iterative waterfilling algorithm proposed above is performed across users with a total power constraint, which should be distinguished from iterative per user waterfilling over frequency with per user power constraints originally proposed for DSL systems [YGC02]. For developing the latter algorithm the power allocation problem in interference channels is modelled as a non-cooperative game, where each user adjusts its transmit power to maximize its own rate while treating interference as noise. In [YGC02] it is proven that under suitable conditions iterative per user waterfilling over frequency with per user power constraints converges to the Nash equilibrium in two-user interference channels. A more comprehensive convergency analysis of this algorithm can be found in [LP06]. As to the iterative waterfilling across users, it will be shown in the following that one can analytically derive the limiting value under certain conditions. In the context of this thesis, iterative waterfilling refers to the procedure described by (4.31) and (4.32).

Assume that after iterative waterfilling all the J users get positive transmit powers which are included in the column vector $\mathbf{p}$ of (4.6). Let z_j denote the corresponding normalized interference plus noise power perceived by user j

which is given by

$$z_j = \sum_{i \neq j} P_i \frac{g_{ji}}{g_{jj}} + \frac{\sigma^2}{g_{jj}} = \mathbf{y}_j \mathbf{p} + \frac{\sigma^2}{g_{jj}}, \tag{4.33}$$

where $\mathbf{y}_j$ is a row vector defined as

$$\mathbf{y}_j = \left(\frac{g_{j1}}{g_{jj}} \quad \dots \quad \frac{g_{j,j-1}}{g_{jj}} \quad 0 \quad \frac{g_{j,j+1}}{g_{jj}} \quad \dots \quad \frac{g_{jJ}}{g_{jj}} \right). \tag{4.34}$$

Hence the final water level P_{W} can be represented by

$$P_{\mathrm{W}} = \frac{1}{J} \sum_j (z_j + P_j) = \frac{1}{J} \left(P_{\mathrm{tot}} + \sum_j \mathbf{y}_j \mathbf{p} + \|\check{\mathbf{n}}\|_1 \right) \tag{4.35}$$

with

$$\check{\mathbf{n}} = \left(\frac{\sigma^2}{g_{11}} \dots \frac{\sigma^2}{g_{JJ}} \right)^{\mathrm{T}} \tag{4.36}$$

being the normalized noise variance vector. Under the assumption that all users get positive transmit powers, the transmit power P_j is simply the difference between the water level P_{W} of (4.35) and the normalized interference plus noise power z_j of (4.33), i.e.,

$$\begin{aligned} P_j &= P_{\mathrm{W}} - z_j \\ &= \frac{P_{\mathrm{tot}}}{J} + \frac{1}{J} \left(\sum_{i \neq j} \mathbf{y}_i - (J-1)\mathbf{y}_j \right) \mathbf{p} + \frac{1}{J} \|\check{\mathbf{n}}\|_1 - \frac{\sigma^2}{g_{jj}}. \end{aligned} \tag{4.37}$$

Defining

$$\mathbf{X} = \begin{pmatrix} \sum_{i \neq 1} \mathbf{y}_i - (J-1)\mathbf{y}_1 \\ \vdots \\ \sum_{i \neq J} \mathbf{y}_i - (J-1)\mathbf{y}_J \end{pmatrix} \tag{4.38}$$

and

$$\mathbf{u} = \frac{P_{\mathrm{tot}}}{J} + \frac{\|\check{\mathbf{n}}\|_1}{J} - \check{\mathbf{n}}, \tag{4.39}$$

then combining (4.37) for $j = 1 \dots J$ leads to a matrix-vector representation

$$\mathbf{p} = \frac{1}{J} \mathbf{X} \cdot \mathbf{p} + \mathbf{u}, \tag{4.40}$$

which represents a system of linear equations. The solution of (4.40) readily follows to be

$$\mathbf{p} = \left(\mathbf{I} - \frac{1}{J}\mathbf{X}\right)^{-1} \mathbf{u}, \tag{4.41}$$

which gives the limiting value of iterative waterfilling. It is worth mentioning that the limiting value (4.41) is conditioned on the knowledge that iterative waterfilling converges to a component-wise positive power vector. However, (4.41) is not necessarily the limiting value even if it is component-wise positive because iterative waterfilling may converge to a different power vector depending on the initial power allocation.

For two-user interference channels (4.41) simplifies to

$$\begin{pmatrix} P_1 \\ P_2 \end{pmatrix} = \begin{pmatrix} \dfrac{g_{22}(g_{12}-g_{11})P_{\text{tot}} + (g_{22}-g_{11})\sigma^2}{g_{11}g_{21} - 2g_{11}g_{22} + g_{12}g_{22}} \\ \dfrac{g_{11}(g_{21}-g_{22})P_{\text{tot}} + (g_{11}-g_{22})\sigma^2}{g_{11}g_{21} - 2g_{11}g_{22} + g_{12}g_{22}} \end{pmatrix}. \tag{4.42}$$

Obviously (4.42) is different from the stationary points given by (4.15). Therefore iterative waterfilling in general leads to a suboptimum solution. As $\frac{P_{\text{tot}}}{\sigma^2}$ approaches infinity, the sum rate resulting from the power allocation of (4.42) can be proven to be

$$R_{\text{sum}} = \log_2\left(1 + \frac{g_{22}\left(g_{12}-g_{11}\right)}{g_{12}\left(g_{21}-g_{22}\right)}\right) + \log_2\left(1 + \frac{g_{11}\left(g_{21}-g_{22}\right)}{g_{21}\left(g_{12}-g_{11}\right)}\right). \tag{4.43}$$

Perron-Frobenius theorem [Sen06, SWB06] ensures that for arbitrary nonnegative matrix $\mathbf{X}$ and positive vector $\mathbf{u}$ the vector $\mathbf{p}$ represented in the form of (4.41) is strictly positive and is a unique solution to (4.40) if and only if $J > \rho(\mathbf{X})$ is true. Unfortunately, the Perron-Frobenius theorem is not valid here since both the matrix $\mathbf{X}$ defined in (4.38) and the vector $\mathbf{u}$ of (4.39) may contain negative elements. Therefore, the power vector $\mathbf{p}$ of (4.41) may not be positive, which is contradictory to our assumption. This indicates the case that one or more users will get zero transmit power after the iterative waterfilling procedure. In this case the exact limiting value of iterative waterfilling is not known. Nevertheless, it is possible to find out all the potential limiting values by means of exhaustive search, i.e., one can exhaustively exclude

a subset of users while constructing $\mathbf{X}$ and $\mathbf{u}$ and calculate the partial power vector $\mathbf{p}$ according to (4.41). The partial power vector $\mathbf{p}$ and a certain number of zero elements corresponding to those excluded users constitute the overall power vector containing the transmit powers of all users. The obtained overall power vector is a potential limiting value of iterative waterfilling if it is component-wise nonnegative.

4.3.7 Noniterative waterfilling

The analysis on the limiting value of iterative waterfilling in the previous subsection also suggests a noniterative waterfilling power allocation algorithm. Namely, one can exhaustively examine the overall power vectors obtained in the same way as to get all potential limiting values. Among all the obtained overall power vectors the one with nonnegative elements only and resulting in the maximum sum rate is selected to be the final solution. This exhaustive search based noniterative waterfilling approach requires to evaluate (4.41)

$$\sum_{j=0}^{J-1} \binom{J}{j} = 2^J - 1 \tag{4.44}$$

times which is the number of strict subsets of $\{1 \dots J\}$ as well as the number of overall power vectors to be checked. In particular, if $J-1$ users are excluded then greedy power allocation results. The power allocation resulting from iterative waterfilling is also specified by one of the $2^J - 1$ overall power vectors. Therefore, it is straightforward to conclude that exhaustive search based noniterative waterfilling power allocation represents an upper bound of iterative waterfilling and greedy power allocation in terms of sum rate. However, for a large number J of users this approach is prohibitively complex although iterations are avoided.

To reduce the complexity of the exhaustive search based noniterative waterfilling power allocation, one can gradually increase the number of excluded users from 0 to $J-1$ till a nonnegative overall power vector is obtained instead of exhaustively excluding all subsets of users. For a certain number j

of excluded users, all the $\binom{J}{j}$ subsets are examined and the resulting overall power vector with nonnegative elements only and yielding the largest sum rate is chosen to be the solution. If none of the resulting overall power vectors is component-wise nonnegative, then the number of excluded users is increased by one. Since the number of users included in (4.41) gradually decreases, this power allocation approach is referred to as decremental noniterative waterfilling in the following. Of course decremental noniterative waterfilling leads to a performance degradation as compared to the exhaustive one. On the other hand, since a smallest possible number of users are excluded while finding a feasible power vector the fairness is improved.

4.4 Performance analysis

In this section we analyze the performance of various power allocation schemes in interference channels by presenting some numerical results. Fig. 4.1 shows a generic two-user interference channel model without assuming any relationship between the channel gains. To visualize the behavior of power allocation some specific cases of the generic model will be considered.

Firstly consider the channel configuration with

$$\frac{g_{12}}{g_{11}} = \frac{g_{21}}{g_{22}} = \beta \tag{4.45}$$

as assumed in [PJSL05]. Under the above restriction a symmetric channel snapshot with $g_{11} = g_{22} = 1$ and an asymmetric channel snapshot with $g_{11} = 1$, $g_{22} = 0.5$ are considered. The ratio between the total transmit power budget P_{tot} and the noise variance σ^2 is defined as pseudo-SNR, which is assumed to range from 0 dB to 30 dB. The ratio between the optimum power allocation P_1^* of (4.20) and the power budget P_{tot} versus the pseudo-SNR and β is plotted in Fig. 4.7 and Fig. 4.8 for the symmetric case and the asymmetric case, respectively. From Fig. 4.7 it can be seen that in the symmetric case the optimal power allocation P_1^* takes one of two values $\frac{P_{\text{tot}}}{2}$ and P_{tot}. In

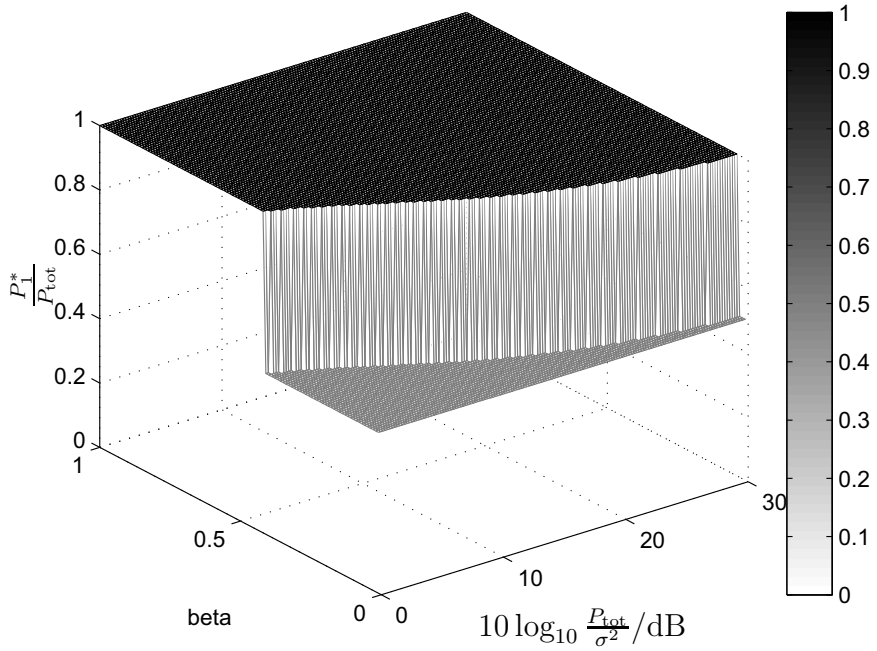

Figure 4.7: $\frac{P_1^*}{P_{\text{tot}}}$ versus pseudo-SNR and β ($g_{11} = g_{22} = 1$)

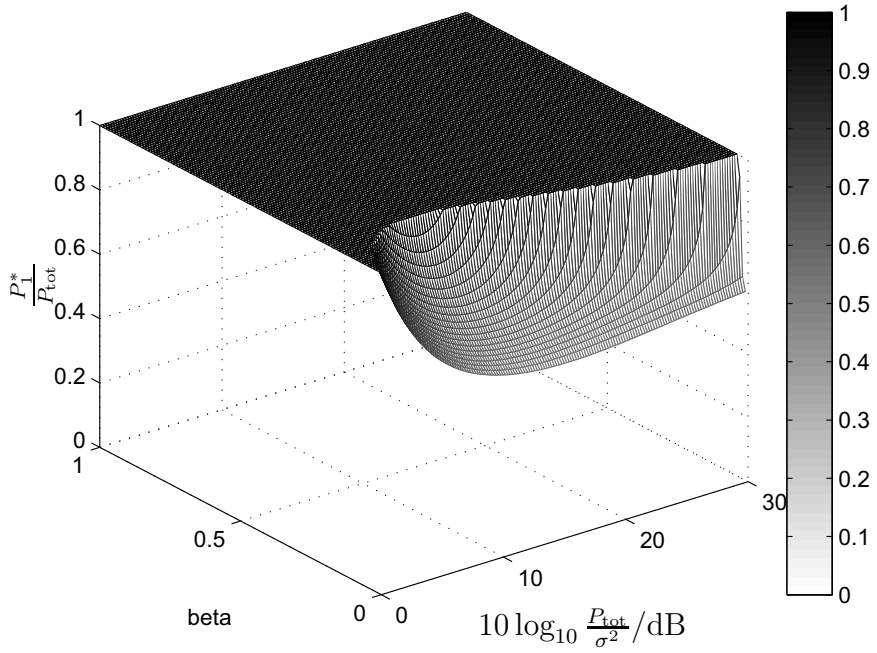

Figure 4.8: $\frac{P_1^*}{P_{\text{tot}}}$ versus pseudo-SNR and β ($g_{11} = 1$, $g_{22} = 0.5$)

other words, either equal or greedy power allocation is optimum according to [PJSL05]

$$P_1^* = \begin{cases} P_{\text{tot}}, & \beta \geq \frac{\sqrt{1+g_{11}P_{\text{tot}}/\sigma^2}-1}{g_{11}P_{\text{tot}}/\sigma^2} \\ \frac{P_{\text{tot}}}{2}, & \text{otherwise} \end{cases} . \tag{4.46}$$

For the asymmetric case, see Fig. 4.8, P_1^* is always greater than $\frac{P_{\text{tot}}}{2}$ as $g_{11} > g_{22}$. Moreover, greedy power allocation is optimum when β is big enough. The exact threshold of β beyond which greedy power allocation is optimum for the two-user interference channel model with (4.45) is derived in [PJSL05].

In the following the power allocation behavior in fading environments without the restriction of (4.45) is investigated. The real and imaginary parts of the complex channel coefficients $\underline{h}_{ji}$, $j, i = 1 \ldots J$, are assumed to be i.i.d. Gaussian variables with zero mean and variance $\frac{\sigma_{ji}^2}{2}$. Therefore, the amplitudes $\left|\underline{h}_{ji}\right|$ follow Rayleigh distributions and the channel gains g_{ji} are Chi-square distributed with two degrees of freedom and mean value of σ_{ji}^2. For each channel realization power allocation is performed. Equal power allocation is used as the initial power allocation in iterative waterfilling. Four exemplary channel models of the two-user interference channel are considered for the investigations, see Table 4.1.

Table 4.1: Exemplary channel models

	σ_{11}^2	σ_{12}^2	σ_{21}^2	σ_{22}^2	remark
I	1	1	1	1	strong interference
II	1	0.001	0.001	1	weak interference
III	1	0.1	0.1	1	moderate interference
IV	1	1	0.001	1	close-to-Z channel

Channel model I models i.i.d. Rayleigh fading channels. In this case the interference links and the useful links are on the average equally strong. Therefore, channel model I describes a strong interference scenario. The strong interference condition and very strong interference condition from information theory point of view are mathematically given in [Sat81]. Channel model II describes a weak interference environment where the average energies of the useful links are 30 dB higher than those of the interference links. For channel model III

the average energies of the interference links are 10 dB smaller than those of the useful links, which corresponds to a moderate interference scenario. Channel models I, II and III are statistically symmetric in the sense that $\mathrm{E}\{g_{11}\} = \mathrm{E}\{g_{22}\}$ and $\mathrm{E}\{g_{12}\} = \mathrm{E}\{g_{21}\}$, whereas channel model IV considers an asymmetric case where one interference link is much weaker than the other. In other words, it represents a close-to-Z channel model.

The ergodic sum rates resulting from the previously discussed power allocation schemes versus the pseudo-SNR are plotted in Figs. 4.9 – 4.12 for the four different channel models. Obviously, the optimum power allocation always presents an upper bound of the sum rate. The exhaustive search based noniterative waterfilling is near-optimum in all the considered scenarios. Furthermore, equal power allocation is inferior to conventional waterfilling independent of the channel models. As the pseudo-SNR increases equal power allocation approaches conventional waterfilling power allocation asymptotically. In all the exemplary channel models greedy power allocation yields the same performance since the strength of the interference links is irrelevant to it. In the high pseudo-SNR regime the sum rate resulting from greedy power allocation is approximately linear with the pseudo-SNR, which conforms to (4.25). It is also observed that greedy power allocation is close to conventional waterfilling in the low pseudo-SNR regime, which can be discerned from (4.28).

Particularly, see Fig. 4.9 corresponding to a strong interference scenario, both exhaustive search based noniterative waterfilling power allocation and greedy power allocation are near-optimum. Actually if $g_{11} = g_{22} = g_{12} = g_{21}$ holds snapshot wise the greedy scheme is strictly optimum, see (4.46). Iterative waterfilling performs worse than exhaustive search based noniterative waterfilling but surpasses decremental noniterative waterfilling. Since the strong crosscoupling interferences are neglected by conventional waterfilling, it has a much worse performance than iterative waterfilling and noniterative waterfilling, especially in the high pseudo-SNR regime. Among all the investigated power allocation strategies SIR balancing yields the lowest sum rate. The significant performance gap between SIR balancing and the optimum power allocation indicates that in strong interference scenarios to trade for balanced SIRs is very expensive in terms of sum rate.

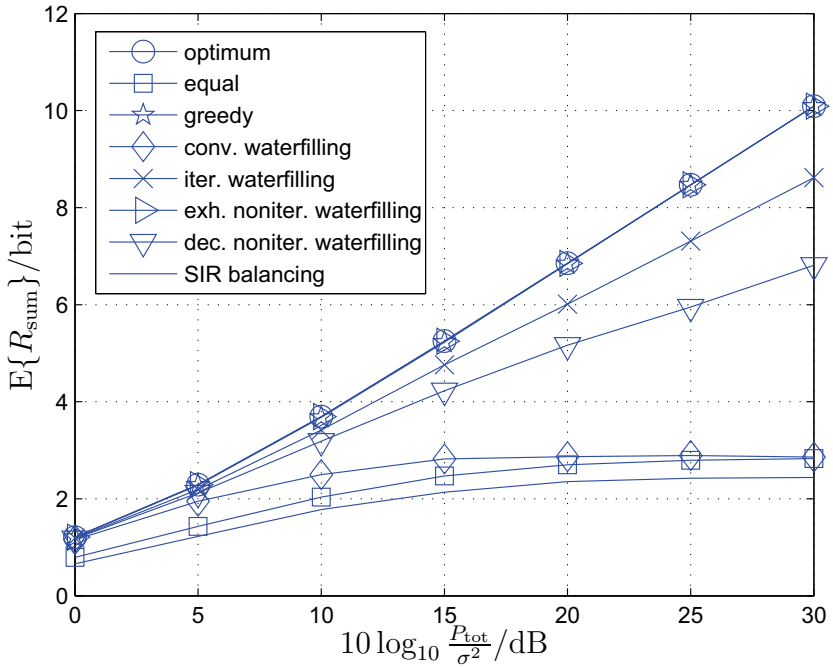

Figure 4.9: Ergodic sum rate in channel model I (strong interference)

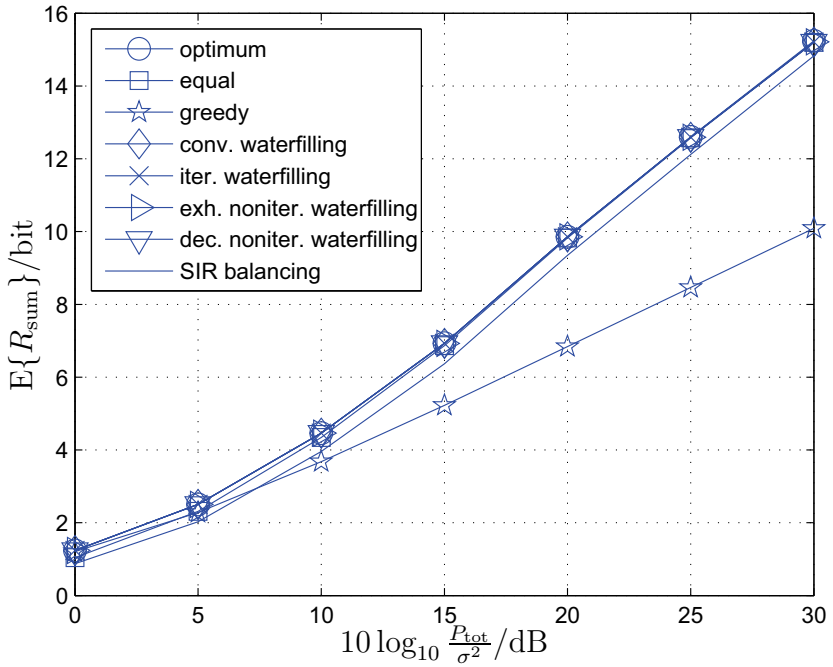

Figure 4.10: Ergodic sum rate in channel model II (weak interference)

Concerning channel model II which describes a weak interference environment, it can be seen from Fig. 4.10 that conventional waterfilling, iterative waterfilling and the noniterative waterfilling approaches are near-optimum. Recall that conventional waterfilling power allocation is optimum in parallel channels which is an extreme case of the weak interference environment. Both iterative waterfilling and noniterative waterfilling which take crosscoupling interferences into consideration show negligible performance gain over conventional waterfilling due to the very weak interference links. Out of the near-optimum power allocation schemes conventional waterfilling is preferable due to its lower complexity. Greedy power allocation performs much worse than the others, especially in the high pseudo-SNR regime of Fig. 4.10. As a matter of fact, greedy power allocation will become near-optimum when the pseudo-SNR approaches infinity, because in noise free scenarios allocating all transmit power to one user obviously makes the sum rate infinite. In weak interference scenarios SIR balancing performs sightly worse than the optimum power allocation and yields a much higher sum rate than greedy power allocation, which means balanced SIRs can be effectively achieved with a minor throughput loss in weak interference scenarios.

In moderate interference scenarios, see Fig. 4.11, it is interesting to observe that iterative waterfilling shows a better performance than greedy power allocation and conventional waterfilling power allocation in the medium range of the investigated pseudo-SNRs, although the performance gain is not so considerable. Decremental noniterative waterfilling power allocation performs similarly as iterative waterfilling. Greedy power allocation gets closer to the near-optimum exhaustive search based noniterative waterfilling power allocation as the pseudo-SNR increases.

Fig. 4.12 corresponds to the asymmetric close-to-Z channel. Because one of the two interference links is still strong enough, greedy power allocation is superior to decremental noniterative waterfilling and iterative waterfilling power allocation, especially in the high pseudo-SNR regime, which is similar to the behavior in channel model I except that here decremental noniterative waterfilling is slightly better than iterative waterfilling. Moreover, iterative waterfilling presents a visible gain over conventional waterfilling in the high pseudo-SNR

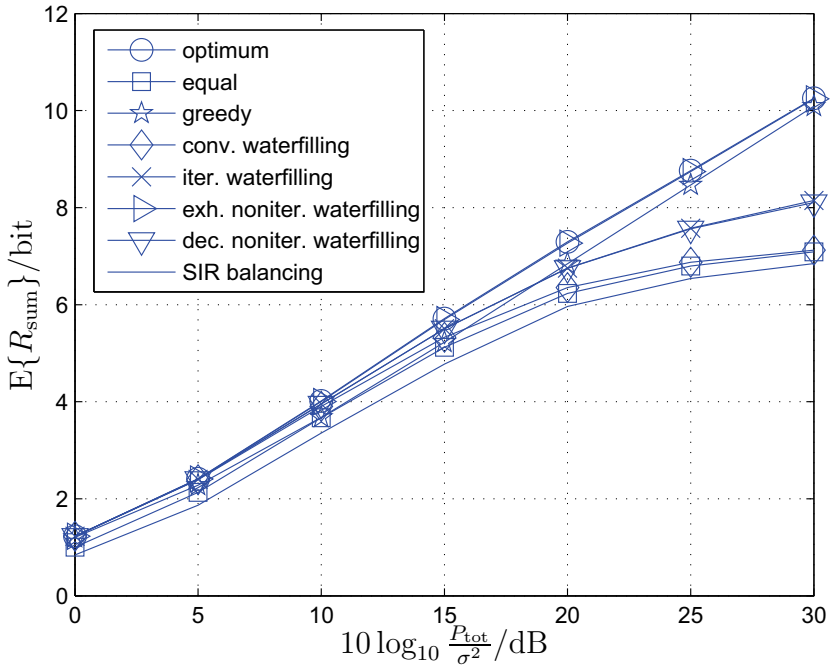

Figure 4.11: Ergodic sum rate in channel model III (moderate interference)

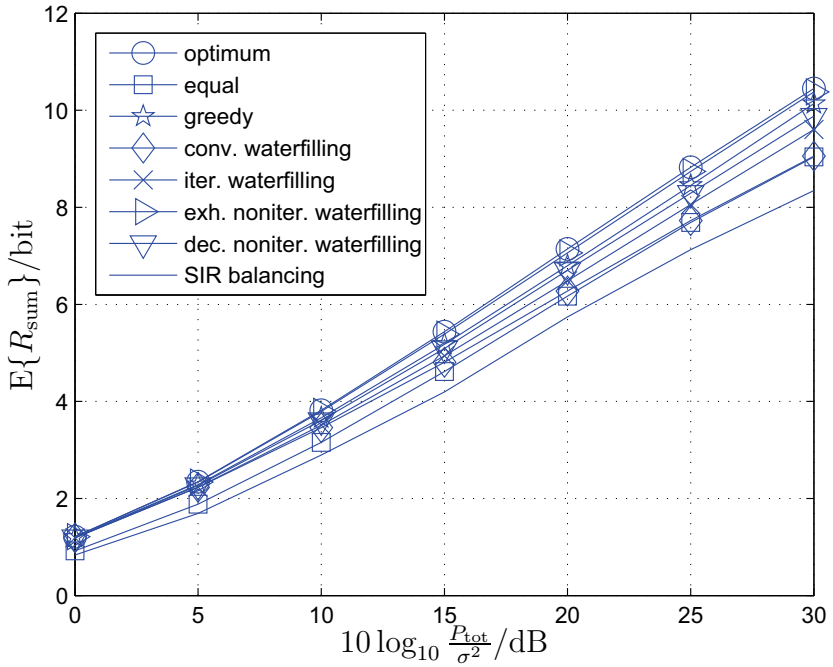

Figure 4.12: Ergodic sum rate in channel model IV (close-to-Z channel)

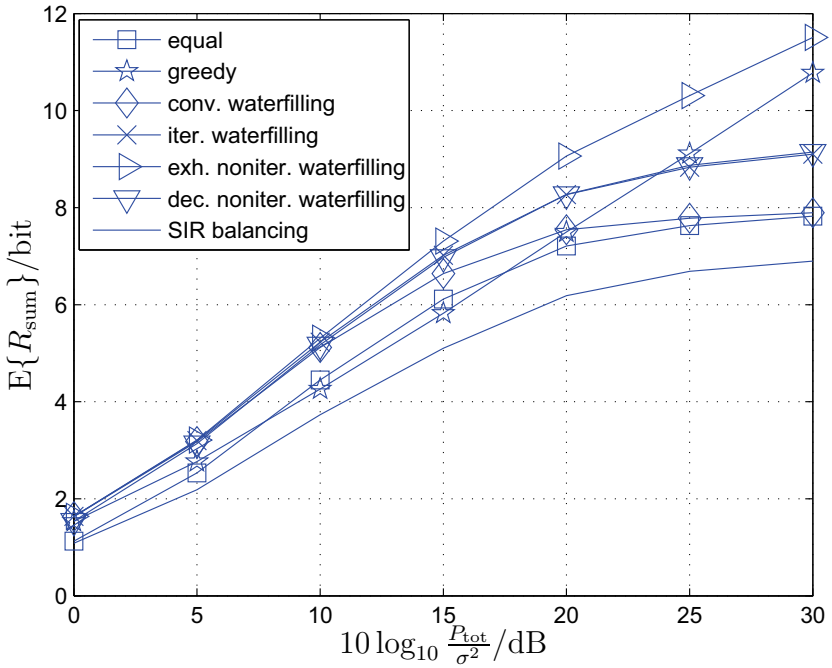

Figure 4.13: Ergodic sum rate in four-user interference channel (moderate interference)

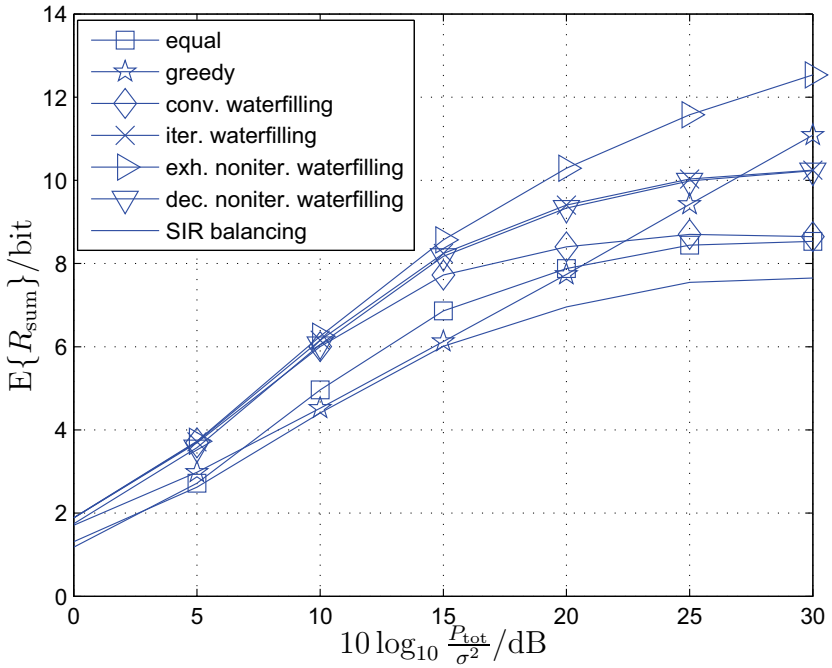

Figure 4.14: Ergodic sum rate in six-user interference channel (moderate interference)

regime. However, unlike in channel model I, here the performance gap is not so significant.

In scenarios with more than two users, the optimum power allocation and the corresponding sum rate are not known. Nevertheless, the suboptimum power allocation schemes are evaluated in Fig. 4.13 and Fig. 4.14 corresponding to $J = 4$ and $J = 6$, respectively. In both cases all useful links have average channel gain $\sigma_{jj}^2 = 1$ and all interference links have average channel gain $\sigma_{ji}^2 = 0.1$, $i \neq j$, i.e., moderate interference scenarios are considered. Comparing Fig. 4.11, Fig. 4.13 and Fig. 4.14 it can be seen that as the number of users increases the performance gain of exhaustive search based noniterative waterfilling power allocation over the other suboptimum power allocation schemes enlarges at a cost of exponentially growing complexity. Moreover, the performance gains of iterative waterfilling and decremental noniterative waterfilling over conventional waterfilling and greedy power allocation also increase in the medium range of the pseudo-SNR.

Although fairness is not the focus of this thesis, it is still interesting to compare the numbers of users getting positive transmit power resulting from different power allocation techniques. Apparently for greedy power allocation only one user gets positive transmit power, whereas for equal power allocation and SIR balancing all users are always active, representing two extremes of the fairness in the sense of the chance being active. For the other power allocation techniques the number of active users depends on the scenario under consideration. As shown in Fig. 4.15 corresponding to a six-user interference channel with moderate interference and pseudo-SNR being 20 dB, with a probability of greater than 0.75 all the 6 users will get positive transmit power after conventional waterfilling. Iterative waterfilling and decremental noniterative waterfilling have similar behavior that in most cases 4 or 5 users will be active. Exhaustive search based noniterative waterfilling is less fair since in most cases fewer users are active. Looking again at the sum rate performance presented in Fig. 4.14, one can easily observe the tradeoff between sum rate and fairness. Actually iterative waterfilling and decremental noniterative waterfilling show a good compromise.

The analysis in this section rely on the presence of thermal noise. In purely in-

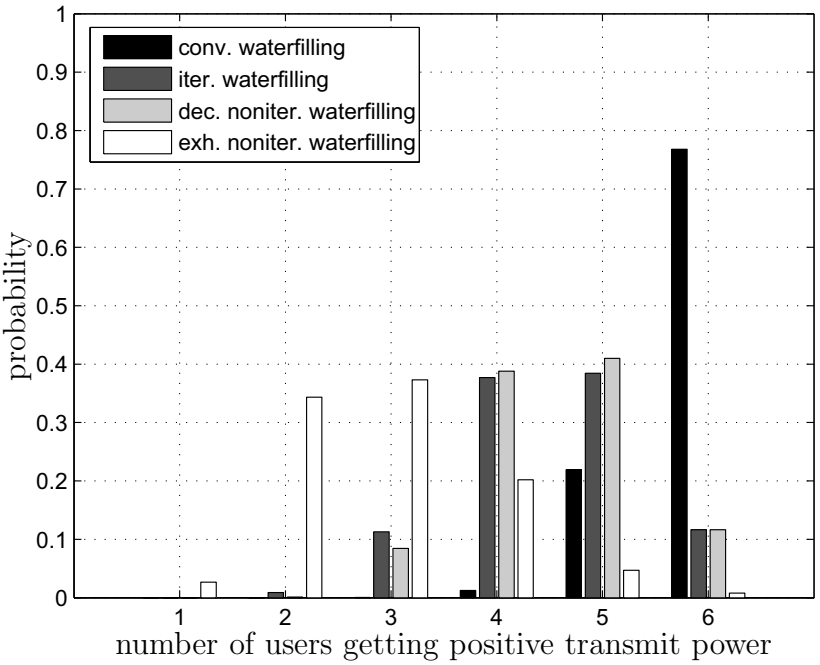

Figure 4.15: Fairness investigation of power allocation techniques in six-user interference channel (moderate interference, $10\log_{10}\frac{P_{\text{tot}}}{\sigma^2} = 20$ dB)

terference limited scenarios, i.e., $\sigma^2 = 0$, the greedy scheme is clearly optimum since it always yields an infinite sum rate, while conventional waterfilling will lead to equal power allocation which yields a finite sum rate. The proposed iterative waterfilling may result in a greedy or non-greedy power allocation in purely interference limited scenarios.

Chapter 5

Subcarrier and power allocation in service area networks

5.1 Preliminary remarks

With the continuously increasing demand for bandwidth consuming mobile communication services, the limited spectrum resources are becoming more and more valuable. Adaptive resource allocation techniques have been proven to be able to make use of the spectrum resources more efficiently and offer substantial performance improvement as compared to fixed resource allocation techniques. Moreover, multi-antenna systems, such as the SA based JOINT system, are drawing a lot of attention recently as they provide an additional dimension of resources in the spatial domain.

This chapter focuses on subcarrier and power allocation in SA networks. DL transmission which is more critical than the UL in data applications is considered. Joint subcarrier and power allocation determines subcarrier allocation and power allocation jointly at the same time and yields the optimum performance. However, such a joint optimization is prohibitively complex, especially in SDMA based systems such as the JOINT system. A possible solution is to decompose the joint optimization problem into two steps. In the first step

subcarrier allocation is determined with the assumption of equal power allocation. Once the subcarrier allocation is determined, the subcarrier specific channel matrix and the modulation matrix of (2.25) in the DL are fixed and the corresponding interference channel model can be obtained, based on which power allocation is performed in the second step. It is worth mentioning that the modulation matrix in the DL is assumed to be independent on the power allocation and to be dependent on subcarrier allocation only. In other words, the modulation matrix is not influenced even if one or more users get zero transmit power after power allocation. As a matter of fact, a higher energy efficiency can be achieved if the inactive users are excluded from the JT stage, which in turn can have an impact on power allocation. This makes the power allocation problem more challenging and also suggests a possibility to further improve the performance of SDMA based systems by joint power allocation and transceiver design [RFLT98, KT02, SB05, SBS05, BK08]. Within the scope of this thesis, however, we restrict ourself to fixed JT.

According to the two-step resource allocation strategy subcarrier allocation in SA networks will be addressed first in Section 5.2. In Section 5.3 power allocation in SA networks is described based on the discussions in Chapter 4.

5.2 Subcarrier allocation in service area networks

5.2.1 Overview

Depending on the optimization objectives the adaptive subcarrier allocation techniques in literature are usually classified into two categories: margin adaptive and rate adaptive. Margin adaptive subcarrier allocation aims at minimizing the total transmit power while meeting the date rate or BER requirements [WCLM99]. The objective of rate adaptive subcarrier allocation techniques is to maximize the sum rate of all users under total or individual power constraints [JL03, RC00].

Either margin adaptive or rate adaptive, the common idea behind adaptive subcarrier allocation is to allocate users to the subcarriers with good channel quality and suffering small interference. In SDMA based systems such as the JOINT system where the additional spatial dimension plays an important role, the correlation among users' spatial signatures has to be taken into consideration as well. In particular, weakly correlated users should be activated on the same subcarrier so that they can be easily spatially separated.

Depending on whether inter-SA interferences are considered, the subcarrier allocation techniques discussed in this chapter are categorized as interference-aware or interference-unaware subcarrier allocation. Interference-aware subcarrier allocation adapts to inter-SA interferences, which implies that subcarrier allocations in different co-channel SAs are mutually dependent. On the contrary, interference-unaware subcarrier allocation ignores inter-SA interferences while determining subcarrier allocation. As a consequence, interference-unaware subcarrier allocations in co-channel SAs become independent of each other and can be carried out separately in parallel, so that the complexity of subcarrier allocation is greatly reduced as compared to interference-aware subcarrier allocation techniques. Another advantage of interference-unaware subcarrier allocation techniques lies in the fact that they can be easily executed at the CUs of individual SAs, whereas interference-aware subcarrier allocation techniques usually necessitate a system-wide central controller or a sophisticated signalling scheme.

5.2.2 Optimum subcarrier allocation

Consider a SA network consisting of K_{S} co-channel SAs. There are N_{F} subcarriers available in each SA. Each SA contains K_{B} BSs and K_{M} MSs. For convenience the number K_{M} of MSs located in each SA is assumed to be a multiple of the number N_{F} of subcarriers, i.e.,

$$K_{\mathrm{M}} = \kappa N_{\mathrm{F}}, \quad \kappa \in \mathbb{N}. \tag{5.1}$$

Furthermore, we impose the restriction that every subcarrier supports the same number K of MSs in each SA. Hence if $\kappa \leq K$ holds all the K_{M} MSs will

be served. In reality adjacent subcarriers within the coherence bandwidth are strongly correlated. Subcarrier allocations in such scenarios usually treat these subcarriers as a unit so that signalling overhead can be saved and complexity of subcarrier allocation is reduced without significant performance degradation [OR05]. For the reason of simplification in the present thesis the fading processes on different subcarriers are assumed to be i.i.d. unless otherwise stated. Therefore, it is necessary to treat individual subcarriers rather than groups of adjacent subcarriers as allocation units. Nevertheless, the subcarrier allocation techniques discussed in this chapter can be extended to realistic scenarios by treating several strongly correlated adjacent subcarriers as one virtual subcarrier properly. All MSs are assumed to have identical traffic pattern and each MS is allowed to be active on at most one subcarrier.

The task of the optimum subcarrier allocation in a SA network is to allocate subcarriers to MSs so that the aggregate rate of all users in the considered system

$$R_{\text{sys}} = \sum_{k_{\text{S}}=1}^{K_{\text{S}}} \sum_{n_{\text{F}}=1}^{N_{\text{F}}} \sum_{k=1}^{K} R_k^{(n_{\text{F}};k_{\text{S}})} \tag{5.2}$$

is maximized. Introducing a subcarrier index n_{F} to (3.39) and assuming that all active users get the same transmit power P, the DL bit rate $R_k^{(n_{\text{F}};k_{\text{S}})}$ of the k-th active MS on subcarrier n_{F} in SA k_{S} is given by

$$R_k^{(n_{\text{F}};k_{\text{S}})} = \log_2 \left(1 + \frac{\dfrac{P}{\left[\left(\underline{\mathbf{H}}^{(n_{\text{F}};k_{\text{S}},k_{\text{S}})} \underline{\mathbf{H}}^{(n_{\text{F}};k_{\text{S}},k_{\text{S}})^{*\text{T}}} \right)^{-1} \right]_{k,k}}}{P \sum\limits_{k'_{\text{S}} \neq k_{\text{S}}} \sum\limits_{k'} \left| \left[\underline{\mathbf{H}}^{(n_{\text{F}};k_{\text{S}},k'_{\text{S}})} \underline{\mathbf{M}}^{(n_{\text{F}};k'_{\text{S}})} \right]_{k,k'} \right|^2 + \sigma^2} \right). \tag{5.3}$$

For the sake of simplicity the subscript "D" standing for DL is dropped from the DL channel matrices. The subcarrier specific DL channel matrices $\underline{\mathbf{H}}^{(n_{\text{F}};k_{\text{S}},k'_{\text{S}})}$, $k'_{\text{S}} = 1 \ldots K_{\text{S}}$, result from subcarrier allocation in SA k_{S}. Introduce the subcarrier and SA specific allocation indicating vector

$$\mathbf{x}^{(n_{\text{F}};k_{\text{S}})} = \left(x_1^{(n_{\text{F}};k_{\text{S}})} \ldots x_{K_{\text{M}}}^{(n_{\text{F}};k_{\text{S}})} \right)^{\text{T}} \tag{5.4}$$

whose elements are binary variables defined according to

$$x_{k_{\text{M}}}^{(n_{\text{F}};k_{\text{S}})} = \begin{cases} 1, & \text{MS } k_{\text{M}} \text{ is active on subcarrier } n_{\text{F}} \text{ in SA } k_{\text{S}} \\ 0, & \text{otherwise} \end{cases}. \tag{5.5}$$

Let $\underline{\mathbf{H}}_{\text{tot}}^{(n_\text{F};k_\text{S},k'_\text{S})}$ denote the total DL channel matrix of dimension $K_\text{M} \times K_\text{B}$ containing the CTFs on subcarrier n_F from the K_B BSs in the k'_S-th SA to the K_M MSs in the k_S-th SA and $\text{extr}(\mathbf{A}, \mathbf{b})$ indicate the operation of extracting the rows of matrix $\mathbf{A}$ corresponding to the non-zero elements of vector $\mathbf{b}$, then $\underline{\mathbf{H}}^{(n_\text{F};k_\text{S},k'_\text{S})}$ of dimension $K \times K_\text{B}$ can be expressed by

$$\underline{\mathbf{H}}^{(n_\text{F};k_\text{S},k'_\text{S})} = \text{extr}\left(\underline{\mathbf{H}}_{\text{tot}}^{(n_\text{F};k_\text{S},k'_\text{S})}, \mathbf{x}^{(n_\text{F};k_\text{S})}\right), \tag{5.6}$$

i.e., $\underline{\mathbf{H}}^{(n_\text{F};k_\text{S},k'_\text{S})}$ includes only the MSs being active on subcarrier n_F.

The optimization of (5.2) is subject to

$$\sum_{k_\text{M}=1}^{K_\text{M}} x_{k_\text{M}}^{(n_\text{F};k_\text{S})} = K \leq K_\text{B}, \quad \forall n_\text{F}, k_\text{S} \tag{5.7}$$

because of the linear ZF constraint, and to

$$\sum_{n_\text{F}=1}^{N_\text{F}} x_{k_\text{M}}^{(n_\text{F};k_\text{S})} \leq 1, \quad \forall k_\text{S}, k_\text{M} \tag{5.8}$$

because each MS is allowed to be active on at most one subcarrier.

The complexity of the optimization problem mainly lies in the following factors:

- The mutual influence among the MSs in the same SA due to their correlated spatial signatures implies that the subcarrier allocation in a SA has to be jointly determined.
- The mutual influence among the MSs in different co-channel SAs due to inter-SA interferences implies that the subcarrier allocation in co-channel SAs has to be jointly determined.

Because of these factors an exhaustive search is in general unavoidable to get the optimum subcarrier allocation in a SA network. For the considered SA network the number of distinct system-wide subcarrier allocations is given by

$$\left(\frac{K_\text{M}!}{(K!)^{N_\text{F}}}\right)^{K_\text{S}}. \tag{5.9}$$

Even for very simple scenarios, e.g., $K_{\mathrm{M}} = 6$, $K = 2$, $N_{\mathrm{F}} = 3$ and $K_{\mathrm{S}} = 4$, there will be 90^4 distinct subcarrier allocations. Therefore, it is practically infeasible to find the optimum subcarrier allocation in multi-SA scenarios due to the prohibitively high complexity.

Note that the exponent K_{S} in (5.9) is a dominant factor that drives the complexity high. In order to reduce the complexity, an intuitive idea is to ignore the inter-SA interferences while performing subcarrier allocation, which allows independent subcarrier allocation in the co-channel SAs. By doing so, the system-wide optimization problem degenerates to multiple separate SA-wide optimization problems, i.e., one can optimize the sum rate of each SA

$$\begin{aligned} R_{\mathrm{SA}} &= \sum_{n_{\mathrm{F}}=1}^{N_{\mathrm{F}}} \sum_{k=1}^{K} R_k^{(n_{\mathrm{F}})} \\ &= \sum_{n_{\mathrm{F}}=1}^{N_{\mathrm{F}}} \sum_{k=1}^{K} \log_2 \left(1 + \frac{P}{\sigma^2 \left[\left(\underline{\mathbf{H}}^{(n_{\mathrm{F}})} \underline{\mathbf{H}}^{(n_{\mathrm{F}})^{*\mathrm{T}}} \right)^{-1} \right]_{k,k}} \right) \end{aligned} \tag{5.10}$$

independently. The subcarrier specific DL channel matrix $\underline{\mathbf{H}}^{(n_{\mathrm{F}})}$ of dimension $K \times K_{\mathrm{B}}$ includes the K active MSs on subcarrier n_{F} in the considered SA and can be represented by

$$\underline{\mathbf{H}}^{(n_{\mathrm{F}})} = \mathrm{extr} \left(\underline{\mathbf{H}}_{\mathrm{tot}}^{(n_{\mathrm{F}})}, \mathbf{x}^{(n_{\mathrm{F}})} \right) \tag{5.11}$$

with $\underline{\mathbf{H}}_{\mathrm{tot}}^{(n_{\mathrm{F}})}$ and $\mathbf{x}^{(n_{\mathrm{F}})}$ denoting subcarrier specific intra-SA channel matrix of dimension $K_{\mathrm{M}} \times K_{\mathrm{B}}$ and subcarrier specific allocation indicating vector of length K_{M} for the considered SA, respectively. The side conditions for optimizing (5.10) are

$$\sum_{k_{\mathrm{M}}=1}^{K_{\mathrm{M}}} x_{k_{\mathrm{M}}}^{(n_{\mathrm{F}})} = K \leq K_{\mathrm{B}}, \quad \forall n_{\mathrm{F}} \tag{5.12}$$

and

$$\sum_{n_{\mathrm{F}}=1}^{N_{\mathrm{F}}} x_{k_{\mathrm{M}}}^{(n_{\mathrm{F}})} \leq 1, \quad \forall k_{\mathrm{M}}. \tag{5.13}$$

Unfortunately, due to matrix inversion in (5.10) an exhaustive search is still inevitable in order to get the SA-wide optimum subcarrier allocation. The number of distinct subcarrier allocations in a SA reads

$$\frac{K_{\mathrm{M}}!}{(K!)^{N_{\mathrm{F}}}} \tag{5.14}$$

and the total number of SA-wide subcarrier allocations to be examined in the considered network is

$$\frac{K_{\mathrm{S}}K_{\mathrm{M}}!}{(K!)^{N_{\mathrm{F}}}}. \tag{5.15}$$

Although the complexity is drastically reduced as compared to the system-wide optimization, such an exhaustive search is still infeasible in a realistic scenario, e.g., with $N_{\mathrm{F}} = 64$, $K_{\mathrm{M}} = 128$ and $K = 2$. Therefore, suboptimum subcarrier allocation techniques which avoid the exhaustive search should be developed. In the following subsections several such techniques are discussed. It is shown that they exploit the potential benefits of adaptive resource allocation to different extents and have different complexities.

5.2.3 Sequential subcarrier allocation

An alternative to joint subcarrier allocation as involved in solving the optimization problem in Subsection 5.2.2 is to determine subcarrier allocation for the MSs one after another in a sequential manner. At each step one conditional MS in the whole system is activated based on previous subcarrier allocations. A reasonable metric used to determine subcarrier allocation at each step could be the sum rate R_{sys} of (5.2), which is obviously interference-aware. The channel matrices involved in calculating the user specific bit rate (5.3) only consider the already activated MSs. The sequential subcarrier allocation procedure stops if all MSs in the system are activated or all subcarriers reach their maximum load.

A straightforward modification to the interference-aware sequential subcarrier allocation is the interference-unaware version, which is performed in different co-channel SAs independently. For SA-wide sequential subcarrier allocation

at each step one conditional MS in a specific SA is activated on a certain subcarrier based on previous subcarrier allocations in this SA. The used metric is the sum rate R_{SA} of (5.10) in the considered SA. This procedure stops if all MSs in the SA are activated or all subcarriers available in the SA reach their maximal load.

Either interference-aware or interference-unaware, a key issue of sequential subcarrier allocation is in which order the MSs are activated. One option is that at each step one of the inactive MSs is chosen based on a certain criterion and is activated. A reasonable criterion could be the sum rate of the network or the SA, depending on whether interference-aware or interference-unaware subcarrier allocation is concerned. A MS is activated if doing so yields a larger sum rate than activating any other MS. For such kind of optimized-order sequential subcarrier allocation, basically at each step every inactive MS in the MS pool and every available subcarrier needs to be examined. The number of times calculating the accumulated bit rate R_{sys} of (5.2) required to determine subcarrier allocation in the whole system is in the order of

$$\mathcal{O}\left(N_{\mathrm{F}} K_{\mathrm{S}}^2 K_{\mathrm{M}}^2\right), \tag{5.16}$$

i.e., the complexity is considerably reduced as compared to an exhaustive search. As to SA-wide sequential subcarrier allocation the complexity is in the order of

$$\mathcal{O}\left(N_{\mathrm{F}} K_{\mathrm{M}}^2\right). \tag{5.17}$$

Therefore, for interference-unaware sequential subcarrier allocation the number of times calculating the accumulated bit rate R_{SA} of a SA involved in the whole system is in the order of

$$\mathcal{O}\left(N_{\mathrm{F}} K_{\mathrm{S}} K_{\mathrm{M}}^2\right), \tag{5.18}$$

which is K_{S} times smaller than (5.16).

An alternative to optimized-order sequential subcarrier allocation could be that at each step a given MS is activated. The order in which the MSs are activated is known, either random or fixed. Since at each step the MS to be activated is known, only the available subcarriers need to be checked. Concerning the complexity, the interference-aware version requires to evaluate (5.2)

$\mathcal{O}\left(N_{\mathrm{F}}K_{\mathrm{M}}K_{\mathrm{S}}\right)$ times and the interference-unaware version requires to evaluate (5.10) $\mathcal{O}\left(N_{\mathrm{F}}K_{\mathrm{M}}K_{\mathrm{S}}\right)$ times. Obviously, the complexity of random- or fixed-order sequential subcarrier allocation is much lower than that of optimized-order sequential subcarrier allocation.

Due to the sequential nature both interference-aware and interference-unaware sequential subcarrier allocation can take advantage of the matrix inversion lemma [GVL86]. The inversion of a matrix that includes one more user can be easily obtained through linear computations with the previously obtained inversion of a smaller dimension matrix, see (3.16)-(3.18). This simplifies practical implementations.

5.2.4 Binary integer programming based subcarrier allocation

Ignoring interferences, the user specific bit rate is a function of its SNR. In conventional cellular networks, the SNR is uniquely determined by the channel gain for a given transmit power and the noise variance. However, in SA networks the correlations among users' spatial signatures have a great impact on their SNRs and impose the most dominant complexity in SA-wide optimum subcarrier allocation, which can be seen in (3.19) being the normalized SNR of a specific user in the UL. Applying channel reciprocity to (3.19) and introducing a subcarrier index n_{F} one directly obtains the subcarrier specific normalized SNR of the K-th active user in the DL

$$\tilde{\gamma}_K^{(n_{\mathrm{F}})} = \frac{\gamma_K^{(n_{\mathrm{F}})}}{\frac{P_K^{(n_{\mathrm{F}})}}{\sigma^2}} = \underline{\mathbf{h}}_K^{(n_{\mathrm{F}})^{*\mathrm{T}}} \underline{\mathbf{h}}_K^{(n_{\mathrm{F}})} - \underline{\mathbf{h}}_K^{(n_{\mathrm{F}})^{*\mathrm{T}}} \underline{\mathbf{H}}'^{(n_{\mathrm{F}})^{\mathrm{T}}} \left(\underline{\mathbf{H}}'^{(n_{\mathrm{F}})^{*}} \underline{\mathbf{H}}'^{(n_{\mathrm{F}})^{\mathrm{T}}} \right)^{-1} \underline{\mathbf{H}}'^{(n_{\mathrm{F}})^{*}} \underline{\mathbf{h}}_K^{(n_{\mathrm{F}})}, \tag{5.19}$$

where $\underline{\mathbf{h}}_k^{(n_{\mathrm{F}})}$ denotes the spatial signature of the k-th active user on subcarrier n_{F} and $\underline{\mathbf{H}}'^{(n_{\mathrm{F}})} = \left(\underline{\mathbf{h}}_1^{(n_{\mathrm{F}})} \ldots \underline{\mathbf{h}}_{K-1}^{(n_{\mathrm{F}})} \right)^{\mathrm{T}}$ contains the spatial signatures of $K-1$ active users. The first term of (5.19) is actually the channel energy of the considered user and the second term depends on the correlations among the spatial signatures of all active users. If $\underline{\mathbf{h}}_K^{(n_{\mathrm{F}})}$ is orthogonal to $\underline{\mathbf{h}}_k^{(n_{\mathrm{F}})}$, $k \neq K$,

then the normalized SNR of the K-th active user is simply given by its channel energy and the corresponding rate reads

$$R_K^{(n_\mathrm{F})} = \log_2\left(1 + \frac{P_K^{(n_\mathrm{F})}}{\sigma^2}\left\|\underline{\mathbf{h}}_K^{(n_\mathrm{F})}\right\|_2^2\right). \tag{5.20}$$

In other words, the spatial signatures of the other users are irrelevant in the case of orthogonality.

The observations above suggest that if the correlations among users' spatial signatures are neglected then the SA-wide subcarrier allocation problem can be simplified. Map the users' subcarrier specific spatial signature vectors $\underline{\mathbf{h}}_{k_\mathrm{M}}^{(n_\mathrm{F})} = \left(\underline{H}_{k_\mathrm{M},1}^{(n_\mathrm{F})} \ldots \underline{H}_{k_\mathrm{M},K_\mathrm{B}}^{(n_\mathrm{F})}\right)^\mathrm{T}$, $k_\mathrm{M} = 1 \ldots K_\mathrm{M}$, onto their squared l_2 norms $\left\|\underline{\mathbf{h}}_{k_\mathrm{M}}^{(n_\mathrm{F})}\right\|_2^2 = \sum_{k_\mathrm{B}} \left|\underline{H}_{k_\mathrm{M},k_\mathrm{B}}^{(n_\mathrm{F})}\right|^2$ which characterize the channel energies. With the binary indicator $x_{k_\mathrm{M}}^{(n_\mathrm{F})}$ being one if MS k_M is active on subcarrier n_F and being zero otherwise, the SA-wide subcarrier allocation problem is written as

$$\max \sum_{n_\mathrm{F}} \sum_{k_\mathrm{M}} x_{k_\mathrm{M}}^{(n_\mathrm{F})} \log_2\left(1 + \frac{P}{\sigma^2}\left\|\underline{\mathbf{h}}_{k_\mathrm{M}}^{(n_\mathrm{F})}\right\|_2^2\right) \tag{5.21}$$

subject to (5.12) and to (5.13). This is a standard binary integer programming (BIP) problem [HL90]. There exist mature algorithms, e.g., the branch-and-bound method [HL90], to solve the BIP problem efficiently. For conventional cellular networks with $K_\mathrm{B} = 1$, the BIP problem degenerates into a maximum weighted bipartite matching problem [NKT89, SR06] which can be efficiently solved via the Hungarian method [NKT89]. This also suggests that the optimum cell-wide subcarrier allocation in conventional cellular networks is solvable without an exhaustive search. Since only channel gains are relevant to the metric, phases of the CTFs are not required.

Obviously, ignoring spatial correlations in SDMA based SA networks will lead to a performance degradation. To which extent the performance is degraded will be evaluated in Chapter 6.

5.2.5 Three dimensional channel gain array based subcarrier allocation

As suggested by (5.19), serving users with high channel gains and weakly correlated spatial signatures on the same subcarrier usually leads to high SNRs. Based on the fact that wide spatial separations between the users imply small correlations among their spatial signatures, see Section 3.1, a low complexity heuristic user selection algorithm based on the channel gain matrix is proposed in [WDM05] to solve the problem of selecting a group of users in a SA for a single subcarrier. This algorithm can be extended to multi-subcarrier cases.

The N_{F} subcarriers, K_{M} MSs and K_{B} BSs of the considered SA form the three dimensions of the channel gain array, see Fig. 5.1 for example. In three dimensional (3-D) channel gain array based subcarrier allocation the MSs are activated one by one. At each step the maximum entry in the channel gain array is selected, the corresponding MS is activated, and then the array is updated properly. Selecting the maximum entry coincides with the idea of activating MSs with high channel gains. Moreover, since the channel gains are mainly determined by the distances between the transmitters and receivers, a MS with high channel gain is probably close to a BS. In order to avoid the case that more than one MSs close to the same BS are activated on the same subcarrier, which implies strongly correlated spatial signatures, once an entry of the channel gain array is selected, the column corresponding to the BS on the subcarrier is excluded. This update mechanism ensures the activated MSs are close to different BSs and thus can be spatially well separated with high probability. Furthermore, as part of update the rows corresponding to the selected MS on all subcarriers of the channel gain array are excluded as well due to the restriction that each MS is allowed to be active on at most one subcarrier. This procedure is repeated till all MSs in the SA are activated or all subcarriers reach their maximal loads. The pseudo code of this algorithm is given in Fig. 5.2. The example shown in Fig. 5.1 demonstrates how the 3-D channel gain array is updated after selecting the first and second maximum entry. In this example MS 3 is activated on subcarrier 1 first and MS 5 is activated on subcarrier 2 afterwards.

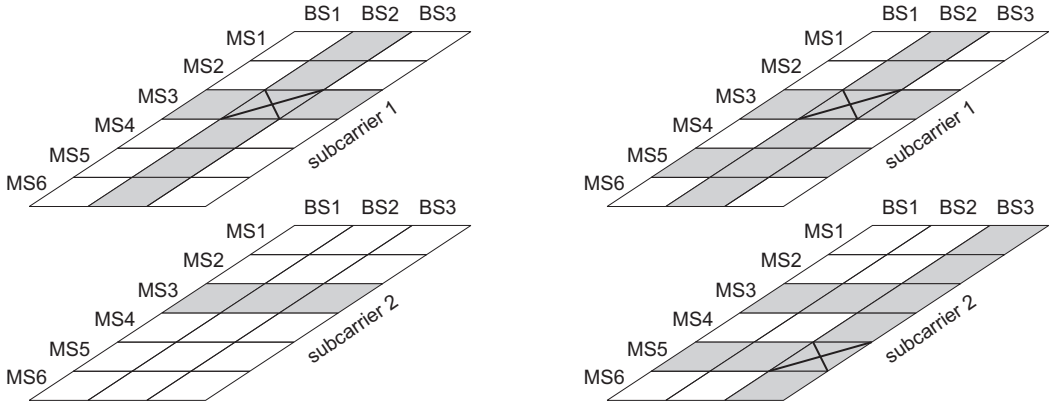

(a) array update after selecting the 1st entry

(b) array update after selecting the 2nd entry

Figure 5.1: 3-D channel gain array based subcarrier allocation ($K_{\mathrm{M}} = 6$, $K_{\mathrm{B}} = 3$, $N_{\mathrm{F}} = 2$). Each tile represents an entry of the 3-D channel gain array. Grey tiles are those being excluded.

for $q = 1 \ldots \min\{K_{\mathrm{M}}, K_{\mathrm{B}} N_{\mathrm{F}}\}$

$$(n_{\mathrm{F}}, k_{\mathrm{M}}, k_{\mathrm{B}}) = \underset{\substack{\check{n}_{\mathrm{F}} = 1 \ldots N_{\mathrm{F}} \\ \check{k}_{\mathrm{M}} = 1 \ldots K_{\mathrm{M}} \\ \check{k}_{\mathrm{B}} = 1 \ldots K_{\mathrm{B}}}}{\arg\max} \left| \underline{H}^{(\check{n}_{\mathrm{F}})}_{\check{k}_{\mathrm{M}}, \check{k}_{\mathrm{B}}} \right|^2$$

activate MS k_{M} on subcarrier n_{F}

$$\left| \underline{H}^{(\check{n}_{\mathrm{F}})}_{k_{\mathrm{M}}, \check{k}_{\mathrm{B}}} \right|^2 = -1, \quad \check{n}_{\mathrm{F}} = 1 \ldots N_{\mathrm{F}},\ \check{k}_{\mathrm{B}} = 1 \ldots K_{\mathrm{B}}$$

$$\left| \underline{H}^{(n_{\mathrm{F}})}_{\check{k}_{\mathrm{M}}, k_{\mathrm{B}}} \right|^2 = -1, \quad \check{k}_{\mathrm{M}} = 1 \ldots K_{\mathrm{M}}$$

Figure 5.2: Pseudo code of 3-D channel gain array based subcarrier allocation

Similar to the interference-unaware sequential subcarrier allocation, the 3-D channel gain array based subcarrier allocation technique also takes the spa-

tial correlations into account. On the other hand, thanks to its elegant entry selection and update mechanism the 3-D channel gain array based approach adapts to channel gains and spatial correlations in an implicit way and thus avoids computationally complex matrix inversions and requires no phase information of the CTFs. Therefore, it has much lower complexity than the interference-unaware sequential subcarrier allocation. As a matter of fact, the 3-D channel gain array based subcarrier allocation can also be interpreted as a sort of interference-unaware sequential subcarrier allocation technique in that the MSs are activated one after another in a sequential fashion. However, in the context of this thesis the term interference-unaware sequential subcarrier allocation is exclusively reserved for the technique described in Subsection 5.2.3.

In the case that the number of subcarriers is not sufficient to accommodate all the users, the entries of the 3-D array can be modified to take fairness into consideration. For instance, normalizing the instantaneous channel gains by the averaged channel gains allows a proportionally fair subcarrier allocation and all MSs have the same chance to be served regardless to whether they are closely located to the BSs or not [WDM05].

Certainly many other suboptimum algorithms for subcarrier allocation exist. For example, the maximum weighted bipartite matching based subcarrier allocation [SR06] proposed for conventional cellular networks can be applied in SA networks by establishing bipartite graphs [Wes00] weighted by channel gains in each cell separately. However, this thesis mainly focuses on the adaptive subcarrier allocation techniques proposed before.

5.2.6 Fixed subcarrier allocation

In addition to the previously discussed adaptive subcarrier allocation techniques, a conventional fixed subcarrier allocation will be considered for reference. Fixed subcarrier allocation means that subcarriers are fixedly or randomly assigned to MSs without adapting to channel conditions or interferences as long as the constraints (5.7) and (5.8) are satisfied. Detailed performance comparison between fixed and adaptive subcarrier allocation techniques will be provided in Chapter 6.

5.3 Power allocation in service area networks

5.3.1 Service area interference channel

As aforementioned power allocation is the second step after subcarrier allocation involved in decoupled subcarrier and power allocation, which is the focus of this section. Power allocation in generic interference channels under total power constraint has been studied in Chapter 4, where various power allocation strategies are discussed and their performances are investigated. However, it is still interesting to analyze power allocation in realistic networks such as OFDM based SA networks.

Rewriting (3.37) in a scalar representation form and introducing the subcarrier index n_{F} yields

$$\begin{aligned}\hat{\underline{d}}_k^{(n_{\mathrm{F}};k_{\mathrm{S}})} &= v_k^{(n_{\mathrm{F}};k_{\mathrm{S}})^{-\frac{1}{2}}}\sqrt{P_k^{(n_{\mathrm{F}};k_{\mathrm{S}})}}\underline{d}_k^{(n_{\mathrm{F}};k_{\mathrm{S}})} \\ &\quad + \sum_{k'_{\mathrm{S}}\neq k_{\mathrm{S}}}\sum_{k'}\left[\underline{\mathbf{H}}^{(n_{\mathrm{F}};k_{\mathrm{S}},k'_{\mathrm{S}})}\underline{\mathbf{M}}^{(n_{\mathrm{F}};k'_{\mathrm{S}})}\right]_{k,k'}\sqrt{P_{k'}^{(n_{\mathrm{F}};k'_{\mathrm{S}})}}\underline{d}_{k'}^{(n_{\mathrm{F}};k'_{\mathrm{S}})} \\ &\quad + \underline{n}_k^{(n_{\mathrm{F}};k_{\mathrm{S}})},\end{aligned} \tag{5.22}$$

where

$$v_k^{(n_{\mathrm{F}};k_{\mathrm{S}})} = \left[\left(\underline{\mathbf{H}}^{(n_{\mathrm{F}};k_{\mathrm{S}},k_{\mathrm{S}})}\underline{\mathbf{H}}^{(n_{\mathrm{F}};k_{\mathrm{S}},k_{\mathrm{S}})^{*\mathrm{T}}}\right)^{-1}\right]_{k,k}. \tag{5.23}$$

Comparing (5.22) with (4.1) it can be seen that a SA network is actually equivalent to a $J = N_{\mathrm{F}}KK_{\mathrm{S}}$ user interference channel. Suppose that user j is located in SA k_{S} and is active on subcarrier n_{F}, and that user i is located in SA k'_{S} and is active on subcarrier n'_{F}, $j, i = 1 \ldots N_{\mathrm{F}}KK_{\mathrm{S}}$. Their indices on the corresponding subcarriers are k and k', respectively. Hence the channel coefficients $\underline{h}_{ji}$ in the equivalent interference channel can be represented by

$$\underline{h}_{ji} = \begin{cases} v_k^{(n_{\mathrm{F}};k_{\mathrm{S}})^{-\frac{1}{2}}}, & n_{\mathrm{F}} = n'_{\mathrm{F}},\ k_{\mathrm{S}} = k'_{\mathrm{S}},\ k = k' \\ 0, & n_{\mathrm{F}} = n'_{\mathrm{F}},\ k_{\mathrm{S}} = k'_{\mathrm{S}},\ k \neq k' \\ \left[\underline{\mathbf{H}}^{(n_{\mathrm{F}};k_{\mathrm{S}},k'_{\mathrm{S}})}\underline{\mathbf{M}}^{(n_{\mathrm{F}};k'_{\mathrm{S}})}\right]_{k,k'}, & n_{\mathrm{F}} = n'_{\mathrm{F}},\ k_{\mathrm{S}} \neq k'_{\mathrm{S}} \\ 0, & n_{\mathrm{F}} \neq n'_{\mathrm{F}} \end{cases}. \tag{5.24}$$

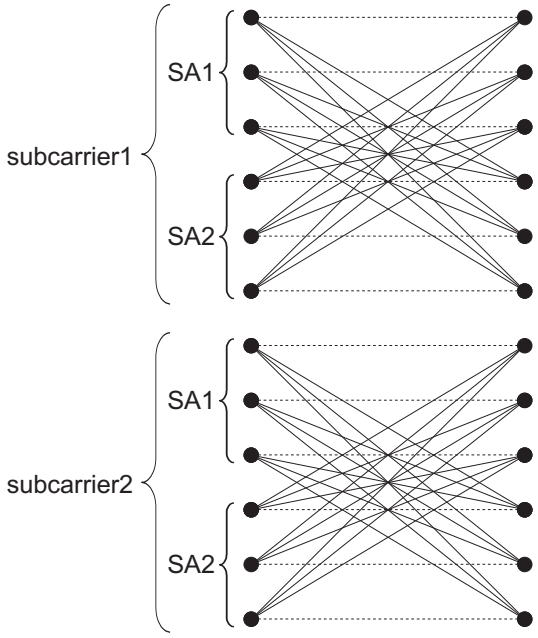

Figure 5.3: SA interference channel model ($K_{\mathrm{S}} = 2$, $N_{\mathrm{F}} = 2$, $K_{\mathrm{M}} = 6$). Solid lines: inter-SA co-channel interference links; dashed lines: useful links

It can be seen that $v_k^{(n_{\mathrm{F}};k_{\mathrm{S}})}$ of (5.23) is essentially the inverse of the useful link gain in the equivalent interference channel. One can also see that the intra-SA interference links vanish due to ZF JT applied in each SA. Only inter-SA interference links exist. Moreover, users active on different orthogonal subcarriers do not interfere with each other. Fig. 5.3 illustrates a 12-user interference channel which corresponds to a SA network with $K_{\mathrm{S}} = 2$ co-channel SAs and $N_{\mathrm{F}} = 2$ subcarriers. Each SA contains $K_{\mathrm{M}} = 6$ MSs.

Due to the inter-subcarrier interference free nature, an OFDM based SA network can be alternatively modelled as multiple subcarrier specific interference channels each having a smaller dimension than the overall interference channel. For instance, the exemplary illustration in Fig. 5.3 can also be viewed as two 6-user interference channels. The channel coefficients of subcarrier specific interference channel model can be represented by

$$\underline{h}_{ji}^{(n_{\mathrm{F}})} = \begin{cases} v_k^{(n_{\mathrm{F}};k_{\mathrm{S}})^{-\frac{1}{2}}}, & k_{\mathrm{S}} = k'_{\mathrm{S}},\ k = k' \\ 0, & k_{\mathrm{S}} = k'_{\mathrm{S}},\ k \neq k' \\ \left[\underline{\mathbf{H}}^{(n_{\mathrm{F}};k_{\mathrm{S}},k'_{\mathrm{S}})}\underline{\mathbf{M}}^{(n_{\mathrm{F}};k'_{\mathrm{S}})}\right]_{k,k'}, & k_{\mathrm{S}} \neq k'_{\mathrm{S}} \end{cases} \tag{5.25}$$

with $n_{\mathrm{F}} = 1 \ldots N_{\mathrm{F}}$ and $j, i = 1 \ldots KK_{\mathrm{S}}$. Although the degrees of freedom in optimizing power allocation are reduced, adopting the subcarrier specific interference channel model of (5.25) rather than the overall interference channel model of (5.24) gives the benefit of much lower complexity in adaptive power allocation because power allocation on different subcarriers are separated. Imagining a realistic OFDM based network whose bandwidth is subdivided into 1024 subcarriers, adaptive power allocation based on the overall interference channel model with a huge number of users would be extremely complex, while subcarrier-wise adaptive power allocation is probably still feasible. In order to distinguish from subcarrier-wise power allocation, the power allocation strategies based on the overall interference channel are termed as system-wide power allocation in the following. Given the total power constraint P_{tot} for system-wide power allocation, subcarrier-wise power allocation is constrained by $\frac{P_{\mathrm{tot}}}{N_{\mathrm{F}}}$.

Since SA networks can be modelled as interference channels, the suboptimum power allocation strategies discussed in Chapter 4 can be readily employed. These power allocation strategies are reviewed in the rest of this chapter, taking the intra-SA interference free and inter-subcarrier interference free transmission into consideration.

5.3.2 Signal-to-interference ratio balancing in service area networks

SIR balancing in an interference channel guarantees that all users perceive the same SIR level. In OFDM based networks such as SA networks, subcarrier-wise SIR balancing makes more sense than system-wide SIR balancing because it is usually sufficient to make co-channel users on the same subcarrier have the same SIR rather than forcing all users in the system to have the same SIR. Moreover, unlike system-wide SIR balancing, subcarrier-wise SIR balancing does not result in an entire system fairness, but it leads to less throughput loss in the meantime. Therefore, only subcarrier-wise SIR balancing in SA networks is addressed in this subsection.

The DL SINR of (3.38) in the absence of noise gives the DL SIR of user k in SA k_S

$$\gamma_k^{(k_\mathrm{S})} = \frac{P_k^{(k_\mathrm{S})}}{v_k^{(k_\mathrm{S})} \sum\limits_{k'_\mathrm{S} \neq k_\mathrm{S}} \sum\limits_{k'} \left| \left[\underline{\mathbf{H}}^{(k_\mathrm{S},k'_\mathrm{S})} \underline{\mathbf{M}}^{(k'_\mathrm{S})} \right]_{k,k'} \right|^2 P_{k'}^{(k'_\mathrm{S})}}. \tag{5.26}$$

Assuming all users active on the considered subcarrier perceive the same SIR level γ, then (5.26) can be rewritten as

$$\frac{1}{\gamma} P_k^{(k_\mathrm{S})} = v_k^{(k_\mathrm{S})} \sum_{k'_\mathrm{S} \neq k_\mathrm{S}} \sum_{k'} \left| \left[\underline{\mathbf{H}}^{(k_\mathrm{S},k'_\mathrm{S})} \underline{\mathbf{M}}^{(k'_\mathrm{S})} \right]_{k,k'} \right|^2 P_{k'}^{(k'_\mathrm{S})}. \tag{5.27}$$

Defining the diagonal matrix

$$\mathbf{V}^{(k_\mathrm{S})} = \begin{pmatrix} v_1^{(k_S)} & & \mathbf{0} \\ & \ddots & \\ \mathbf{0} & & v_K^{(k_\mathrm{S})} \end{pmatrix} \tag{5.28}$$

and stacking $\mathbf{V}^{(k_\mathrm{S})}$ of (5.28) for $k_\mathrm{S} = 1 \ldots K_\mathrm{S}$ into a diagonal matrix yields

$$\mathbf{V} = \begin{pmatrix} \mathbf{V}^{(1)} & & \mathbf{0} \\ & \ddots & \\ \mathbf{0} & & \mathbf{V}^{(K_\mathrm{S})} \end{pmatrix}, \tag{5.29}$$

which is related to the useful link gains of the subcarrier specific interference channel. The interference link gains of the subcarrier specific interference channel are contained in the matrix

$$\mathbf{W} = \begin{pmatrix} \mathbf{W}^{(1,1)} & \ldots & \mathbf{W}^{(1,K_\mathrm{S})} \\ \vdots & & \vdots \\ \mathbf{W}^{(K_\mathrm{S},1)} & \ldots & \mathbf{W}^{(K_\mathrm{S},K_\mathrm{S})} \end{pmatrix}. \tag{5.30}$$

with $\mathbf{W}^{(k_\mathrm{S},k'_\mathrm{S})} = \left\{ w_{k,k'}^{(k_\mathrm{S},k'_\mathrm{S})} \right\}$ defined as

$$w_{k,k'}^{(k_\mathrm{S},k'_\mathrm{S})} = \begin{cases} \left| \left[\underline{\mathbf{H}}^{(k_\mathrm{S},k'_\mathrm{S})} \underline{\mathbf{M}}^{(k'_\mathrm{S})} \right]_{k,k'} \right|^2, & k_\mathrm{S} \neq k'_\mathrm{S} \\ 0, & k_\mathrm{S} = k'_\mathrm{S} \end{cases}. \tag{5.31}$$

Hence the diagonal blocks of $\mathbf{W}$ are zero matrices. The overall power vector

$$\mathbf{p} = \left(\mathbf{p}^{(1)^{\mathrm{T}}} \dots \mathbf{p}^{(K_{\mathrm{S}})^{\mathrm{T}}}\right)^{\mathrm{T}} \tag{5.32}$$

corresponding to the subcarrier specific interference channel is composed of SA specific power vectors

$$\mathbf{p}^{(k_{\mathrm{S}})} = \left(P_1^{(k_{\mathrm{S}})} \dots P_K^{(k_{\mathrm{S}})}\right)^{\mathrm{T}}, \quad k_{\mathrm{S}} = 1 \dots K_{\mathrm{S}}. \tag{5.33}$$

With the above introduced notations (5.27) can be represented by

$$\frac{1}{\gamma} \cdot \mathbf{p} = \mathbf{VW} \cdot \mathbf{p}, \tag{5.34}$$

which is analogous to (4.8). In effect, $\mathbf{VW}$ can be interpreted as the normalized interference link gain matrix which describes an interference channel. According to the Perron-Frobenius theorem the balanced SIR level on the considered subcarrier is given by

$$\gamma = \frac{1}{\rho\left(\mathbf{VW}\right)} \tag{5.35}$$

and the vector $\frac{P_{\mathrm{tot}}}{N_{\mathrm{F}} \left\| \mathbf{p}_{\rho(\mathbf{VW})} \right\|_1} \mathbf{p}_{\rho(\mathbf{VW})}$ contains the allocated transmit powers.

5.3.3 Greedy power allocation in service area networks

As discussed in Chapter 4, the essential idea behind greedy power allocation in interference channels is to invest all transmit power budget to only one user at a time so that capacity limiting interferences are avoided. Concerning OFDM based SA networks, however, applying such a greedy scheme is obviously inefficient in terms of sum rate due to the inter-subcarrier interference free nature.

An intuitive idea to improve the performance of the system-wide greedy scheme in OFDM based SA networks is to apply subcarrier-wise greedy power allocation, i.e., for each subcarrier choose one MS which has the largest useful link gain

$$g_{\max}^{(n_{\mathrm{F}})} = \max \left\{ \frac{1}{v_k^{(n_{\mathrm{F}};k_{\mathrm{S}})}} \right\}, \quad n_{\mathrm{F}} = 1 \dots N_{\mathrm{F}}. \tag{5.36}$$

Since the chosen MSs are active on uncoupled subcarriers, apparently one could optimize the sum rate by distributing the total transmit power among these MSs according to the waterfilling principle rather than allocating power to all subcarriers evenly, namely

$$P^{(n_\mathrm{F})} = \left(P_\mathrm{W} - \frac{\sigma^2}{g_\mathrm{max}^{(n_\mathrm{F})}} \right)^+, \tag{5.37}$$

subject to

$$\sum_{n_\mathrm{F}} P^{(n_\mathrm{F})} = P_\mathrm{tot}. \tag{5.38}$$

5.3.4 Conventional waterfilling in service area networks

It is straightforward to apply conventional waterfilling power allocation in a SA network by modelling it as an interference channel. Such a system-wide waterfilling problem can be formulated as

$$P_k^{(n_\mathrm{F};k_\mathrm{S})} = \left(P_\mathrm{W} - \sigma^2 v_k^{(n_\mathrm{F};k_\mathrm{S})} \right)^+ \tag{5.39}$$

subject to

$$\sum_{n_\mathrm{F}} \sum_{k_\mathrm{S}} \sum_{k} P_k^{(n_\mathrm{F};k_\mathrm{S})} = P_\mathrm{tot}. \tag{5.40}$$

Modelling the SA network as multiple subcarrier specific interference channels, subcarrier-wise waterfilling

$$P_k^{(n_\mathrm{F};k_\mathrm{S})} = \left(P_\mathrm{W}^{(n_\mathrm{F})} - \sigma^2 v_k^{(n_\mathrm{F};k_\mathrm{S})} \right)^+ \tag{5.41}$$

reduces the complexity as compared to system-wide waterfilling. The power constraint for all subcarriers are the same, namely

$$\sum_{k_\mathrm{S}} \sum_{k} P_k^{(n_\mathrm{F};k_\mathrm{S})} = \frac{P_\mathrm{tot}}{N_\mathrm{F}}, \quad \forall n_\mathrm{F}. \tag{5.42}$$

In addition to system-wide waterfilling and subcarrier-wise waterfilling as described above, in SA networks one can also think of SA-wide waterfilling and subcarrier-wise SA-wide waterfilling which have different complexities. However, they are not addressed in this thesis.

5.3.5 Iterative waterfilling in service area networks

System-wide iterative waterfilling power allocation in SA networks means that the transmit power of user k active on subcarrier n_{F} in SA k_{S} is iteratively updated according to

$$P_k^{(n_{\mathrm{F}};k_{\mathrm{S}})}(l) = \left(P_{\mathrm{W}}(l) - \left(\sum_{k'_{\mathrm{S}}} \sum_{k'} w_{k,k'}^{(n_{\mathrm{F}};k_{\mathrm{S}},k'_{\mathrm{S}})} P_{k'}^{(n_{\mathrm{F}};k'_{\mathrm{S}})}(l-1) + \sigma^2 \right) v_k^{(n_{\mathrm{F}};k_{\mathrm{S}})} \right)^+ . \tag{5.43}$$

In all iterations the power constraint

$$\sum_{n_{\mathrm{F}}} \sum_{k_{\mathrm{S}}} \sum_{k} P_k^{(n_{\mathrm{F}};k_{\mathrm{S}})}(l) = P_{\mathrm{tot}} \tag{5.44}$$

must be met.

To reduce the complexity of system-wide iterative waterfilling which may be infeasible in realistic OFDM based SA networks one can perform subcarrier-wise iterative waterfilling as follows

$$P_k^{(n_{\mathrm{F}};k_{\mathrm{S}})}(l) = \left(P_{\mathrm{W}}^{(n_{\mathrm{F}})}(l) - \left(\sum_{k'_{\mathrm{S}}} \sum_{k'} w_{k,k'}^{(n_{\mathrm{F}};k_{\mathrm{S}},k'_{\mathrm{S}})} P_{k'}^{(n_{\mathrm{F}};k'_{\mathrm{S}})}(l-1) + \sigma^2 \right) v_k^{(n_{\mathrm{F}};k_{\mathrm{S}})} \right)^+ \tag{5.45}$$

subject to

$$\sum_{k_{\mathrm{S}}} \sum_{k} P_k^{(n_{\mathrm{F}};k_{\mathrm{S}})}(l) = \frac{P_{\mathrm{tot}}}{N_{\mathrm{F}}}, \quad \forall n_{\mathrm{F}}, l. \tag{5.46}$$

Similarly, decremental noniterative waterfilling can also be applied subcarrier-wise based on subcarrier specific interference channel model, but system-wide decremental noniterative waterfilling which is impractical in SA networks will be excluded from performance evaluation in Chapter 6. The exhaustive search based noniterative waterfilling will not be investigated either due to its prohibitively high complexity in SA networks.

Chapter 6

Performance evaluation of adaptive resource allocation in JOINT

6.1 Preliminary remarks

This chapter focuses on evaluating the performance of adaptive resource allocation in SA networks. Both quantitative and qualitative behaviors of various resource allocation techniques depend quite a lot on the scenario under consideration such as network configuration, user distribution and channel condition. For instance, changing the SA size or cluster size will alter the interference level and the interferer diversity which in turn affect the performance of interference adaptive resource allocation techniques. As another example, frequency selectivity of the channels can influence the gain of adaptive subcarrier allocation a lot. Therefore, a common physical scenario is absolutely necessary for a fair performance comparison. For this purpose a reference scenario will be introduced in Section 6.2 first. In order to investigate the characteristics of various resource allocation techniques under different circumstances several variations based on the reference scenario will also be considered later on. The figure of merit used in performance evaluation is described in Section 6.2 as well.

As mentioned before joint subcarrier and power allocation is decomposed into two separate stages for complexity reason, hence the performance should be investigated in two steps accordingly. In Section 6.3 the performance of subcarrier allocation with equal power allocation will be analyzed first. How various subcarrier allocation techniques benefit from adapting to frequency selectivity, spatial correlation and interferences will be examined. Afterwards in Section 6.4 the simulation results of different power allocation strategies in conjunction with a specific subcarrier allocation technique will be presented and discussed.

6.2 Simulation model

6.2.1 Reference scenario

A fair performance evaluation necessitates a common scenario. To this end we will mainly consider the reference multi-SA scenario depicted in Fig. 6.1. It represents a SA network consisting of $K_{\mathrm{S}} = 4$ SAs and each SA is composed of $K_{\mathrm{B}} = 3$ cells. The BSs equipped with single antenna elements are located at the center of their corresponding cells. The cell radius is 250 m. Universal frequency reuse is assumed, i.e., the cluster size r is one. $N_{\mathrm{F}} = 8$ subcarriers are available in each SA. Moreover, it is assumed that the same number N_{F} of MSs are geographically randomly located in each cell with uniform distribution function. Thus each SA contains $K_{\mathrm{M}} = K_{\mathrm{B}}N_{\mathrm{F}}$ MSs. The number K of MSs allowed to be simultaneously active on each subcarrier in each SA is equal to the upper bound K_{B}, unless otherwise stated. As a consequence, all the MSs will be served and the system will be fully loaded after performing subcarrier allocation. The MSs and the BSs are assumed to be synchronized.

The 12-cell scenario can alternatively be configured as a conventional cellular network with $K_{\mathrm{S}} = 12$ cells, i.e., the SA size K_{B} is one, see Fig. 6.2. The cluster size r is one as well. Based on the same physical scenario with different network configurations the behavior of various resource allocation techniques

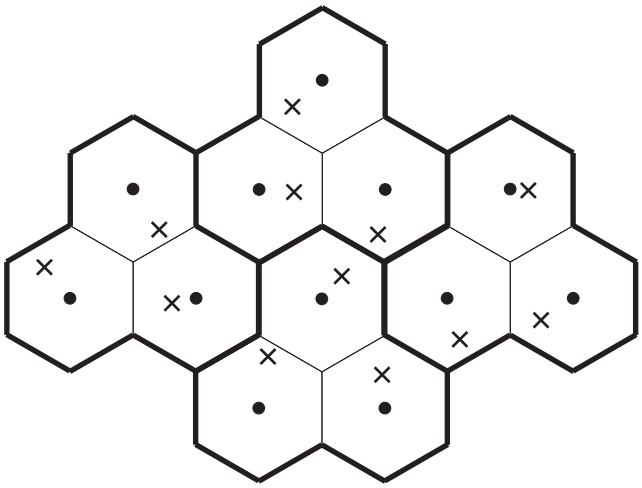

Figure 6.1: SA network with $K_{\mathrm{S}} = 4$, $K_{\mathrm{B}} = 3$, $r = 1$

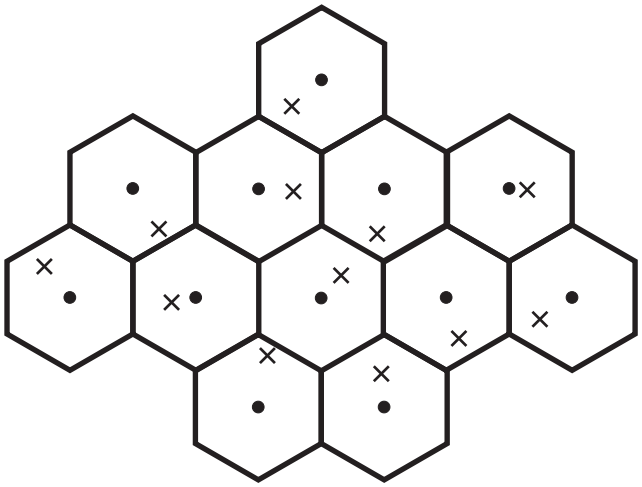

Figure 6.2: Conventional cellular network with $K_{\mathrm{S}} = 12$, $K_{\mathrm{B}} = 1$, $r = 1$

in SA networks and in conventional cellular networks will be compared in the following sections.

Establishing a proper channel model is an important prerequisite for evaluating wireless communication systems. There are a variety of path loss models available for describing the channel attenuation behavior. The main difference among them is an offset in the typical SNRs to be expected for a given pseudo-SNR. Hence for the sake of simplicity the distance dependent average channel

gains will be modelled by

$$\bar{G}(d) = \left(\frac{4\pi d}{\lambda}\right)^{-3} g_{\mathrm{T}} g_{\mathrm{R}} \tag{6.1}$$

in the following investigations. λ in (6.1) indicates the wavelength which is assumed to be 0.0545 m. The corresponding carrier frequency is 5.5 GHz. g_{T} and g_{R} denote the transmit antenna gain and receive antenna gain respectively, both being assumed to be one. (6.1) actually describes a single slope path loss model with path loss exponent of 3. Taking Rayleigh fading into account but ignoring shadowing, the subcarrier specific instantaneous channel transfer function can be represented by

$$\underline{H}^{(n_{\mathrm{F}})} = \bar{G}\left(I^{(n_{\mathrm{F}})} + \mathrm{j}Q^{(n_{\mathrm{F}})}\right), \tag{6.2}$$

where $I^{(n_{\mathrm{F}})}$ and $Q^{(n_{\mathrm{F}})}$ are i.i.d. Gaussian variables with zero mean and variance of 0.5. These Rayleigh fading processes on different subcarriers are assumed to be independent, which represents an extreme case of frequency selectivity, unless otherwise stated.

A total transmit power budget is assumed for the considered scenario. As described in Chapter 4 the quantity eventually relevant to the performance in a generic interference channel is the ratio between the total transmit power P_{tot} and the noise variance σ^2, which is termed pseudo-SNR. Equivalently, one can also specify the per resource pseudo-SNR, which is defined as the ratio between the average transmit power $\bar{P}$ per user per subcarrier and the noise variance σ^2 per subcarrier. Actually the per resource pseudo-SNR is physically more meaningful in a realistic network. In the simulations the per resource pseudo-SNR is assumed to be 150 dB, which corresponds to an almost noise free case, since we are interested in interference limited scenarios.

6.2.2 Figure of merit

The adaptive subcarrier and power allocation techniques discussed in Chapter 5 aim at optimizing the accumulated bit rate R_{sys} in the system. In reality, however, the performance is usually measured by the spectral efficiency η,

which can be obtained by normalizing the sum rate R_{sys} of (5.2) to the number of channel resources in the system, i.e.,

$$\eta = \frac{R_{\text{sys}}}{r K_{\text{S}} K_{\text{B}} N_{\text{F}}}. \tag{6.3}$$

The cluster size r in the denominator of the above expression is necessary because the number of subcarriers in the system required to achieve the performance has to be taken into account for a fair comparison.

6.3 Performance of subcarrier allocation

6.3.1 Performance evaluation in the reference service area scenario

In this subsection, the performance of different suboptimum subcarrier allocation techniques with equal power allocation in the SA network illustrated in Fig. 6.1 is investigated.

The fixed subcarrier allocation considered here can be described as follows: In every SA, K_{B} MSs are grouped together for each of the N_{F} subcarriers in a way that in each of the K_{B} cells exactly one MS is randomly selected for the subcarrier. Since N_{F} MSs are assumed to be located in each cell, this procedure ensures that the MSs within the same cell are active on different subcarriers and co-channel MSs are always located in different cells. The optimized-order sequential subcarrier allocation will not be examined due to its prohibitively high complexity. For the sake of simplicity sequential subcarrier allocation exclusively refers to the random-order sequential subcarrier allocation in the following.

Fig. 6.3 shows the complementary cumulative distribution functions (CCDFs) of the spectral efficiencies corresponding to various subcarrier allocation techniques. First of all, it is interesting to note that the performance of fixed

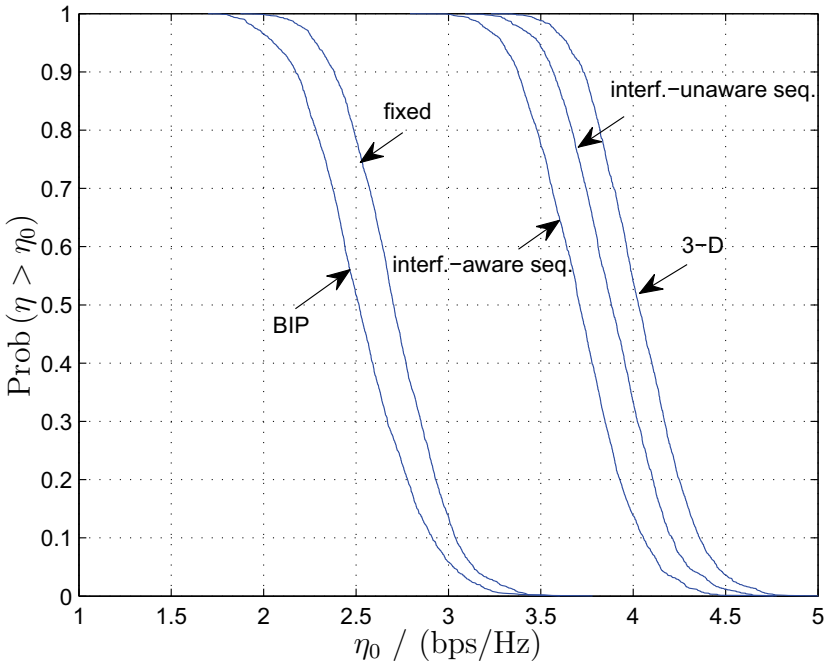

Figure 6.3: Spectral efficiency CCDFs in a SA network with $K_{\mathrm{B}} = 3$, $r = 1$, $K_{\mathrm{S}} = 4$ and $N_{\mathrm{F}} = 8$

subcarrier allocation is even better than BIP based subcarrier allocation. Recall that the BIP based approach only adapts to channel energies without taking spatial correlations into account. In contrast, the fixed subcarrier allocation implicitly adapts to spatial correlations to some extent by grouping MSs located in different cells together without considering channel gains. The observed performance difference implies that the correlation of users' spatial signatures is a more critical factor in subcarrier allocation than channel gains. Adapting to both channel gains and spatial correlations, sequential subcarrier allocation and 3-D channel gain array based subcarrier allocation show significant performance improvement over BIP based subcarrier allocation and fixed subcarrier allocation. Among them the 3-D channel gain array based approach yields the best performance although its complexity is much lower than that of the other adaptive techniques. The intelligent user selection mechanism makes it a promising adaptive subcarrier allocation technique.

Furthermore, it is surprising to note that the performance of interference-aware

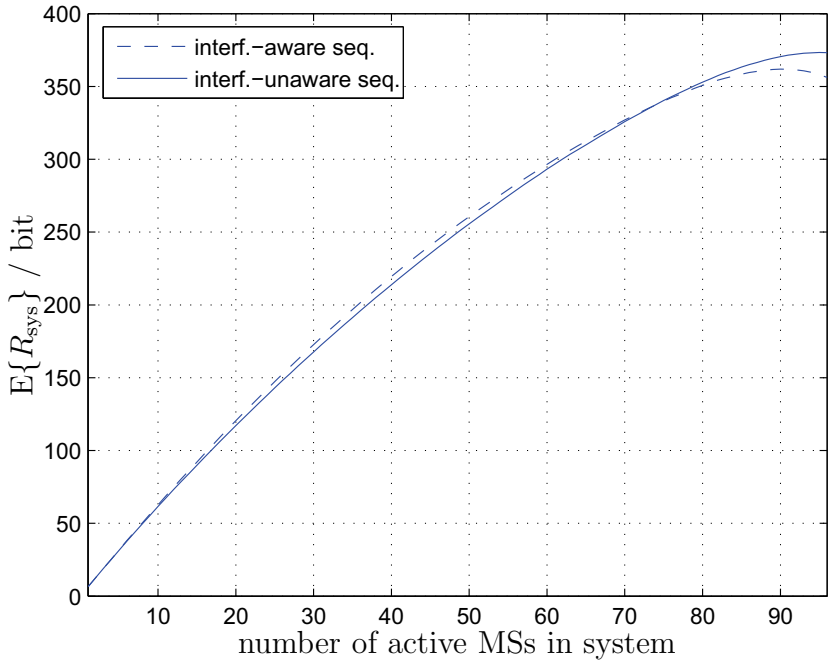

Figure 6.4: Averaged sum rate versus number of active MSs in a SA network with $K_{\mathrm{B}} = 3$, $r = 1$, $K_{\mathrm{S}} = 4$ and $N_{\mathrm{F}} = 8$

sequential subcarrier allocation is even worse than that of interference-unaware sequential subcarrier allocation, although the former additionally adapts to inter-SA interferences. To understand this phenomenon, the aggregated rate averaged over many simulations versus the number of MSs which are already activated in the system is plotted in Fig. 6.4. It can be seen that the sum rate resulting from interference-aware sequential subcarrier allocation is actually greater than that of interference-unaware sequential subcarrier allocation when there are not too many active MSs. However, when more and more MSs get active at a certain point it becomes inferior to interference-unaware sequential subcarrier allocation and in the range close to full system load the sum rate even drops instead of ramping up. The reason behind is that subcarrier allocation sequentially adapting to interferences caused by a few active MSs at the beginning phase may turn out to be unfavorable due to changed interference situation later on when the system approaches its full load. It is impractical to predict the interferences beforehand. This behavior suggests that an interfer-

Table 6.1: Ergodic spectral efficiency and outage spectral efficiency in a SA network with $K_{\mathrm{B}} = 3$, $r = 1$, $K_{\mathrm{S}} = 4$ and $N_{\mathrm{F}} = 8$

	$\mathrm{E}\{\eta\}$/ (bps/Hz)	η_{out}/ (bps/Hz)
fixed subcarrier allocation	2.71	2.38
BIP based subcarrier allocation	2.53	2.17
3-D channel gain array based subcarrier allocation	4.04	3.73
interference-unaware sequential subcarrier allocation	3.89	3.57
interference-aware sequential subcarrier allocation	3.71	3.38

ence adaptive subcarrier allocation technique with reasonable complexity, such as the interference-aware sequential subcarrier allocation, does not work well in fully loaded systems. It is not worth adapting to interferences in subcarrier allocation. It will be shown later, however, that power allocation can benefit from interference adaptation.

To enable a more precise comparison the spectral efficiency performance is quantified in terms of ergodic spectral efficiency $\mathrm{E}\{\eta\}$ and outage spectral efficiency η_{out}, which are listed in Table 6.1. The outage spectral efficiency is obtained according to

$$\mathrm{Prob}\left\{\eta < \eta_{\mathrm{out}}\right\} = P_{\mathrm{out}} \tag{6.4}$$

with the outage probability P_{out} being 0.1. In other words, with a probability of 0.1 the spectral efficiency η is smaller than the outage spectral efficiency η_{out}.

6.3.2 Service area networks versus conventional cellular networks

The major motivation of the SA concept is to reduce the capacity limiting interferences. To verify this quantitatively in Fig. 6.5 the spectral efficiency CCDFs for the conventional cellular network shown in Fig. 6.2 are plotted. The corresponding outage spectral efficiencies and ergodic spectral efficiencies are

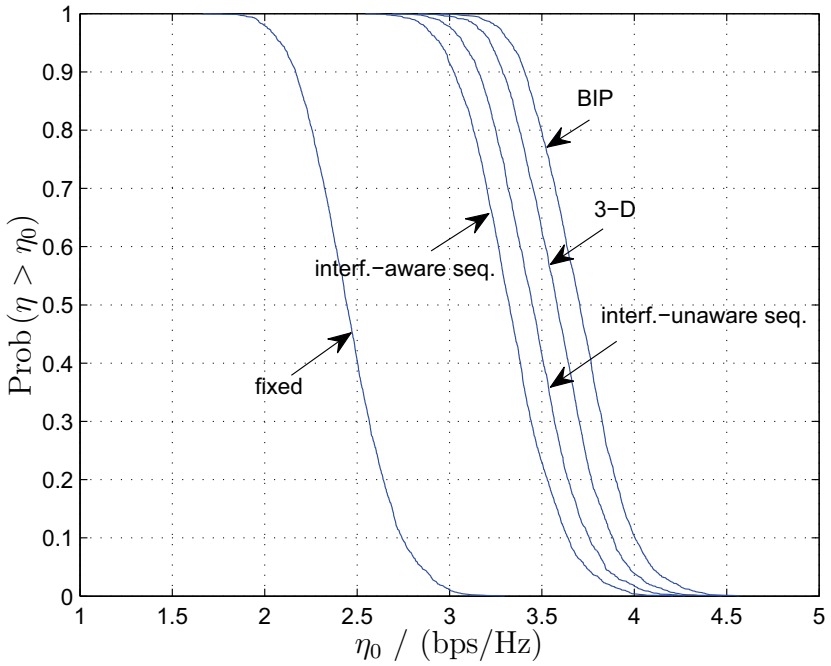

Figure 6.5: Spectral efficiency CCDFs in a conventional cellular network with $K_{\mathrm{B}} = 1$, $r = 1$, $K_{\mathrm{S}} = 12$ and $N_{\mathrm{F}} = 8$

Table 6.2: Ergodic spectral efficiency and outage spectral efficiency in a conventional cellular network with $K_{\mathrm{B}} = 1$, $r = 1$, $K_{\mathrm{S}} = 12$ and $N_{\mathrm{F}} = 8$

	$\mathrm{E}\{\eta\}$/ (bps/Hz)	η_{out}/ (bps/Hz)
fixed subcarrier allocation	2.45	2.17
BIP based subcarrier allocation	3.70	3.41
3-D channel gain array based subcarrier allocation	3.58	3.29
interference-unaware sequential subcarrier allocation	3.45	3.16
interference-aware sequential subcarrier allocation	3.33	3.02

listed in Table 6.2. Comparing these numerical results with those presented in Subsection 6.3.1 it can be seen that the SA network surpasses the conventional cellular network when using the same subcarrier allocation technique, except the BIP based subcarrier allocation. Since in each cell of a conventional cellular network every subcarrier can only support up to one user, the spatial correlation issue which is important in SA networks becomes irrelevant. Con-

sequently, the BIP based subcarrier allocation which shows poor performance in SA networks turns out to be the optimum cell-wide subcarrier allocation technique in conventional cellular networks and outperforms the others.

The comparison verifies the fact that capacity limiting interferences are reduced by employing the SA architecture and JT/JD. More precisely, the MSs close to the center of a SA suffer smaller interferences than those located at the same position in conventional cellular networks, while the MSs close to SA border experience similar interference levels as those being close to cell border in conventional cellular networks [DWA06]. Generally speaking, the spectral efficiency will become higher as the SA size increases. However, the performance enhancement is at a cost of complexity.

In high user density scenarios, e.g., typical urban areas, conventional cellular networks are severely interference limited. Hence the SA concept should be applied to reduce interferences and to improve the system performance. In low user density scenarios such as rural areas, however, it could be sufficient to deploy conventional cellular networks in order to save infrastructure cost. As conventional cellular networks are special cases of SA networks with SA size one, in principle SA networks with adjustable SA sizes can achieve the compromise between performance and complexity. This can be accomplished by replacing centralized signal processing with decentralized signal processing at individual BSs [WAD07]. Meanwhile, by doing so the performance of the MSs close to SA borders can be improved.

6.3.3 Exploitation of frequency selectivity

The performance of adaptive subcarrier allocation heavily relies on the frequency selectivity of the channels. Frequency selectivity characterizes the correlation among adjacent subcarriers. In previous subsections an extreme case of frequency selectivity is considered, i.e., for a specific channel between one MS and one BS the fading processes on different subcarriers are totally independent of each other and identically distributed. The opposite case is that the fading processes over the whole bandwidth are fully correlated, i.e.,

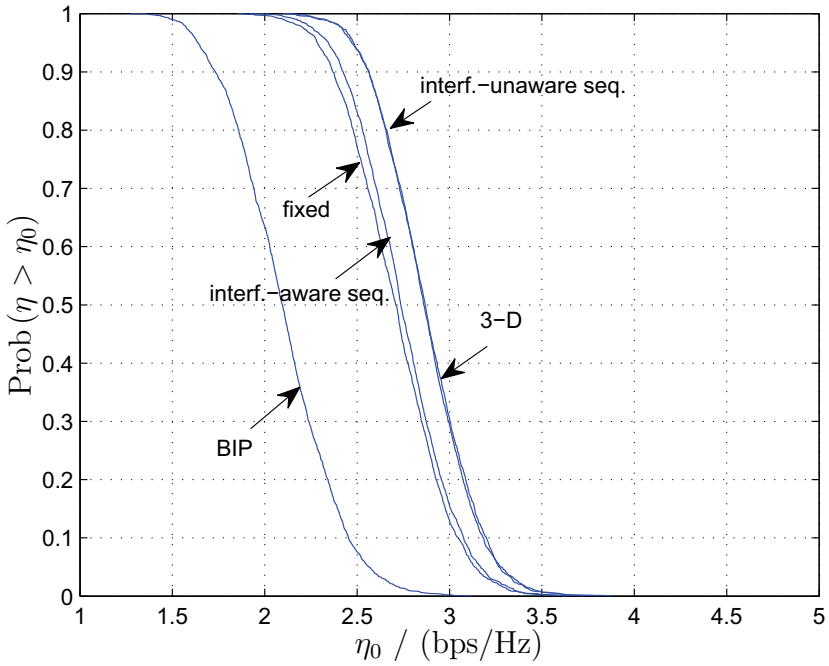

Figure 6.6: Spectral efficiency CCDFs in a SA network with $K_{\mathrm{B}} = 3$, $r = 1$, $K_{\mathrm{S}} = 4$ and $N_{\mathrm{F}} = 8$, flat fading

Table 6.3: Ergodic spectral efficiency and outage spectral efficiency in a flat fading scenario ($N_{\mathrm{F}} = 8$, $K_{\mathrm{B}} = 3$, $r = 1$, $K_{\mathrm{S}} = 4$)

	$\mathrm{E}\{\eta\}$/ (bps/Hz)	η_{out}/ (bps/Hz)
fixed subcarrier allocation	2.71	2.37
BIP based subcarrier allocation	2.10	1.73
3-D channel gain array based subcarrier allocation	2.87	2.57
interference-unaware sequential subcarrier allocation	2.87	2.56
interference-aware sequential subcarrier allocation	2.74	2.42

at a certain time instant the channel coefficients on all subcarriers are identical, which is known as flat fading. In order to evaluate to which extent the frequency selectivity affects subcarrier allocation, in Fig. 6.6 the performance of different subcarrier allocation techniques in flat fading scenario is investi-

gated. The corresponding ergodic and outage spectral efficiencies are listed in Table 6.3.

Comparing Fig. 6.6 and Table 6.3 with the results given in Subsection 6.3.1, it can be observed that fixed subcarrier allocation in a flat fading scenario has almost the same performance as in the i.i.d. fading case, since it does not harness frequency selectivity at all. For the other subcarrier allocation techniques which exploit frequency selectivity the performance degrades significantly in a flat fading scenario, especially for the interference-aware/-unaware sequential subcarrier allocation and the 3-D channel gain array based subcarrier allocation. In an i.i.d. fading scenario these techniques outperform fixed subcarrier allocation considerably, while in the flat fading case they only show a little performance improvement. This suggests that exploiting frequency selectivity of the channels is very beneficial. Moreover, the performance gap between BIP based subcarrier allocation and fixed subcarrier allocation becomes larger as compared to the i.i.d. fading case, which means even for frequency non-selective channels the way how the users are combined has a great impact on the performance. Indeed, in a flat fading scenario the BIP based subcarrier allocation adapts nothing at all, because the user specific channel energies $\left\|\underline{\mathbf{h}}_{k_\mathrm{M}}^{(n_\mathrm{F})}\right\|_2^2$ are identical on all subcarriers and the metric to be maximized in (5.21) for BIP based subcarrier allocation will be exactly the same regardless to how subcarriers are allocated as long as the number of MSs to be served is not greater than that the system can accommodate. Note that in scenarios where a lot of users compete for a limited number of subcarriers the BIP based subcarrier allocation can still benefit from multiuser diversity even for flat fading channels.

6.3.4 Adaptation of spatial correlation

As described in Chapter 3, multiple users in a SA can share a common subcarrier and part of the transmit energy has to be sacrificed for interference cancellation due to the correlated spatial signatures. The energy efficiency

ε_k of (3.26) is a proper measure of spatial correlation. In principle, grouping users together whose spatial signatures are weakly correlated yields high energy efficiencies.

Spatial correlation is a vital issue in SDMA based systems. Different subcarrier allocation techniques handle spatial correlations in different ways, which can be examined by comparing their energy efficiency CCDFs. Using the same scenario as in Subsection 6.3.1, from Fig. 6.7 it can be seen that the energy efficiency resulting from BIP based subcarrier allocation is significantly worse than the others. This is because the BIP based approach determines the subcarrier allocation exclusively according to absolute channel energies without considering spatial correlations. On the contrary, although the considered fixed subcarrier allocation technique doesn't adapt to channel gains, it ensures that co-channel users are physically located in different cells and thus implicitly avoids, at least to some extent, grouping strongly spatially correlated users together. As a consequence, its energy efficiency is much better than that of the BIP based approach. The energy efficiency performance is further improved by adapting to spatial correlations more effectively, as shown by the interference-aware/-unaware sequential subcarrier allocation and the 3-D channel gain array based subcarrier allocation. The interference-aware sequential subcarrier allocation yields a little smaller energy efficiency than the 3-D channel gain array based subcarrier allocation and the interference-unaware sequential subcarrier allocation, because adapting to interferences impairs the impact of spatial correlations on subcarrier allocation. Moreover, interference-unaware sequential subcarrier allocation outperforms 3-D channel gain array based subcarrier allocation in terms of energy efficiency, since in the former approach energy efficiency explicitly plays a role. Recall that the interference-unaware sequential subcarrier allocation sequentially optimizes the aggregate rate which is a function of the SNRs and the SNR is proportional to the product of energy efficiency and channel energy.

In short, the results shown in Fig. 6.7 indicate that spatial correlations are more important than absolute channel gains in subcarrier allocation. Nevertheless, it should be emphasized that the energy efficiency is not a unique concern for adaptive subcarrier allocation, because grouping users with weak spatial

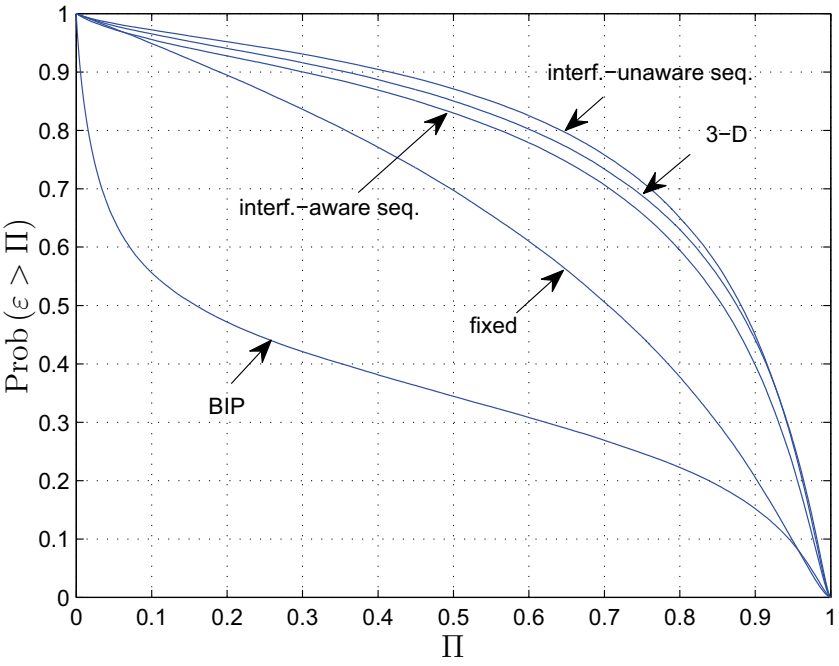

Figure 6.7: Energy efficiency CCDFs in a SA network with $K_{\mathrm{B}} = 3$, $K = 3$, $r = 1$, $K_{\mathrm{S}} = 4$ and $N_{\mathrm{F}} = 8$

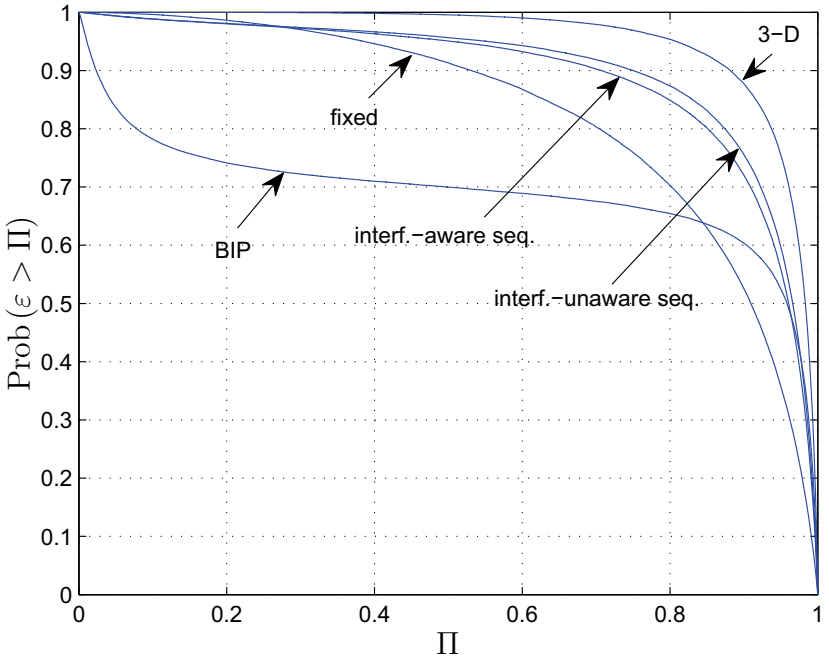

Figure 6.8: Energy efficiency CCDFs in a SA network with $K_{\mathrm{B}} = 3$, $K = 2$, $r = 1$, $K_{\mathrm{S}} = 4$ and $N_{\mathrm{F}} = 8$

correlations but low channel gains together can yield a small spectral efficiency. In fact, it is necessary to adapt to both spatial correlations and channel gains to obtain a good performance, as sequential subcarrier allocation and 3-D channel gain array based subcarrier allocation do.

It has been shown in Chapter 3 that the correlations among users' spatial signatures depend on the user distribution. Closely located co-channel users usually have strongly correlated spatial signatures. Besides, spatial correlations can also be affected by the load of a subcarrier, which is described by the ratio $\frac{K}{K_{\mathrm{B}}}$ between the number of subcarrier-sharing users and the maximum user capability of the subcarrier. Previously a fully loaded system is considered. Now we use the same physical scenario as in Subsection 6.3.1 but impose the restriction that each subcarrier is allowed to support up to $K = 2$ instead of $K = K_{\mathrm{B}} = 3$ MSs simultaneously, i.e., a load of $\frac{2}{3}$ is assumed. The remaining users are not served. The corresponding energy efficiency CCDFs are plotted in Fig. 6.8. One can easily see that the energy efficiencies are improved for all subcarrier allocation techniques, especially the BIP based subcarrier allocation. Furthermore, the 3-D channel gain array based subcarrier allocation results in higher energy efficiency than interference-unaware sequential subcarrier allocation, which is opposite to the fully loaded case. The reason is that multiuser diversity is exploited by the 3-D channel gain array based subcarrier allocation but not by the random-order sequential subcarrier allocation considered here.

The spectral efficiency performance corresponding to the non-fully loaded case is presented in Fig. 6.9 and Table 6.4. The most interesting observation is that the BIP based subcarrier allocation performs considerably better than in the fully loaded case. It even outperforms sequential subcarrier allocations as it harnesses multiuser diversity. On the other hand, however, the other subcarrier allocation techniques yield smaller spectral efficiencies as compared to the fully loaded case, which implies the improved energy efficiency is depleted for spectral efficiency from a system point of view. Nevertheless, it can be concluded that the higher the system load is, the more crucial spatial correlations are.

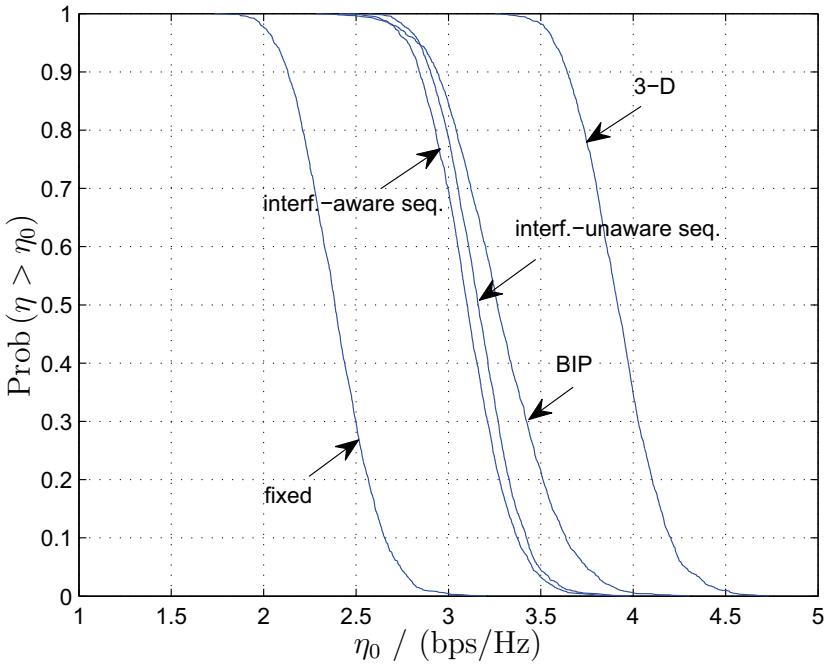

Figure 6.9: Spectral efficiency CCDFs in SA network with $K_{\mathrm{B}} = 3$, $K = 2$, $r = 1$, $K_{\mathrm{S}} = 4$ and $N_{\mathrm{F}} = 8$

Table 6.4: Ergodic spectral efficiency and outage spectral efficiency in a SA network with $K_{\mathrm{B}} = 3$, $K = 2$, $r = 1$, $K_{\mathrm{S}} = 4$ and $N_{\mathrm{F}} = 8$

	$\mathrm{E}\{\eta\}$/ (bps/Hz)	η_{out}/ (bps/Hz)
fixed subcarrier allocation	2.39	2.13
BIP based subcarrier allocation	3.28	2.94
3-D channel gain array based subcarrier allocation	3.92	3.64
interference-unaware sequential subcarrier allocation	3.16	2.90
interference-aware sequential subcarrier allocation	3.11	2.84

6.3.5 Interferer diversity and interference adaptation

Interferer diversity reflects to which extent the interferences originating from geographically distributed users are averaged [TV05]. A small interferer di-

versity means a minor interference averaging effect, i.e., the interference seen by a user is contributed by a single or few dominant interferers and is colorful. Contrarily, a very large interferer diversity indicates a strong interference averaging effect, i.e., the interference perceived by a user is more or less evenly contributed by many interferers and can be well approximated by white Gaussian noise. In [DWA06] it has been shown that SA networks have larger interferer diversity than conventional cellular networks. This is because the interferences from several neighboring cells, which are very likely to be dominant in conventional cellular networks, are eliminated in SA networks as intra-SA interferences. Recall that conventional cellular networks are special cases of SA networks with SA size one. In general, interferer diversity will become larger as the SA size increases. Besides SA size, the cluster size also has a great impact on interferer diversity. With the increase of the cluster size, not only interferences get significantly smaller due to distance incurred signal attenuation but also interferer diversity becomes much larger.

Interferer diversity influences the behavior of interference adaptive subcarrier allocation techniques, which can be verified by comparing interference-aware sequential subcarrier allocation and interference-unaware sequential subcarrier allocation in different scenarios. Recall that in case of universal frequency reuse with cluster size one, interference-aware sequential subcarrier allocation does yield a little higher accumulated rate than interference-unaware sequential subcarrier allocation for moderate system load, although for full system load the former performs worse, see Fig. 6.4. Whereas in case of frequency planning with cluster size being three, see Fig. 6.10, the curves for interference-aware and interference-unaware sequential subcarrier allocation almost overlap for the whole range, which means interference-aware sequential subcarrier allocation gains nothing from interference adaptation due to a large interferer diversity. This confirms that a small interferer diversity is beneficial to interference adaptive subcarrier allocation.

The spectral efficiency CCDFs for frequency planning with cluster size being three are depicted in Fig. 6.11 and the corresponding ergodic and outage spectral efficiencies are given in Table 6.5. Since interferences decrease considerably and become much less colorful as the cluster size increases, adapting to inter-

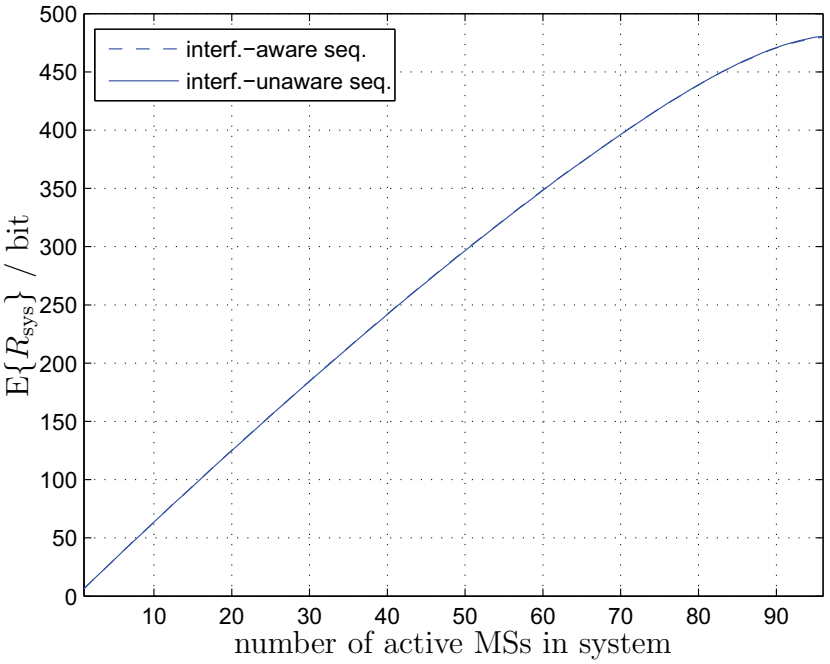

Figure 6.10: Averaged sum rate versus number of active MSs in a SA network with $K_{\mathrm{B}} = 3$, $r = 3$, $K_{\mathrm{S}} = 4$ and $N_{\mathrm{F}} = 8$

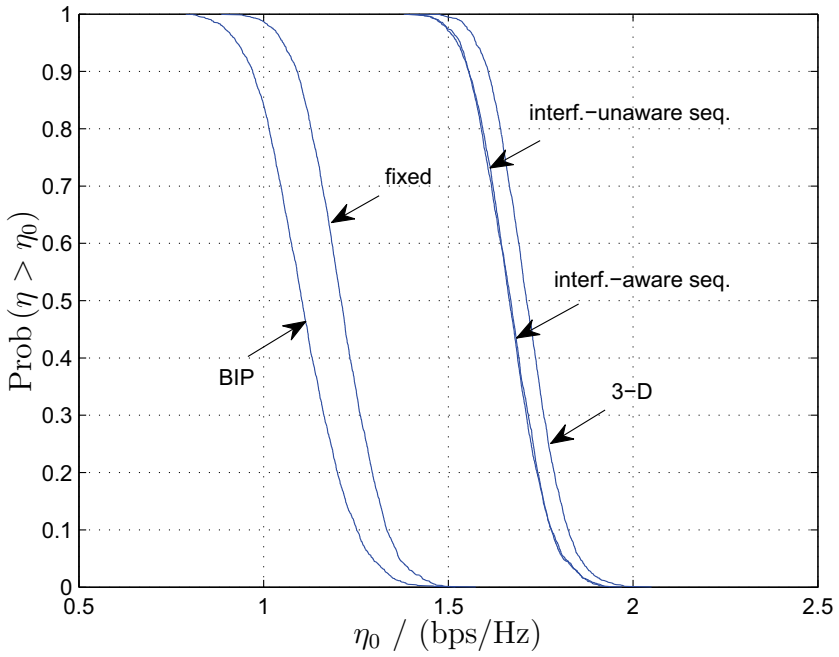

Figure 6.11: Spectral efficiency CCDFs in a SA network with $K_{\mathrm{B}} = 3$, $r = 3$, $K_{\mathrm{S}} = 4$ and $N_{\mathrm{F}} = 8$

Table 6.5: Ergodic spectral efficiency and outage spectral efficiency in a SA network with $K_{\mathrm{B}} = 3$, $r = 3$, $K_{\mathrm{S}} = 4$ and $N_{\mathrm{F}} = 8$

	$\mathrm{E}\{\eta\}$/ (bps/Hz)	η_{out}/ (bps/Hz)
fixed subcarrier allocation	1.21	1.09
BIP based subcarrier allocation	1.11	0.97
3-D channel gain array based subcarrier allocation	1.71	1.61
interference-unaware sequential subcarrier allocation	1.67	1.56
interference-aware sequential subcarrier allocation	1.67	1.56

ferences by interference-aware sequential subcarrier allocation has marginal influence on subcarrier allocation. As a consequence, there is no appreciable performance difference between interference-aware sequential subcarrier allocation and interference-unaware sequential subcarrier allocation. Moreover, for all of the subcarrier allocation techniques the spectral efficiencies in case of frequency planning degrade a lot in comparison to universal frequency reuse. Therefore, one can conclude that universal frequency reuse is more spectrum efficient than frequency planning when a proper subcarrier allocation technique is applied.

6.4 Performance of power allocation

6.4.1 Power allocation in the reference service area scenario

It has been revealed in Chapter 4 that in generic interference channels different power allocation strategies behave differently depending on the strength of the interference links. In the present section realistic SA networks are considered for analyzing the performance of various power allocation strategies discussed in Chapter 5.

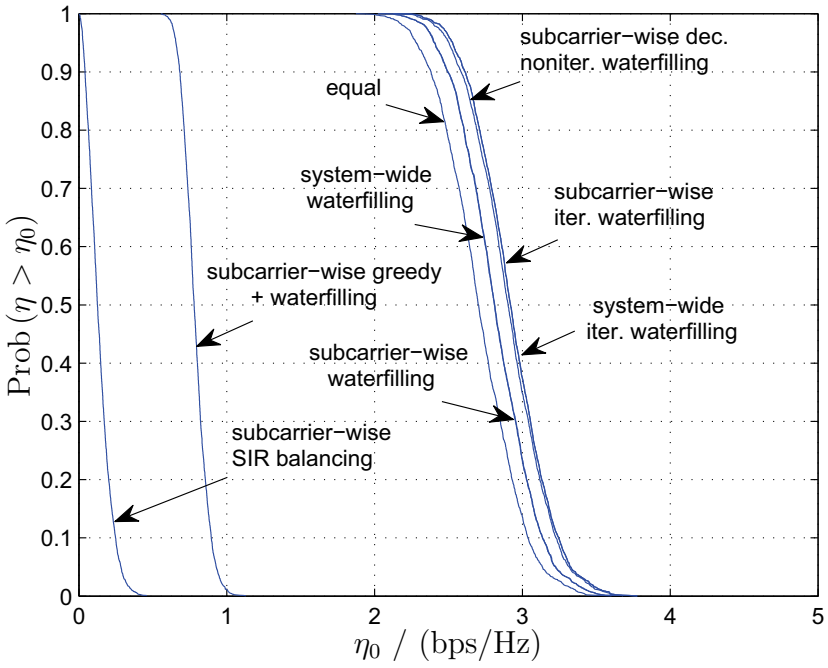

Figure 6.12: Spectral efficiency CCDFs in a SA network with $K_{\mathrm{B}} = 3$, $r = 1$, $K_{\mathrm{S}} = 4$ and $N_{\mathrm{F}} = 8$, applying fixed subcarrier allocation

Table 6.6: Ergodic spectral efficiency and outage spectral efficiency in a SA network with $K_{\mathrm{B}} = 3$, $r = 1$, $K_{\mathrm{S}} = 4$ and $N_{\mathrm{F}} = 8$, applying fixed subcarrier allocation

	$\mathrm{E}\{\eta\}$/ (bps/Hz)	η_{out}/ (bps/Hz)
equal power allocation	2.71	2.38
subcarrier-wise SIR balancing	0.14	0.04
subcarrier-wise greedy + waterfilling	0.79	0.68
system-wide waterfilling	2.82	2.50
subcarrier-wise waterfilling	2.82	2.49
system-wide iterative waterfilling	2.93	2.61
subcarrier-wise iterative waterfilling	2.93	2.61
subcarrier-wise decremental noniterative waterfilling	2.91	2.58

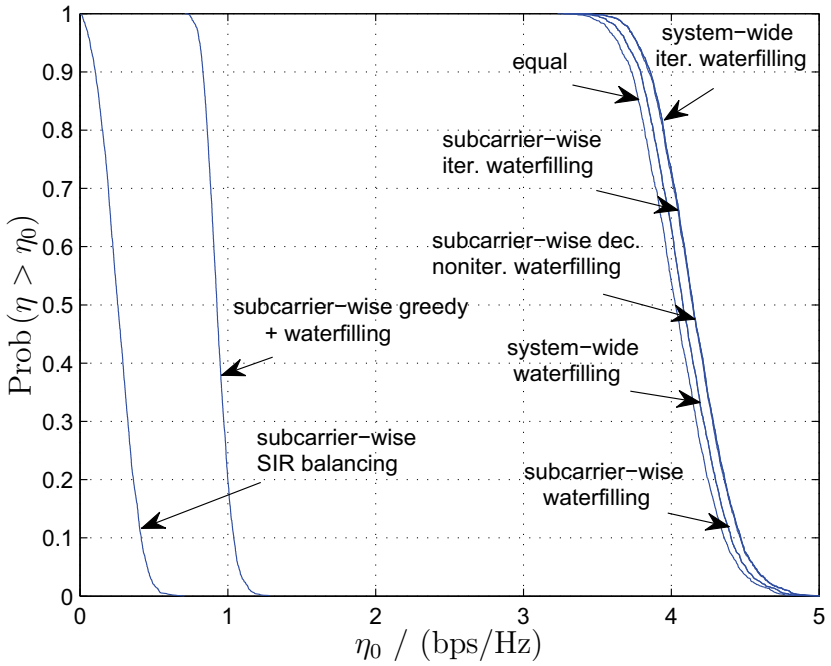

Figure 6.13: Spectral efficiency CCDFs in a SA network with $K_{\mathrm{B}} = 3$, $r = 1$, $K_{\mathrm{S}} = 4$ and $N_{\mathrm{F}} = 8$, applying 3-D channel gain array based subcarrier allocation

Table 6.7: Ergodic spectral efficiency and outage spectral efficiency in a SA network with $K_{\mathrm{B}} = 3$, $r = 1$, $K_{\mathrm{S}} = 4$ and $N_{\mathrm{F}} = 8$, applying 3-D channel gain array based subcarrier allocation

	$\mathrm{E}\{\eta\}$/ (bps/Hz)	η_{out}/ (bps/Hz)
equal power allocation	4.04	3.73
subcarrier-wise SIR balancing	0.26	0.10
subcarrier-wise greedy + waterfilling	0.93	0.83
system-wide waterfilling	4.09	3.79
subcarrier-wise waterfilling	4.09	3.79
system-wide iterative waterfilling	4.16	3.86
subcarrier-wise iterative waterfilling	4.16	3.86
subcarrier-wise decremental noniterative waterfilling	4.15	3.85

For reference let's first consider fixed subcarrier allocation as the subcarrier allocation technique being applied before power allocation. Using the reference scenario described in Subsection 6.2.1, the spectral efficiency CCDFs resulting from different power allocation strategies are plotted in Fig. 6.12. The corresponding ergodic and outage spectral efficiencies are listed in Table 6.6. It can be seen that subcarrier-wise iterative waterfilling performs as well as system-wide iterative waterfilling and shows marginal performance improvement over subcarrier-wise decremental noniterative waterfilling. Ignoring inter-SA interferences, system-wide waterfilling and subcarrier-wise waterfilling are inferior to the interference adaptive power allocation strategies including iterative waterfilling and decremental noniterative waterfilling. Recalling that interference-aware subcarrier allocation with affordable complexity is not so favorable, this actually suggests that interferences should be considered by power allocation rather than by subcarrier allocation. Equal power allocation yields significantly higher spectral efficiency than subcarrier-wise greedy power allocation. As the cost of subcarrier-wise fairness, subcarrier-wise SIR balancing performs the worst in terms of spectral efficiency. In short, the observed behavior of various power allocation strategies conforms to the results in generic interference channels with moderate interferences, which implies that the considered scenario can be treated as a moderate interference scenario in a statistical sense. Moreover, subcarrier-wise iterative waterfilling and subcarrier-wise waterfilling perform almost the same as system-wide iterative waterfilling and system-wide waterfilling, respectively. Therefore, subcarrier-wise power allocation strategies are preferable in OFDM based SA networks due to their lower complexity.

Due to its outstanding performance and low complexity as demonstrated in Section 6.3, the 3-D channel gain array based subcarrier allocation is chosen as the adaptive subcarrier allocation technique applied before power allocation in the following. The corresponding results are shown in Fig. 6.13 and Table 6.7. Compared to the performance resulting from fixed subcarrier allocation, the spectral efficiencies are enhanced. Furthermore, the performance gain of iterative waterfilling over equal power allocation applying 3-D channel gain array based subcarrier allocation shrinks as compared to applying fixed subcarrier allocation. Indeed, the better a subcarrier allocation technique per-

forms, the less gain can be obtained by adaptive power allocation. According to this trend, for an adaptive subcarrier allocation which offers very good performance it would be sufficient to apply equal power allocation rather than adaptive power allocation without much performance degradation.

6.4.2 Power allocation in a conventional cellular network

The performance of power allocation in the conventional cellular network depicted in Fig. 6.2 is addressed in this subsection. Because of the increased interferences as compared to a SA network, in the conventional cellular network the spectral efficiency performance of most considered power allocation strategies degrades, see Fig. 6.14 and Table 6.8. Note that subcarrier-wise greedy

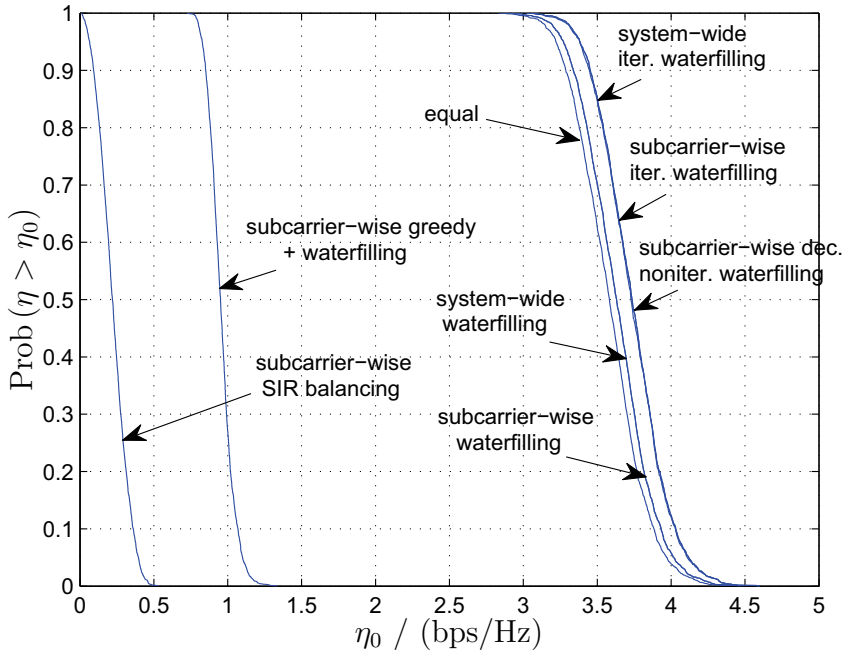

Figure 6.14: Spectral efficiency CCDFs in a conventional cellular network with $K_{\mathrm{B}} = 1$, $r = 1$, $K_{\mathrm{S}} = 12$ and $N_{\mathrm{F}} = 8$, applying 3-D channel gain array based subcarrier allocation

Table 6.8: Ergodic spectral efficiency and outage spectral efficiency in a conventional cellular network with $K_{\mathrm{B}} = 1$, $r = 1$, $K_{\mathrm{S}} = 12$ and $N_{\mathrm{F}} = 8$, applying 3-D channel gain array based subcarrier allocation

	$\mathrm{E}\{\eta\}$/ (bps/Hz)	η_{out}/ (bps/Hz)
equal power allocation	3.58	3.29
subcarrier-wise SIR balancing	0.22	0.09
subcarrier-wise greedy + waterfilling	0.95	0.85
system-wide waterfilling	3.63	3.34
subcarrier-wise waterfilling	3.63	3.34
system-wide iterative waterfilling	3.74	3.45
subcarrier-wise iterative waterfilling	3.74	3.45
subcarrier-wise decremental noniterative waterfilling	3.73	3.45

power allocation performs better than in a SA network due to improved energy efficiency. Moreover, it can be observed that the performance gain of interference adaptive power allocation strategies including iterative waterfilling and decremental noniterative waterfilling over interference nonadaptive power allocation strategies such as system-wide and subcarrier-wise waterfilling enlarges a little bit as compared to the SA network due to the fact that the conventional cellular network has smaller interferer diversity.

6.4.3 Power allocation in a frequency planned network

In the case of universal frequency reuse, the inter-SA interference links can be as strong as the useful links if the MSs are close to the border of the SAs. While under the assumption of random distribution of MSs, such a scenario can actually be viewed as a moderate interference scenario in a statistical sense, which is already shown before. A weak interference scenario is obtained if the cluster size is sufficiently large. Considering a frequency planned SA network with cluster size being three, it can been observed from Fig. 6.15 and Table 6.9 that there is no appreciable performance difference among iterative waterfilling, decremental noniterative waterfilling and conventional waterfilling power

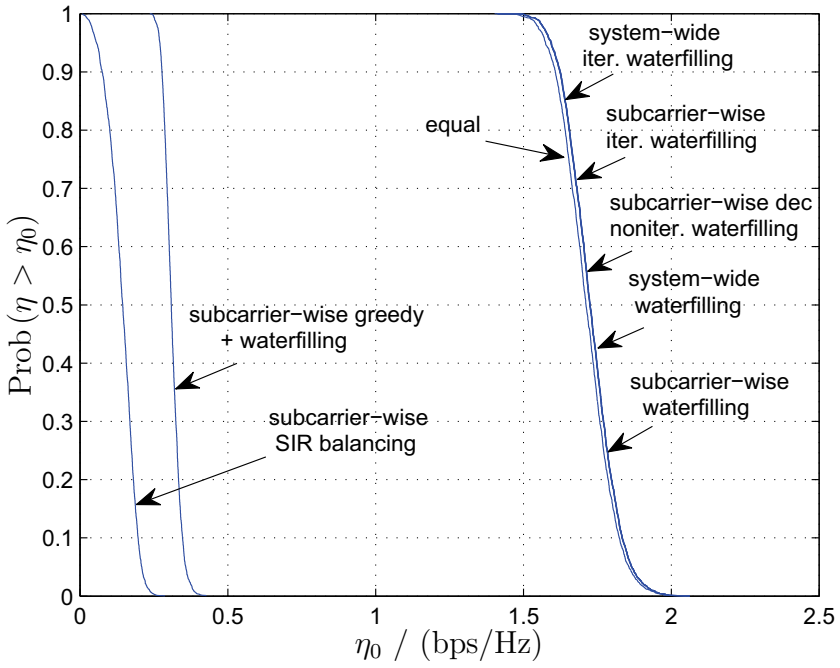

Figure 6.15: Spectral efficiency CCDFs in a SA network with $K_{\mathrm{B}} = 3$, $r = 3$, $K_{\mathrm{S}} = 4$ and $N_{\mathrm{F}} = 8$, applying 3-D channel gain array based subcarrier allocation

Table 6.9: Ergodic spectral efficiency and outage spectral efficiency in a SA network with $K_{\mathrm{B}} = 3$, $r = 3$, $K_{\mathrm{S}} = 4$ and $N_{\mathrm{F}} = 8$, applying 3-D channel gain array based subcarrier allocation

	$\mathrm{E}\{\eta\}$/ (bps/Hz)	η_{out}/ (bps/Hz)
equal power allocation	1.71	1.61
subcarrier-wise SIR balancing	0.14	0.08
subcarrier-wise greedy + waterfilling	0.31	0.28
system-wide waterfilling	1.73	1.62
subcarrier-wise waterfilling	1.73	1.62
system-wide iterative waterfilling	1.73	1.63
subcarrier-wise iterative waterfilling	1.73	1.62
subcarrier-wise decremental noniterative waterfilling	1.73	1.62

allocation strategies, which conforms to the behavior in generic interference channels with weak interference links. Furthermore, the spectral efficiencies in the case of frequency planning obviously degrade as compared to the case of universal frequency reuse.

Chapter 7

Summary

7.1 English

The present thesis focuses on resource allocation in the SA based JOINT system. As a B3G air interface proposal, the JOINT system aims at reducing capacity limiting interferences, which is achieved by deploying the novel SA architecture and by applying joint signal processing in each SA. The BSs inside a SA made up from a cluster of adjacent cells are coordinated, which enables joint transmission in the DL and joint detection in the UL to separate the signals of multiple MSs in the spatial domain. Consequently, multiple MSs are allowed to be simultaneously active on the same frequency slot without causing interference to each other. Since intra-SA interferences are completely eliminated, the SA based JOINT system outperforms conventional cellular systems at a cost of complexity.

Besides SDMA based interference cancellation as applied in JOINT, adaptive resource allocation is also known to be an effective means to increase network capacity. The use of OFDMA in SA networks provides the possibility of performance optimization by adaptive subcarrier allocation. In order to avoid an exhaustive search required to find the optimum subcarrier allocation in SA networks, suboptimum subcarrier allocation techniques are studied with the

assumption of equal power allocation. Among them the proposed 3-D channel gain array based subcarrier allocation provides substantial performance gain over fixed subcarrier allocation at a low complexity. The significance of the frequency selectivity of wireless channels, the correlation among users' spatial signatures and the presence of interferences to adaptive subcarrier allocation is also assessed through simulations. It is demonstrated that exploiting frequency selectivity is very beneficial. The spatial correlations are more critical than absolute channel gains in SDMA based SA networks, especially for fully loaded systems. The benefit from adapting to interferences depends on the interferer diversity. In SA networks it is not worth applying interference-adaptive subcarrier allocation with a reasonable complexity, especially for the case of frequency planning.

Power allocation is a vital issue in interference limited networks. Motivated by the prohibitively high complexity required for finding the optimum power allocation in generic interference channels with total power constraint, several suboptimum schemes are investigated. The behavior of different power allocation schemes depends quite a lot on the strength of the interference links. For instance, in strong interference scenarios the greedy scheme which simply allocates all transmit power to the best user is shown to be near-optimum, whereas conventional waterfilling should be used in weak interference environments due to its near-optimum performance and relatively low complexity. The proposed iterative waterfilling and decremental noniterative waterfilling are preferable in moderate interference scenarios. Based on the analysis in generic interference channels, various power allocation strategies as the second step after subcarrier allocation in SA networks are evaluated. Simulation results indicate that a SA network with universal frequency reuse can essentially be considered as a moderate interference scenario where iterative waterfilling shows its superiority. In case of frequency planning, e.g., with cluster size being three, the network is equivalent to a weak interference scenario and conventional waterfilling is sufficient to provide a good performance. Moreover, subcarrier-wise power allocation yields almost the same performance as system-wide power allocation strategies at a lower complexity. It is also revealed that the performance gain of adaptive power allocation over equal power allocation shrinks as the performance of the afore applied subcarrier allocation technique improves.

7.2 Deutsch

Die vorliegende Dissertation befaßt sich mit der Ressourcenvergabe in dem Service Area basierten JOINT System. Als ein Luftschnittstellenkonzept für Mobilfunksysteme jenseit der dritten Generation zielt das JOINT System durch die neuartige Service Area Architektur und gemeinsame Singalverarbeitung in jeder Service Area auf eine Reduktion der Interferenzen, welche die Netzwerkkapazität begrenzen. Die Koordination der Basisstationen innerhalb einer Service Area, die aus einen Cluster benachbarter Zellen besteht, ermöglicht eine räumliche Trennung der Signale mehrerer Mobilstationen durch Joint Detection in der Aufwärtsstrecke und Joint Transmission in der Abwärtsstrecke. Als Folge davon können mehrere Mobilstationen in dem selben Frequenzband gleichzeitig interferenzfrei aktiv sein. Da die Interferenzen innerhalb einer Service Area völlig eliminiert werden, ist die Performanz eines Service Area basierten Mobilfunksystems besser als die Performanz eines konventionellen zellularen Mobilfunksystems, wofür aber ein erhöhter Aufwand zu investieren ist.

Neben SDMA basierter Interferenzreduktion wie in JOINT, ist adaptierte Ressourcenallokation als ein weiteres effizientes Mittel zur Erhöhung der Netzwerkkapazität bekannt. Die Benutzung von OFDMA in Service Area basierten Netzwerken bietet die Möglichkeit, die Systemperfomanz durch adaptive Subträgerallokation zu optimieren. Um die zur optimalen Subträgerallokation in Service Area basierten Netzwerken benötigte erschöpfende Suche zu vermeiden, werden suboptimale Subträgerallokationsverfahren unter der Annahme einer gleichmäßgen Verteilung der Sendeleistung untersucht. Von diesen Verfahren liefert die 3-dimensionale Funkfeldgewinnarray basierte Subträgerallokation erheblichen Performanzgewinn gegenüber fester Subträgerallokation bei niedrigen Aufwand. Die Bedeutung der Frequenzselektivität der Funkkanäle, der Korrelation zwischen räumlichen Signaturen der Teilnehmer und der Existenz der Interferenzen für adaptierte Subträgerallokation wird durch Computersimulationen bewertet. Es wird dargestellt, dass das Ausnutzen der Frequenzselektivität sehr vorteilhaft ist. Die räumlichen Korrelationen sind bedeutender als der absoluter Funkfeldgewinn in SDMA basierten Netzwerken, besonders in Fällen voller Last. Der Gewinn der Interferenzadatption hängt von der Interfererdiversität ab. In Service Area basierten Netzwerken, besonders im Falle

von Frequenzplanung, lohnt sich interferenzadaptive Subträgerallokation mit einem angemessenen Aufwand nicht.

Leistungsallokation ist ein unerlässliches Thema in Netzwerken, deren Kapazität durch Interferenzen begrenzt ist. Aufgrund des untragbar höheren Aufwandes, den die optimale Leistungsallokation in allgemeinen Interferenzkanälen mit Summenleistungsbeschränkung erfordert, werden verschiedene suboptimale Leistungsallokationsverfahren untersucht. Das Verhalten der unterschiedlichen Leistungsallokationsverfahren hängt stark von der Größe der Interferenzkanalkoeffizienten ab. In Szenarien mit starker Interferenz ist beispielsweise die gierige Leistungsallokation, die alle verfügbare Sendeleistung dem besten Teilnehmer zuordnet, fast optimal, während konventionelles Waterfilling wegen seiner fast optimaler Performanz und seines relativ niedrigen Aufwandes eingesetzt werden sollte. Die vorgeschlagene iterative Waterfilling und dekrementale nichtiterative Waterfilling sind in Szenarien mit mittelmäßiger Interferenz vorzuziehen. Basierend auf den Untersuchungen in allgemeinen Interferenzkanälen werden verschiedene Leistungsallokationsverfahren als zweiter Schritt nach der Subträgerallokation in Service Area basierten Netzwerken untersucht. Die Ergebnisse der Simulationen zeigen, dass ein Service Area basiertes Gleichwellennetz tatsächlich als ein Szenario mit mittelmäßiger Interferenz, wo iteratives Waterfilling überlegen ist, angesehen werden kann. Im Falle von Frequenzplanung, zum Beispiel wenn die Clustergröße drei ist, entspricht das Netzwerk einem Szenario mit schwacher Interferenz und konventionelles Waterfilling ist hinreichend, um eine gute Performanz zu erzielen. Darüber hinaus bieten subträgerweise Leistungsallokationsverfahren fast die gleiche Performanz wie systemweite Leistungsallokationsverfahren bei einem niedrigeren Aufwand. Es wird auch gezeigt, dass sich der durch adaptive Leistungsallokation erzielte Performanzgewinn gegenüber gleichmäßiger Leistungsverteilung verringert, wenn ein leistungsfähiges Subträgerallokationsverfahren zuvor durchgeführt wurde.

Appendix A

List of frequently used abbreviations and symbols

A.1 Abbreviations

AWGN	additive white gaussian noise
B3G	beyond 3rd generation
BER	bit error rate
BIP	binary integer programming
BS	base station
CCDF	complementary cumulative distribution function
CDMA	code division multiple access
CIR	carrier-to-interference ratio
CSI	channel state information
CTF	channel transfer function
CU	central unit
DL	downlink
DSL	digital subscriber line
FDD	frequency division duplex
FDMA	frequency division multiple access
ICI	inter-channel interference
ISI	inter-symbol interference
JCE	joint channel estimation
JD	joint detection
JOINT	joint transmission and detection integrated network

JT	joint transmission
MF	matched filter
MIMO	multiple-input multiple-output
MMSE	minimum mean square error
MS	mobile station
OFDM	orthogonal frequency division multiplexing
OFDMA	orthogonal frequency division multiple access
pdf	probability density function
QoS	quality of service
SA	service area
SDMA	space division multiple access
SINR	signal-to-interference-plus-noise ratio
SIR	signal-to-interference ratio
SISO	single-input single-output
SNR	signal-to-noise ratio
TDD	time division duplex
TDMA	time division multiple access
UL	uplink
ZF	zero forcing

A.2 Symbols

$\underline{d}_j$	transmitted data symbol of user j in an interference channel
$\hat{\underline{d}}_j$	received data symbol of user j in an interference channel
$\underline{d}_k^{(n_\mathrm{F};k_\mathrm{S})}$	transmitted data symbol of the k-th active MS on subcarrier n_F in SA k_S
$\hat{\underline{d}}_k^{(n_\mathrm{F};k_\mathrm{S})}$	estimated data symbol of the k-th active MS on subcarrier n_F in SA k_S
$\underline{\mathbf{d}}^{(k_\mathrm{S})}$	SA specific data vector
$\hat{\underline{\mathbf{d}}}^{(k_\mathrm{S})}$	SA specific estimated data vector
$\underline{\mathbf{D}}^{(k_\mathrm{S})}$	SA specific demodulation matrix
$\underline{e}_{k_\mathrm{B}}$	receive signal at BS k_B in the UL
$\underline{\mathbf{e}}^{(k_\mathrm{S})}$	SA specific receive signal vector in the UL
F_{ji}	normalized interference link gain between transmitter i and receiver j in an interference channel
$\mathbf{F}$	normalized interference link gain matrix of an interference channel

g_{ji}	channel gain between transmitter i and receiver j in an interference channel
$\bar{G}$	distance dependent average channel gain
$\underline{h}_{ji}$	channel coefficient between transmitter i and receiver j in an interference channel
$\underline{h}_{ji}^{(n_\mathrm{F})}$	channel coefficient between transmitter i and receiver j in subcarrier specific interference channels
$\underline{\mathbf{h}}_{k}^{(n_\mathrm{F})}$	spatial signature of the k-th active MS on subcarrier n_F
$\underline{\mathbf{h}}_{k_\mathrm{M}}^{(n_\mathrm{F})}$	spatial signature of MS k_M on subcarrier n_F
$\underline{\mathbf{h}}_{\mathrm{D},k}$	user specific spatial signature in the DL
$\underline{\mathbf{h}}_{\mathrm{U},k}$	user specific spatial signature in the UL
$\underline{H}_{k_\mathrm{M},k_\mathrm{B}}^{(n_\mathrm{F})}$	subcarrier specific DL channel transfer function from BS k_B to MS k_M in a considered SA
$\underline{H}_{\mathrm{D},k,k_\mathrm{B}}^{(k_\mathrm{S},k'_\mathrm{S})}$	DL channel transfer function from BS k_B in SA k'_S to MS k in SA k_S
$\underline{H}_{\mathrm{U},k_\mathrm{B},k}^{(k_\mathrm{S},k'_\mathrm{S})}$	UL channel transfer function from MS k in SA k'_S to BS k_B in SA k_S
$\underline{\mathbf{H}}^{(n_\mathrm{F};k_\mathrm{S},k'_\mathrm{S})}$	DL channel matrix between the BSs in SA k'_S and the MSs active on subcarrier n_F in SA k_S
$\underline{\mathbf{H}}_{\mathrm{D}}^{(k_\mathrm{S},k'_\mathrm{S})}$	DL channel matrix between the BSs in SA k'_S and the active MSs in SA k_S
$\underline{\mathbf{H}}_{\mathrm{U}}^{(k_\mathrm{S},k'_\mathrm{S})}$	UL channel matrix between the active MSs in SA k'_S and the BSs in SA k_S
$\underline{\mathbf{H}}'^{(n_\mathrm{F})}$	subcarrier specific DL channel matrix between the $K-1$ active MSs and the BSs in a SA
$\underline{\mathbf{H}}'_{\mathrm{U}}$	UL channel matrix between the $K-1$ active MSs and the BSs in a SA
$\underline{\mathbf{H}}_{\mathrm{tot}}^{(n_\mathrm{F};k_\mathrm{S},k'_\mathrm{S})}$	total DL channel matrix between the BSs in SA k'_S and all the MSs in SA k_S on subcarrier n_F
$I^{(n_\mathrm{F})}$	real part of subcarrier specific Rayleigh fading component
$\mathbf{I}$	identity matrix
J	number of users in an interference channel
K	number of active MSs per subcarrier per SA
K_B	number of cells per SA
K_M	number of MSs per SA
K_S	number of co-channel SAs in a multi-SA scenario
l	iteration index in iterative waterfilling
$\underline{\mathbf{M}}^{(n_\mathrm{F};k_\mathrm{S})}$	subcarrier and SA specific modulation matrix
$\underline{n}_j$	noise at receiver side of user j in an interference channel

$\underline{n}_{k_\mathrm{B}}$	noise at the input of the k_B-th BS in UL transmission
$\underline{n}_k^{(n_\mathrm{F};k_\mathrm{S})}$	noise at the input of the k-th active MS on subcarrier n_F in SA k_S in DL transmission
$\underline{\mathbf{n}}^{(k_\mathrm{S})}$	SA specific noise vector
$\underline{\tilde{\mathbf{n}}}$	enhanced noise vector at receiver output in the UL
N_F	number of subcarriers available in each SA
P	transmit power of each user in subcarrier allocation stage
$\bar{P}$	average transmit power per user per subcarrier
P_1^*	optimum transmit power allocated to user 1 in two-user interference channels
P_j	transmit power of user j in an interference channel
$P_k^{(n_\mathrm{F};k_\mathrm{S})}$	transmit power of MS k active on subcarrier n_F in SA k_S
P_tot	total transmit power budget
P_W	waterfilling level
$\mathbf{p}$	total power vector
$\mathbf{p}^{(k_\mathrm{S})}$	SA specific power vector
$\mathbf{P}^{(k_\mathrm{S})}$	SA specific power matrix
$Q^{(n_\mathrm{F})}$	imaginary part of subcarrier specific Rayleigh fading component
r	cluster size
R_j	bit rate of user j in an interference channel
$R_k^{(n_\mathrm{F};k_\mathrm{S})}$	DL bit rate of MS k active on subcarrier n_F in SA k_S
R_sum	sum rate
R_sys	system-wide accumulated bit rate
R_SA	SA-wide accumulated bit rate
$\underline{s}_{k_\mathrm{B}}$	transmit signal of BS k_B in the DL
$\underline{\mathbf{s}}^{(k_\mathrm{S})}$	SA specific transmit signal vector
$v_k^{(n_\mathrm{F};k_\mathrm{S})}$	inverse of the useful channel gain of MS k active on subcarrier n_F in SA k_S
$w_{k,k'}^{(k_\mathrm{S},k'_\mathrm{S})}$	interference link gain between the k'-th MS in SA k'_S and the k-th MS in SA k_S in subcarrier specific interference channel model
$x_{k_\mathrm{M}}^{(n_\mathrm{F};k_\mathrm{S})}$	binary subcarrier allocation indicator for MS k_M on subcarrier n_F in SA k_S
$\mathbf{x}^{(n_\mathrm{F};k_\mathrm{S})}$	subcarrier allocation indicating vector for subcarrier n_F in SA k_S
z_j	normalized interference plus noise power with respect to the j-th user in an interference channel
β	ratio between interference link gain and useful link gain in two-user interference channels

γ	achieved SIR level after SIR balancing power allocation
γ_j	SINR of user j in an interference channel
$\gamma_k^{(k_\mathrm{S})}$	SINR of MS k in SA k_S
$\gamma_k^{(n_\mathrm{F})}$	SNR of MS k on subcarrier n_F in the DL
$\tilde{\gamma}_k^{(n_\mathrm{F})}$	normalized SNR of MS k on subcarrier n_F in the DL
ε_k	user specific energy efficiency
η	spectral efficiency
η_out	outage spectral efficiency
ρ	spectral radius
σ^2	noise variance
σ_{ji}^2	mean value of Chi-square distributed channel gain g_{ji} in an interference channel

Literature

[80299] *IEEE 802.11a Working Group, Part 11: Wireless LAN Medium Access Control (MAC) and Physical Layer (PHY) specifications– Amendment 1: High-Speed Physical Layer in the 5 GHz band.* 1999.

[80203] *IEEE 802.11g Working Group, Part 11: Wireless LAN Medium Access Control (MAC) and Physical Layer (PHY) specifications– Amendment 4: Further Higher-Speed Physical Layer Extension in the 2.4 GHz Band.* 2003.

[Aei73] Aein, J.: Power balancing in systems employing frequency reuse. *COMSAT Technical Review*, vol. 3, 1973, pp. 277–300.

[Ahl71] Ahlswede, R.: Multi-way communication channels. *IEEE International Symposium on Information Theory (ISIT)*, Tsahkadsor USSR, 1971, pp. 103–135.

[AN82] Alavi, H.; Nettleton, R.: Downstream power control for a spread spectrum cellular mobile radio system. *IEEE Global Telecommunication Conference (GLOBECOM'82)*, 1982, pp. 84–88.

[And05] Andrews, J. G.: Interference cancellation for cellular systems: A contemporary overview. *IEEE Wireless Communications*, vol. 12, 2005, pp. 19–29.

[AS65] Abramowitz, M.; Stegun, I.: *Handbook of Mathematical Functions.* New York: Dover, 1965.

[Bin90] Bingham, J.: Multicarrier modulation for data transmission: An idea whose time has come. *IEEE Communications Magazine*, vol. 28, 1990, pp. 5–14.

[BK08] Böhnke, R.; Kammeyer, K.: Weighted sum rate maximization for MIMO-OFDM systems with linear and dirty paper precoding.

7th International ITG Conference on Source and Channel Coding (SCC 2008), Ulm, 2008.

[BS06] Boche, H.; Schubert, M.: A general theory for SIR balancing. *EURASIP Journal on Wireless Communications and Networking*, vol. 2006, 2006.

[Car78] Carleial, A.: Interference channels. *IEEE Transactions on Information Theory*, vol. 24, 1978, pp. 60–70.

[CCB95] Chow, P. S.; Cioffi, J. M.; Bingham, J. A. C.: A practical discrete multitone transceiver loading algorithm for data transmission over spectrally shaped channels. *IEEE Transactions on Communications*, vol. 43, 1995, pp. 773–775.

[Che01] Cherubini, G.: Optimum upstream power back-off and multiuser detection for VDSL. *IEEE Global Telecommunications Conference (GLOBECOM'01)*, 2001, pp. 375–380.

[CLTC98] Chen, J.-T.; Liang, J.; Tsa, H.-S.; Chen, Y.-K.: Joint MLSE receiver with dynamic channel description. *IEEE Journal on Selected Areas in Communications*, vol. 16, 1998, pp. 1604–1615.

[Cos83] Costa, M. H. M.: Writing on dirty paper. *IEEE Transactions on Information Theory*, vol. 29, 1983, pp. 439–441.

[Cov72] Cover, T.: Broadcast channels. *IEEE Transactions on Information Theory*, vol. 18, 1972, pp. 2–14.

[CT91] Cover, T. M.; Thomas, J. A.: *Elements of Information Theory*. John Wiley & Sons, 1991.

[CTC91] Chow, P. S.; Tu, J. C.; Cioffi, J. M.: A discrete multitone transceiver system for HDSL applications. *IEEE Journal on Selected Areas in Communications*, vol. 9, 1991, pp. 895–908.

[CV93] Cheng, R.; Verdu, S.: Gaussian multiaccess channels with ISI: capacity region and multiuser water-filling. *IEEE Transactions on Information Theory*, vol. 39, 1993, pp. 773–785.

[CYM+06] Cendrillon, R.; Yu, W.; Moonen, M.; Verlinden, J.; Bostoen, T.: Optimal multiuser spectrum balancing for digital subscriber lines. *IEEE Transactions on Communications*, vol. 54, 2006, pp. 922–933.

[DWA06] Deng, S.; Weber, T.; Ahrens, A.: Interference statistics in the downlink of service area based mobile radio networks. *11th International OFDM-Workshop (InOWo'06)*, Hamburg, 2006, pp. 31–35.

[ETS97a] ETSI: *Digital video broadcasting (DVB); Framing structure, channel coding, and modulation for digital terrestial television.* Technical Report EN 300 744, European Telecommunication and Standardization Institute (ETSI), 1997.

[ETS97b] ETSI: *Radio broadcasting systems; digital audio broadcasting (DAB) to mobile, portable and fixed receivers.* Technical Report EN 300 401, European Telecommunication and Standardization Institute (ETSI), 1997.

[ETS99] ETSI: *Broadband radio access networks (BRAN); HIPERLAN Type 2 technical specification, Part I: physical layer.* 1999.

[Ett76] Etten, W.: Maximum likelihood receiver for multiple channel transmission systems. *IEEE Transactions on Communications*, vol. 24, 1976, pp. 276–283.

[ETW06] Etkin, R.; Tse, D.; Wang, H.: Gaussian interference channel capacity to within one bit: the symmetric case. *IEEE Information Theory Workshop (ITW)*, Chengdu, 2006, pp. 601–605.

[EV-01] *Cdma2000 High Rate Packet Data Air Interface Specication.* TIA/EIA/3GPP2 Standard IS-856/3GPP2 C.S.0024, v3.0, 2001.

[FG98] Foschini, G.; Gans, M.: On limits of wireless communications in a fading environment when using multiple antennas. *Wireless Personal Communications*, vol. 6, 1998, pp. 311–335.

[FGH05] Fuchs, M.; Galdo, G. D.; Haardt, M.: A novel tree-based scheduling algorithm for the downlink of multi-user MIMO systems with ZF beamforming. *IEEE International Conference Acoustics, Speech, and Signal Processing (ICASSP)*, Philadelphia, PA, 2005, pp. 1121–1124.

[FGH06] Fuchs, M.; Galdo, G. D.; Haardt, M.: Low complexity spatial scheduling prosched for MIMO systems with multiple base stations and a central controller. *International ITG/IEEE Workshop on Smart Antennas (WSA)*, Guenzburg, Germany, 2006.

[Fis02] Fischer, R. F. H.: *Precoding and Signal Shaping for Digital Transmission.* New York: John Wiley & Sons, 2002.

[FM93] Foschini, G. J.; Miljanic, Z.: A simple distributed automonous power control algorithm and its convergence. *IEEE Transactions on Vehicular Technology*, vol. 42, 1993, pp. 641–646.

[Gar99] Garg, V. K.: *IS-95 CDMA and cdma2000*. Prentice Hall PTR, 1999.

[GVL86] Golub, G. H.; Van Loan, C. F.: *Matrix Computations*. 2. edition. Baltimore: Johns Hopkins University Press, 1986.

[Har06] Harte, L.: *Introduction to 802.16 WiMAX, Wireless Broadband Technology, Operation and Services*. Althos Publishing, 2006.

[HBHD+06] Hoeher, P. A.; Badri-Hoeher, S.; Deng, S.; Krakowski, C.; Xu, W.: Single antenna interference cancellation (SAIC) for cellular TDMA networks by means of joint delayed-decision feedback sequence estimation. *IEEE Transactions on Wireless Communications*, vol. 5, 2006, pp. 1234–1237.

[HG86] Hahne, E. L.; Gallager, R. G.: Round robin scheduling for fair flow control in data communication networks. *IEEE International Conference on Communications (ICC)*, 1986, pp. 103–107.

[HH87] Hughes-Hartogs, D.: *Ensemble modem structure for imperfect transmission media*. 1987. United States Patent 4,679,227.

[HHA03] Hafeez, A.; Hui, D.; Arslan, H.: Interference cancellation for EDGE via two-user joint demodulation. *IEEE Vehicular Technology Conference (VTC 2003-Fall)*, Orlando, Florida, 2003, pp. 1025–1029.

[HK81] Han, T. S.; Kobayashi, K.: A new achievable rate region for the interference channel. *IEEE Transactions on Information Theory*, vol. IT-27, 1981, pp. 49–60.

[HL90] Hillier, F.; Lieberman, G.: *Introduction to Operations Research*. New York: McGraw-Hill, 1990.

[JL03] Jang, J.; Lee, K. B.: Transmit power adaptation for multiuser OFDM systems. *IEEE Journal on Selected Areas in Communications*, vol. 21, 2003, pp. 171–178.

[JLL02] Jang, J.; Lee, K. B.; Lee, Y.-H.: Frequency-time domain transmit power adaptation for a multicarrier system in fading channels. *IEE Electronics Letters*, vol. 38, 2002, pp. 218–220.

[Jor06] Jorswieck, E. A.: Uplink throughput maximization with combined sum and individual power constraints. *IEEE Communications Letters*, vol. 10, 2006, pp. 816–818.

[JPP00] Jalali, A.; Padovani, R.; Pankaj, R.: Data throughput of CDMA-HDR: a high efficiency-high data rate personal communication wireless system. *IEEE Vehicular Technology Conference (VTC2000)*, Tokyo, Japan, 2000.

[Kal89] Kalet, I.: The multitone channel. *IEEE Transactions on Communications*, vol. 37, 1989, pp. 119–124.

[KAS05] Kulkarni, G.; Adlakha, S.; Srivastava, M.: Subcarrier allocation and bit loading algorithms for OFDMA-based wireless networks. *IEEE Transactions on Mobile Computing*, vol. 4, 2005, pp. 652–662.

[KH95] Knopp, R.; Humblet, P.: Information capacity and power control in single cell multiuser communications. *IEEE International Conference on Communications (ICC)*, vol. 1, Seattle, 1995, pp. 331–335.

[KHK05] Kim, K.; Han, Y.; Kim, S.-L.: Joint subcarrier and power allocation in uplink OFDMA systems. *IEEE Communications Letters*, vol. 9, 2005, pp. 526–528.

[KKB96] Klein, A.; Kaleh, G. K.; Baier, P. W.: Zero forcing and minimum mean-square-error equalization for multiuser detection in code-division multiple-access channels. *IEEE Transactions on Vehicular Technology*, vol. 45, 1996, pp. 276–287.

[KL00] Kivanc, D.; Liu, H.: Subcarrier allocation and power control for OFDMA. *Conference on Signals, Systems and Computers*, 2000, pp. 147–151.

[KL03] Kapoor, S.; Li, J.: *Initial Contribution on a System Meeting MBWA Characteristics*. IEEE 802.20 Working Group on Mobile Broadband Wireless Access, 2003.

[Kle96] Klein, A.: *Multi-User Detection of CDMA Signals – Algorithms and Their Application to Cellular Mobile Radio*. Fortschrittberichte VDI, Reihe 10, no. 423. Düsseldorf: VDI-Verlag, 1996.

[Koc07] Koch, M.: *Power Line Communications (PLC). Coordination of Distributed Generation and Key Aspects for Inter-working with UMTS*. WiKu-Verlag Verlag für Wissenschaft und Kultur, 2007.

[Kra01] Kramer, G.: Genie-aided outer bounds on the capacity of interference channels. *IEEE International Symposium on Information Theory (ISIT)*, Washington, DC, 2001.

[KT02] Koutsopoulos, I.; Tassiulas, L.: Adaptive resource allocation in SDMA-based wireless broadband networks with OFDM signaling. *IEEE 21st Annual Joint Conference of the IEEE Computer and Communications Societies (INFOCOM 2002)*, vol. 3, 2002, pp. 1376–1385.

[Lee97] Lee, W. C. Y.: *Mobile Communications Engineering: Theory and Applications*. McGraw-Hill, 1997.

[Liu05] Liu, Y.: *Modelling and Simulation of Service Area Based OFDM Air Interface for Beyond 3G Mobile Radio Systems*. PhD thesis, University of Kaiserslautern, Germany, 2005.

[LP06] Luo, Z.-Q.; Pang, J.-S.: Analysis of iterative waterfilling algorithm for multiuser power control in digital subscriber lines. *EURASIP Journal on Applied Signal Processing*, vol. 2006, 2006, pp. 1–10.

[LZ06] Leshem, A.; Zehavi, E.: Bargaining over the interference channel. *IEEE International Symposium on Information Theory (ISIT)*, Seattle, WA, 2006, pp. 2225–2229.

[Mac08] Maciel, T. F.: *Suboptimal Resource Allocation for Multi-User MIMO-OFDMA Systems*. PhD thesis, TU Darmstadt, Germany, 2008.

[Man05] Maniatis, I.: *Joint Channel Estimation in Service Area Based OFDM Air Interface for Beyond 3G Mobile Radio Systems*. PhD thesis, University of Kaiserslautern, Germany, 2005.

[MB05] Mohanram, C.; Bhashyam, S.: A sub-optimal joint subcarrier and power allocation algorithm for multiuser OFDM. *IEEE Communications Letters*, vol. 9, 2005, pp. 685–687.

[MBQ04] Meurer, M.; Baier, P. W.; Qiu, W.: Receiver orientation versus transmitter orientation in linear MIMO transmission systems. *EURASIP Journal on Applied Signal Processing*, vol. 9, 2004, pp. 1191–1198.

[MBW+00] Meurer, M.; Baier, P. W.; Weber, T.; Lu, Y.; Papathanassiou, A.: Joint transmission: advantageous downlink concept for CDMA

mobile radio systems using time division duplexing. *IEE Electronics Letters*, vol. 11, 2000, pp. 900–901.

[MD79] Mac Donald, V. H.: The cellular concept. *The Bell System Technical Journal*, vol. 58, 1979, pp. 15–41.

[Meh91] Mehta, M. L.: *Random Matrices*. San Diego: Academic Press, 1991.

[MF07] Marsch, P.; Fettweis, G.: A framework for optimizing the uplink performance of distributed antenna systems under a constrained backhaul. *IEEE International Conference on Communications (ICC)*, Glasgow, Scotland, 2007, pp. 975–979.

[MPS02] Muenz, G.; Pfletschinger, S.; Speidel, J.: An efficient waterfilling algorithm for multiple access OFDM. *IEEE Global Telecommunications Conference 2002 (GLOBECOM'02)*, Taipei, Taiwan, 2002.

[Mül01] Müller, R. R.: Multiuser receivers for randomly spread signals: Fundamental limits with and without decision-feedback. *IEEE Transactions on Information Theory*, vol. 47, 2001, pp. 268–283.

[MWS+02] Maniatis, I.; Weber, T.; Sklavos, A.; Liu, Y.; Costa, E.; Haas, H.; Schulz, E.: Pilots for joint channel estimation in multi-user OFDM mobile radio systems. *IEEE 7th International Symposium on Spread Spectrum Techniques & Applications (ISSSTA'02)*, Prague, Czech, 2002, pp. 44–48.

[NA83] Nettleton, R. W.; Alavi, H.: Power control for a spread spectrum cellular mobile radio system. *IEEE Vehicular Technology Conference (VTC1983)*, 1983, pp. 242–246.

[NKT89] Nemhauser, G. L.; Kan, A. H. G. R.; Todd, M. J.: *Handbooks in Operations Research and Management Science, Volume 1: Optimization*. Amsterdam: North-Holland, 1989.

[OR05] Olonbayar, S.; Rohling, H.: Multiuser diversity and subcarier allocation in OFDM-FDMA systems. *10th International OFDM-Workshop (InOWo'05)*, Hamburg, 2005, pp. 275–279.

[PJ04] Pietrzyk, S.; Janssen, G. J. M.: Performance evaluation of bit loading, subcarrier allocation, and power control algorithms for cellular OFDMA systems. *Personal Wireless Communications*. vol. 3260/2004. pp. 349–363. Springer, 2004.

[PJSL05] Park, T.; Jang, J.; Shin, O.-S.; Lee, K. B.: Transmit power allocation for a downlink two-user interference channel. *IEEE Communications Letters*, vol. 9, 2005, pp. 13–15.

[PL04] Park, C. S.; Lee, K. B.: Transmit power allocation for BER performance improvement in multicarrier systems. *IEEE Transactions on Communications*, vol. 52, 2004, pp. 1658–1663.

[Rap96] Rappaport, T. S.: *Wireless Communications – Principles and Practice*. Prentice Hall PTR, 1996.

[RC00] Rhee, W.; Cioffi, J. M.: Increase in capacity of multiuser OFDM system using dynamic subchannel allocation. *IEEE Vehicular Technology Conference (VTC2000)*, Tokyo, Japan, 2000, pp. 1085–1089.

[RFLT98] Rashid-Farrokhi, F.; Liu, K. J. R.; Tassiulas, L.: Transmit beamforming and power control for cellular wireless systems. *IEEE Journal on Selected Areas in Communications*, vol. 16, 1998, pp. 1437–1450.

[RG97] Rohling, H.; Grünheid, R.: Performance comparison of different multiple access schemes for thedownlink of an OFDM communication system. *47th IEEE Vehicular Technology Conference (VTC1997)*, vol. 3, 1997, pp. 1365–1369.

[RGG01] Rohling, H.; Grünheid, R.; Galda, D.: OFDM transmission technique for the 4th generation of mobile communication systems. *6th International OFDM-Workshop 2001 (InOWo'01)*, Hamburg, 2001.

[SAE03] Shen, Z.; Andrews, J. G.; Evans, B. L.: Optimal power allocation in multiuser OFDM systems. *IEEE Global Communications Conference*, San Francisco, CA, 2003, pp. 337–341.

[Sas04] Sason, I.: On achievable rate regions for the Gaussian interference channel. *IEEE Transactions on Information Theory*, vol. 50, 2004, pp. 1345–1356.

[Sat81] Sato, H.: The capacity of the Gaussian interference channel under strong interference. *IEEE Transactions on Information Theory*, vol. 27, 1981, pp. 786–788.

[SB05] Schubert, M.; Boche, H.: Iterative multiuser uplink and downlink beamforming under SINR constraints. *IEEE Transactions on Signal Processing*, vol. 53, 2005, pp. 2324–2334.

[SBS05] Schubert, M.; Boche, H.; Stanczak, S.: Joint power control and multiuser receiver design - fairness issues and cross-layer optimization. *14th IST Mobile & Wireless Communications Summit*, Dresden, Germany, 2005.

[SCS98] Starr, T.; Cioffi, J. M.; Silverman, P. J.: *Understanding Digital Subscriber Line Technology*. Prentice Hall PTR, 1998.

[Sen06] Seneta, E.: *Non-negative Matrices and Markov Chains*. 2nd edition. Springer-Verlag, 2006.

[SH04] Schoeneich, H.; Hoeher, P. A.: Iterative semi-blind single-antenna cochannel interference cancellation and tight lower bound for joint maximum-likelihood sequence estimation. *Signal Processing*, vol. 84, 2004, pp. 1991–2004.

[Sha61] Shannon, C. E.: Two-way communication channels. *4th Berkeley Symposium on Mathematical Statistics and Probability*, Berkeley, CA, 1961.

[SL03] Song, G.; Li, Y.: Adaptive subcarrier and power allocation in OFDM based on maximizing utility. *IEEE Vehicular Technology Conference (VTC 2003-Spring)*, 2003.

[SMW+01] Sklavos, A.; Maniatis, I.; Weber, T.; Baier, P. W.; Costa, E.; Haas, H.; Schulz, E.: Joint channel estimation in multiuser OFDM systems. *Proc. 6th International OFDM-Workshop (InOWo'01)*, Hamburg, 2001, pp. 3–1 – 3–4.

[SR06] Stimming, C.; Rohling, H.: Multi-user diversity and self-organized resource allocation in cellular OFDM-systems. *11th International OFDM-Workshop (InOWo'06)*, Hamburg, 2006, pp. 273–277.

[SRR87] Saleh, A.; Rustako, A.; Roman, R.: Distributed antennas for indoor radio communications. *IEEE Transactions on Communications*, vol. 35, 1987, pp. 1245–1251.

[SS00] Sonalkar, R. V.; Shively, R. R.: An efficient bit-loading algorithm for DMT applications. *IEEE Communications Letters*, vol. 4, 2000, pp. 80–82.

[SS04] Spencer, Q. H.; Swindlehurst, A. L.: Channel allocation in multi-user MIMO wireless communications systems. *IEEE International Conference on Communications (ICC)*, vol. 5, 2004, pp. 3035–3039.

[SSH04] Spencer, Q. H.; Swindlehurst, A. L.; Haardt, M.: Zero-forcing methods for downlink spatial multiplexing in multi-user MIMO channels. *IEEE Transactions on Siganal Processing*, vol. 52, 2004, pp. 461–471.

[SWB06] Stanczak, S.; Wiczanowski, M.; Boche, H.: *Resource Allocation in Wireless Networks – Theory and Algorithms*. Lecture Notes in Computer Science (LNCS 4000). Springer-Verlag, 2006.

[TE92] Tassiulas, L.; Ephremides, A.: Stability properties of constrained queueing systems and scheduling policies for maximum throughput in multihop radio networks. *IEEE Transactions on Automatic Control*, vol. 37, 1992, pp. 1936–1948.

[Tel99] Telatar, I. E.: Capacity of multi-antenna Gaussian channels. *European Transactions on Telecommunications*, vol. 10, 1999, pp. 585–595.

[TV05] Tse, D.; Viswanath, P.: *Fundamentals of Wireless Communication*. Cambridge University Press, 2005.

[TXX+05] Tao, X.; Xu, J.; Xu, X.; Tang, C.; Zhang, P.: Group cell FuTURE B3G TDD system. *China Communications*, vol. October, 2005, pp. 62–68.

[Ver98] Verdu, S.: *Multiuser Detection*. Cambridge University Press, 1998.

[vNP00] van Nee, R.; Prasad, R.: *OFDM for Wireless Multimedia Communications*. Boston: Artech House, 2000.

[WAD07] Weber, T.; Ahrens, A.; Deng, S.: Decentralized interference cancellation in mobile radio networks. *IEEE Wireless Communications and Networking Conference (WCNC)*, Hong Kong, 2007.

[WCLM99] Wong, C. Y.; Cheng, R. S.; Lataief, K. B.; Murch, R. D.: Multiuser OFDM with adaptive subcarrier, bit, and power allocation. *IEEE Journal on Selected Areas in Communications*, vol. 17, 1999, pp. 1747–1758.

[WDM05] Weber, T.; Deng, S.; Meurer, M.: Dynamic resource allocation in JOINT. *10th International OFDM-Workshop (InOWo'05)*, Hamburg, 2005, pp. 270–274.

[Wes00] West, D. B.: *Introduction to Graph Theory*. 2nd edition. Prentice Hall, 2000.

[WSEA04] Wong, I. C.; Shen, Z.; Evans, B. L.; Andrews, J. G.: A low complexity algorithm for proportional resource allocation in OFDMA systems. *IEEE Workshop on Signal Processing Systems 2004 (SIPS'04)*, Austin, USA, 2004.

[WSLW03] Weber, T.; Sklavos, A.; Liu, Y.; Weckerle, M.: The air interface concept JOINT for beyond 3G mobile radio networks. *15th International Conference on Wireless Communications (WIRELESS 2003)*, vol. 1, Calgary, 2003, pp. 25–33.

[Wu00] Wu, Q.: Optimum transmitter power control in cellular systems with heterogeneous SIR thresholds. *IEEE Transactions on Vehicular Techonology*, vol. 49, 2000, pp. 1424–1429.

[WW97] Willink, T. J.; Wittke, P. H.: Optimization and performance evaluation of multicarrier transmission. *IEEE Transactions on Information Theory*, vol. 43, 1997, pp. 426–440.

[XL06] Xu, M.; Lin, D.: Low-complexity user selection strategies in the downlink of multi-user channels. *The 8th International Conference Advanced Communication Technology (ICACT 2006)*, vol. 1, 2006.

[XTWZ06] Xu, X.; Tao, X.; Wu, C.; Zhang, P.: Group cell architecture for future mobile communication system. *ICN/ICONS/MCL*, 2006, pp. 199–203.

[YGC02] Yu, W.; Ginis, G.; Cioffi, J.: Distributed multiuser power control for digital subscriber lines. *IEEE Journal on Selected Areas in Communications*, vol. 20, 2002, pp. 1105–1115.

[YL02] Yin, H.; Liu, H.: Performance of space-division multiple-access (SDMA) with scheduling. *IEEE Transactions on Wireless Communications*, vol. 1, 2002, pp. 611–618.

[Zan92] Zander, J.: Performance of optimum transmitter power control in cellular radio systems. *IEEE Transactions on Vehicular Techonology*, vol. 41, 1992, pp. 57–62.

[ZCZ+06] Zheng, H.; Chen, X.; Zhou, S.; Wang, J.; Zhou, Y.; Kim, J. S.: An efficient user selection algorithm for zero-forcing beamforming in downlink multiuser MIMO systems. *IEICE Transactions on Communications*, vol. E89-B(9), 2006, pp. 2641–2645.

[ZL04] Zhang, Y. J.; Letaief, K. B.: Multiuser adaptive subcarrier-and-bit allocation with adaptive cell selection for OFDM systems. *IEEE Transactions on Wireless Communications*, vol. 3, 2004, pp. 1566–1575.

[ZL05] Zhang, Y. J.; Letaief, K. B.: An efficient resource-allocation scheme for spatial multiuser access in MIMO/OFDM systems. *IEEE Transactions on Communications*, vol. 53, 2005, pp. 107–116.

[ZT03] Zheng, L.; Tse, D. N. C.: Diversity and multiplexing: A fundamental tradeoff in multiple-antenna channels. *IEEE Transactions on Information Theory*, vol. 49, 2003, pp. 1073–1096.

[ZTZ+05] Zhang, P.; Tao, X.; Zhang, J.; Wang, Y.; Li, L.; Wang, Y.: A vision from the future: beyond 3G TDD. *IEEE Communications Magazine*, vol. 43, 2005, pp. 38–44.

List of Figures

1.1 General MIMO system 4

1.2 Conventional cellular architecture with cluster size three 7

1.3 SA architecture with SA size three 7

1.4 Multiuser MIMO scenarios in a service area, uplink 9

1.5 Multiuser MIMO scenarios in a service area, downlink 9

2.1 Generalized linear data transmission 21

2.2 UL transmission model 22

2.3 DL transmission model 25

2.4 TDD frame structure of JOINT 28

3.1 pdf of the SNR γ_k under the i.i.d. assumption of (3.4), $10 \log \frac{P_k}{\sigma^2} = 10$ dB 30

3.2 pdf of the bit rate R_k under the i.i.d. assumption of (3.4), $10 \log \frac{P_k}{\sigma^2} = 10$ dB 31

3.3 pdf of the energy efficiency ε_k under the i.i.d. assumption of (3.4) 33

3.4 Exemplary 2-cell scenario 35

3.5 Energy efficiency of MS1 in the 2-cell scenario 36

3.6 UL transmission model in a multi-SA scenario 39

3.7 DL transmission model in a multi-SA scenario 41

4.1 Two-user interference channel model 47

4.2 Two-user parallel channel model 48

4.3 Z channel model 48

4.4 Objective function $R_{\mathrm{sum}}(P_1)$ for $P_{\mathrm{tot}} = 1$ 51

4.5 Conventional waterfilling 55

4.6 Iterative waterfilling 57

4.7 $\frac{P_1^*}{P_{\mathrm{tot}}}$ versus pseudo-SNR and β ($g_{11} = g_{22} = 1$) 62

4.8 $\frac{P_1^*}{P_{\mathrm{tot}}}$ versus pseudo-SNR and β ($g_{11} = 1$, $g_{22} = 0.5$) 62

4.9 Ergodic sum rate in channel model I (strong interference) 65

4.10 Ergodic sum rate in channel model II (weak interference) 65

4.11 Ergodic sum rate in channel model III (moderate interference) . 67

4.12 Ergodic sum rate in channel model IV (close-to-Z channel) . . . 67

4.13 Ergodic sum rate in four-user interference channel (moderate interference) 68

4.14 Ergodic sum rate in six-user interference channel (moderate interference) 68

4.15 Fairness investigation of power allocation techniques in six-user interference channel (moderate interference, $10 \log_{10} \frac{P_{\mathrm{tot}}}{\sigma^2} = 20$ dB) 70

5.1 3-D channel gain array based subcarrier allocation ($K_{\mathrm{M}} = 6$, $K_{\mathrm{B}} = 3$, $N_{\mathrm{F}} = 2$). Each tile represents an entry of the 3-D channel gain array. Grey tiles are those being excluded. 82

5.2 Pseudo code of 3-D channel gain array based subcarrier allocation 82

5.3 SA interference channel model ($K_S = 2$, $N_F = 2$, $K_M = 6$). Solid lines: inter-SA co-channel interference links; dashed lines: useful links 85

6.1 SA network with $K_S = 4$, $K_B = 3$, $r = 1$ 93

6.2 Conventional cellular network with $K_S = 12$, $K_B = 1$, $r = 1$ . . . 93

6.3 Spectral efficiency CCDFs in a SA network with $K_B = 3$, $r = 1$, $K_S = 4$ and $N_F = 8$ 96

6.4 Averaged sum rate versus number of active MSs in a SA network with $K_B = 3$, $r = 1$, $K_S = 4$ and $N_F = 8$ 97

6.5 Spectral efficiency CCDFs in a conventional cellular network with $K_B = 1$, $r = 1$, $K_S = 12$ and $N_F = 8$ 99

6.6 Spectral efficiency CCDFs in a SA network with $K_B = 3$, $r = 1$, $K_S = 4$ and $N_F = 8$, flat fading 101

6.7 Energy efficiency CCDFs in a SA network with $K_B = 3$, $K = 3$, $r = 1$, $K_S = 4$ and $N_F = 8$ 104

6.8 Energy efficiency CCDFs in a SA network with $K_B = 3$, $K = 2$, $r = 1$, $K_S = 4$ and $N_F = 8$ 104

6.9 Spectral efficiency CCDFs in SA network with $K_B = 3$, $K = 2$, $r = 1$, $K_S = 4$ and $N_F = 8$ 106

6.10 Averaged sum rate versus number of active MSs in a SA network with $K_B = 3$, $r = 3$, $K_S = 4$ and $N_F = 8$ 108

6.11 Spectral efficiency CCDFs in a SA network with $K_B = 3$, $r = 3$, $K_S = 4$ and $N_F = 8$ 108

6.12 Spectral efficiency CCDFs in a SA network with $K_B = 3$, $r = 1$, $K_S = 4$ and $N_F = 8$, applying fixed subcarrier allocation 110

6.13 Spectral efficiency CCDFs in a SA network with $K_B = 3$, $r = 1$, $K_S = 4$ and $N_F = 8$, applying 3-D channel gain array based subcarrier allocation 111

6.14 Spectral efficiency CCDFs in a conventional cellular network with $K_{\mathrm{B}} = 1$, $r = 1$, $K_{\mathrm{S}} = 12$ and $N_{\mathrm{F}} = 8$, applying 3-D channel gain array based subcarrier allocation 113

6.15 Spectral efficiency CCDFs in a SA network with $K_{\mathrm{B}} = 3$, $r = 3$, $K_{\mathrm{S}} = 4$ and $N_{\mathrm{F}} = 8$, applying 3-D channel gain array based subcarrier allocation 115

List of Tables

1.1 Selected publications on resource allocation 14

4.1 Exemplary channel models 63

6.1 Ergodic spectral efficiency and outage spectral efficiency in a SA network with $K_{\mathrm{B}} = 3$, $r = 1$, $K_{\mathrm{S}} = 4$ and $N_{\mathrm{F}} = 8$ 98

6.2 Ergodic spectral efficiency and outage spectral efficiency in a conventional cellular network with $K_{\mathrm{B}} = 1$, $r = 1$, $K_{\mathrm{S}} = 12$ and $N_{\mathrm{F}} = 8$ 99

6.3 Ergodic spectral efficiency and outage spectral efficiency in a flat fading scenario ($N_{\mathrm{F}} = 8$, $K_{\mathrm{B}} = 3$, $r = 1$, $K_{\mathrm{S}} = 4$) 101

6.4 Ergodic spectral efficiency and outage spectral efficiency in a SA network with $K_{\mathrm{B}} = 3$, $K = 2$, $r = 1$, $K_{\mathrm{S}} = 4$ and $N_{\mathrm{F}} = 8$ . . 106

6.5 Ergodic spectral efficiency and outage spectral efficiency in a SA network with $K_{\mathrm{B}} = 3$, $r = 3$, $K_{\mathrm{S}} = 4$ and $N_{\mathrm{F}} = 8$ 109

6.6 Ergodic spectral efficiency and outage spectral efficiency in a SA network with $K_{\mathrm{B}} = 3$, $r = 1$, $K_{\mathrm{S}} = 4$ and $N_{\mathrm{F}} = 8$, applying fixed subcarrier allocation 110

6.7 Ergodic spectral efficiency and outage spectral efficiency in a SA network with $K_{\mathrm{B}} = 3$, $r = 1$, $K_{\mathrm{S}} = 4$ and $N_{\mathrm{F}} = 8$, applying 3-D channel gain array based subcarrier allocation 111

6.8 Ergodic spectral efficiency and outage spectral efficiency in a conventional cellular network with $K_{\mathrm{B}} = 1$, $r = 1$, $K_{\mathrm{S}} = 12$ and $N_{\mathrm{F}} = 8$, applying 3-D channel gain array based subcarrier allocation 114

6.9 Ergodic spectral efficiency and outage spectral efficiency in a SA network with $K_{\mathrm{B}} = 3$, $r = 3$, $K_{\mathrm{S}} = 4$ and $N_{\mathrm{F}} = 8$, applying 3-D channel gain array based subcarrier allocation 115

Thesen

1. The coordination of the BSs inside the same SA allows spatial separation of the signals of multiple MSs by means of joint transmission in the downlink and joint detection in the uplink.
2. SA based networks outperform conventional cellular networks by reducing capacity limiting interferences at a cost of complexity.
3. It is prohibitively complex to find the optimum subcarrier allocation in a SA network due to the correlated spatial signatures and the inter-SA interferences.
4. Adaptive resource allocation in SA networks can potentially benefit from adapting to frequency selectivity, to spatial correlations and to interferences.
5. Frequency selectivity of wireless channels is very beneficial to subcarrier allocation.
6. Spatial correlations are more critical than absolute channel gains in SDMA based SA networks, especially for fully loaded systems.
7. Arranging users with weakly correlated spatial signatures into the same subcarrier-sharing group results in high energy efficiencies.
8. The proposed 3-dimensional channel gain array based subcarrier allocation shows outstanding performance at a low complexity in SA based networks thanks to its elegant way of adapting to spatial correlations and channel gains.
9. It is not worth adapting to interferences in subcarrier allocation, especially in frequency planned networks for which the interferer diversity is large.
10. Universal frequency reuse is more spectrum efficient than frequency planning when a proper subcarrier allocation technique is applied.

11. Sum rate maximizing power allocation in interference channels with total power constraint is difficult to obtain due to the non-convexity of the optimization problem.

12. Allocating all transmit power to the best user is near-optimum in strong interference scenarios.

13. Conventional waterfilling power allocation should be used in weak interference scenarios due to its near-optimum performance and relatively low complexity.

14. The proposed iterative and noniterative waterfilling algorithms are preferable in moderate interference scenarios.

15. Exhaustive search based noniterative waterfilling power allocation is near-optimum, but is impractical if the number of users in the interference channel is large.

16. Classical SIR balancing power allocation is unfavorable in sum rate orientated applications.

17. SA networks can be interpreted as interference channels with vanishing intra-SA and inter-subcarrier interference links.

18. Interferences should be considered in power allocation rather than in subcarrier allocation.

19. Subcarrier-wise power allocation yields almost the same performance as system-wide power allocation at a lower complexity.

20. A SA network with universal frequency reuse can essentially be considered as a moderate interference scenario, while a SA network with frequency planning is equivalent to a weak interference scenario.

21. The performance gain of adaptive power allocation over equal power allocation shrinks as the performance of the subcarrier allocation technique applied before improves.